Syntheses and Properties of Kinetically Stabilized Tin–carbon Double-bond Compounds

Yoshiyuki MIZUHATA

Syntheses and Properties of Kinetically Stabilized Tin–carbon Double-bond Compounds

Department of Chemistry, Graduate School of Science

Kyoto University

Yoshiyuki MIZUHATA

March, 2006

Contents

Abbreviations

The following abbreviations are used in the text.

Ad	1-adamantyl
AIBN	2,2'-azobis(isobutyronitrile)
Anal.	elemental analysis
aq.	aqueous
Ar	an aryl group
B3LYP	Becke's 3-parameter hybrid with Lee, Young and Parr's correation functional
Bbt	2,6-bis[bis(trimethylsilyl)methyl]-4-[tris(trimethylsilyl)methyl]phenyl
BPO	benzoyl peroxide
br	broad
Bu	butyl
calcd	calculated
cat.	catalyst
Ch	chalcogen (Group 16 Elements)
Cp	cyclopentadienyl
Cp*	pentamethylcyclopentadienyl
d	doublet
δ	chemical shift of NMR signal in ppm
DBU	1,8-diazbicyclo[5.4.0]undec-7-ene
dec.	decomposition
DEPT	distortionless enhancement by polarization transfer
Dip	2,6-diisopropylphenyl
Dis	bis(trimethylsilyl)methyl
Ditp	2,2"-diisopropylphenyl-*m*-terphenyl-2'-yl
ε	molar extinction coefficient
equiv.	equivalents

EI	electron impact
Et	ethyl
FAB	fast atom bombardment
GIAO	gauge-independent atomic orbitals
GPC	gel permeation chromatography
h	hour(s)
η	hapto (eta)
HOMO	highest occupied molecular orbital
HPLC	high performance liquid chromatography
HRMS	high-resolution mass spectra
IR	infrared
J	coupling constants in NMR
LANL2DZ	Los Alamos national laboratory 2 double-zeta
LDA	lithium diisopropylamide
LTMP	lithium 2,2,6,6-tetramethylpieridide
LUMO	lowest unoccupied molecular orbital
m	multiplet
m	*meta*
Me	methyl
Mes	mesityl (2,4,6-trimethylphenyl)
Mes*	supermesityl [2,4,6-tri(*t*-butyl)phenyl]
mp	melting point
MS	mass spectrum
n	normal
NBS	*N*-bromosuccinimide
NICS	Nucleus-Independent Chemical Shift
NMR	nuclear magnetic resonance
NOE	nuclear Overhauser effect
o	*ortho*

ORTEP	Oak Ridge thermal ellipsoid plot
p	*para*
Ph	phenyl
Pn	pnictogen (Group 15 Elements)
q	quartet
quant.	quantitative
R, R', R"	an organic group
ref.	reference
rt	room temperature
s	singlet
sh	shoulder
t	triplet
t	tertiary
Tbt	2,4,6-tris[bis(trimethylsilyl)methyl]phenyl
THF, thf	tetrahydrofuran
Tip	2,4,6-triisopropylphenyl
Titp	2,2",4,4"-tetraisopropylphenyl-*m*-terphenyl-2'-yl
TMP	2,2,6,6-tetramethylpiperidide
UV/vis	ultraviolet and visible
X	halogen

Chapter 1

General Introduction

1.1 Breaking of "Classical Double-bond Rule"

It has been well-known that the second-row elements of the Periodic Table, such as boron, carbon, nitrogen, and oxygen are able to form multiple pπ-pπ bonds. Owing to such feature, a wide variety of organic chemistry has been developed for a long time.

In contrast to the second-row elements, their heavier congeners had been thought for many years to be incapable of forming stable molecules having pπ-pπ bondings.[1] In other words, it was believed that elements having a principal quantum number greater than 2 cannot form pπ-pπ bonds with themselves or with other elements. Such a view is referred to as the "classical double-bond rule". This interpretation was rationalized by the long bond-distances between heavier elements, which do not allow the sufficient overlapping of p-orbitals.

The breakthrough in this field was the isolation of the first stable distannene (Sn=Sn, **1**)[2] in 1973, phosphaalkene (P=C, **2**)[3] in 1978, and silene (Si=C, **3**),[4] diphosphene (P=P, **4**),[5] and disilene (Si=Si, **5**)[6] in 1981. In all cases, introduction of bulky ligands on the central atoms prevented them from oligomerization to make such reactive species isolable as stable compounds. These sensational works evidenced that the double-bond compounds of heavier main group elements could be isolated as stable species without oligomerization (or side-reaction) when they were well "kinetically stabilized" with bulky substituents.

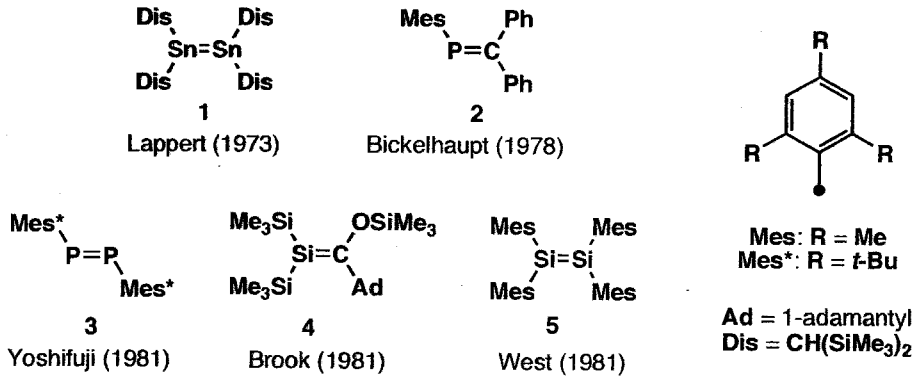

After this breakthrough, significant and exciting progress has been made in the chemistry of unsaturated compounds of heavier main group elements, especially in the field of group 14 elements by taking advantages of steric protection. Until now, a variety stable compounds having double bonds between group 14–group 14, group 14–group 15, group 14–group 16 elements have been successfully synthesized and characterized. In addition to these double-bond species, the double-bond compounds between group 14–group 13 elements, silaborene[7] and 1,3-disila-2-gallata- and indataallenic anions have been synthesized very recently.[8]

1.2 Multiply Bonded Systems Containing Tin Atom(s)

In Figure 1-1 are shown the radii of atomic orbitals (maximal electron-density), which are calculated for group 14 elements.[9] It may be expected that the sizes of the *n*s and *n*p orbitals increase monotonously going down the periodic table from C to Pb, since the principal quantum number (*n*) increases. Unexpectedly, however, one can see that the sizes of orbitals change irregularly. The irregularity in Si→Ge and Sn→Pb are most likely interpreted in terms of so-called "d-block contraction" and "relativistic effect".[10] Anyway, one can see obviously two boundary lines drawn between carbon and silicon, and between germanium and tin. Taking into consideration of the second boundary line, that is, the large difference of the orbital sizes between Ge and Sn, it should be expected that the properties of silicon and/or germanium compounds may differ from those of tin and/or lead compounds.

In fact, the compounds doubly bonded to tin are less stable than the corresponding silicon or germanium compounds, and the investigations about them are still insufficient due to the difficulty in the synthesis of such unstable species.

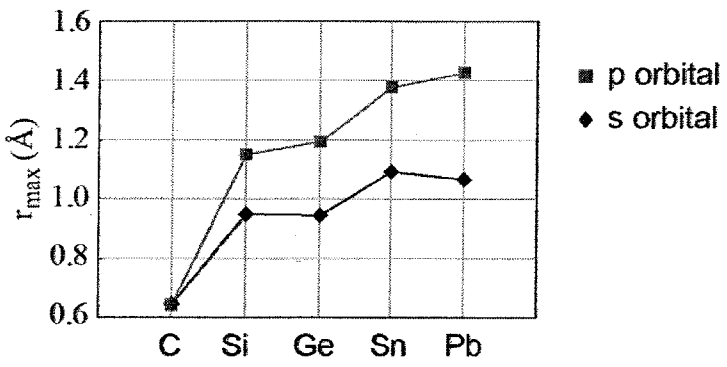

Figure 1-1.

1.2.1 >Sn=E<, >Sn=E=E<, and –Sn≡E– (E = Group 14 Elements)

1.2.1.1 Ethylene Analogues

Distannenes (>Sn=Sn<). As mentioned previously, the chemistry of distannenes >Sn=Sn<, the ethylene analogues of tin atoms, has the longest history among all heavy alkene analogues of the type >E=E'< (E, E' are group 14 elements).[11] The first stable compound with an Sn=Sn double bond, **1** was reported by Lappert nearly 30 years ago.[2] Since then, distannenes **6-11** were synthesized and characterized.[12] However, almost of all distannenes ($R_2Sn=SnR_2$) known to date undergo ready dissociation into two molecules of the corresponding stannylenes (R_2Sn:) in solution. Tetrasilyl-substituted distannene **11** reported by Sekiguchi certainly forms the stable double bond in the solid state and in solution.

Furthermore, **1** and **7-10** possess *trans*-bent structures with substantial out-of-plane angles and Sn–Sn distances [2.768(1)-2.910(1) Å] approximately equal to or greater than those of the corresponding Sn–Sn single bond. However, the Sn=Sn bond length in **11** is very short, 2.6683(10) Å, being the shortest one among all acyclic distannenes ever reported. Moreover, the sp^2 Sn atoms have planar geometry (the sum of the bond angles around them is 359.98°) along with the very small bend angle of only 1.22(5)°.

Due to the distannene–stannylenes equilibrium in solution, the ^{119}Sn NMR signals of these distannenes except **11** were observed at low temperature or not observed (only signal assignable to stannylne was reported). The signals assignable to the central tin atom of the distannenes were observed at 740 (**1**), 427 (**6**), and 630.7 (**11**) ppm.

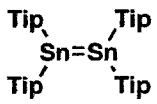

6
Masamune (1985)

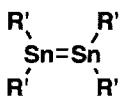

7
Weidenburuch (1992)

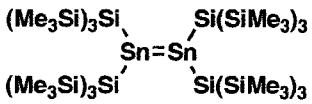

8
Klinkhammer (1995)

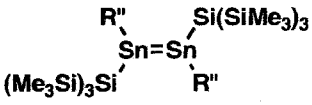

9
Klinkhammer (1998)

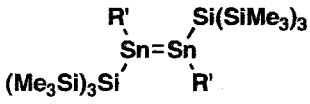

10
Weidenburuch (1999)

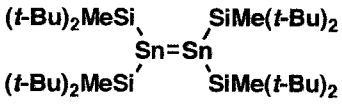

11
Sekiguchi (2004)

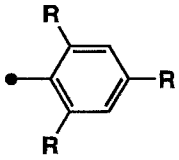

Tip: R = *i*-Pr
R": R = CF_3

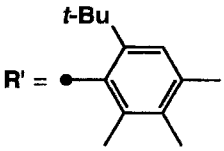

Germastannenes (>Sn=Ge<). The first report of germastannene **12** appeared in 1996 by Escudié.[13] However, **12** was stable only below –20 °C, and it underwent ready dissociation into Tip_2Sn: **13** and Mes_2Ge: **14** at room temperature to afford germadistannirane **15** as the final isolable product. Germastannenes **16-19** stable at ambient temperature were reported in 2003 by Weidenbruch and Sekiguchi.[14] The most striking feature of **17** was its ready isomerization to the symmetrically substituted germastannene **18** by heating at 50 °C in C_6D_6 solution.

The experimental results showed that the behavior of germastannenes (double bond vs. divalent species) is totally controlled by their substituents: germastannenes **12** and **16** having only aryl groups undergo dissociation in solution at ambient temperature, whereas all of three germastannenes **17-19** bearing silyl substituents form the stable double bonds in both the solid

state and even in the solution. The ^{119}Sn NMR spectra of all germastannenes showed a signal at 268-525 ppm, which is characteristic region for doubly bonded tin derivatives.

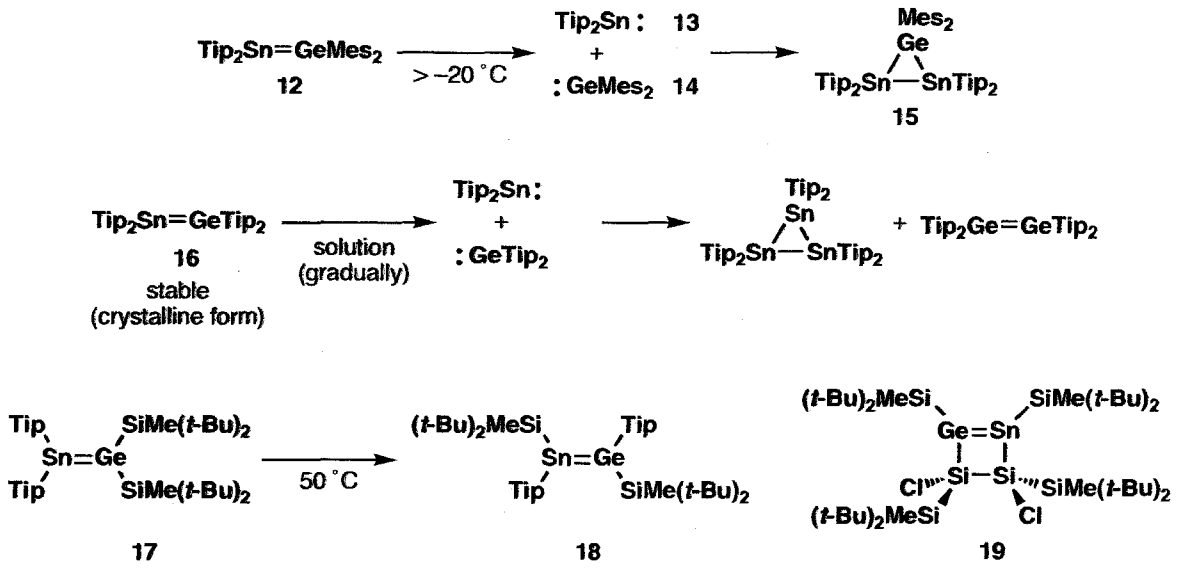

Silastannenes (>Sn=Si<). The first stable silastannene **20** was reported by Sekiguchi in 2002.[15] The ^{119}Sn NMR spectrum of **20** showed a downfield-shifted resonance of the doubly bonded Sn atom at +516.7 ppm, which was characteristic of sp^2 Sn atoms. The sp^2 Si atom in **20** resonated at an unusually high field, +27.4 ppm, in a sharp contrast to the vast majority of other doubly bonded Si atoms. Such a phenomenon should be definitely ascribed to the inverted polarity Si^+=Sn^- due to the electronic environments around the double bond, that is, the electron-donating silyl substituents on the sp^2 Si atom and the electron-withdrawing aryl groups on the sp^2 Sn atom.

The length of the Si=Sn double bond **20** was determined as 2.4188(14) Å, which was just between the typical values of Si=Si (2.138-2.289 Å) and Sn=Sn (2.590-3.087 Å) double-bond lengths. The shortening of the Si=Sn double bond compared with the Si–Sn single bond (average value 2.60 Å) was ca. 7%.

The Si=Sn double bond of **20** was rather strong and did not dissociate in solution into a silylene and a stannylene.

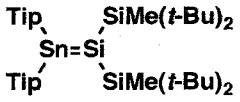

20

Stannenes (>Sn=C<). The chemistry of stannenes has been less developed than that of silenes and germenes. The structural analyses of the Sn=C double-bond compounds ever reported are limited to only two types, both of which are thermodynamically stabilized by heteroatoms such as B and/or N. While Berndt reported a series of diboryl-substituted stannenes **21**-**24** having an extremely short Sn=C bond [**21** (2.025 Å), **23** (2.036 Å) and **24** (2.032 Å)],[16] the formal Sn=C compounds such as **25**,[17] **26**, **27**,[18] and **28**[19], the Sn–C bond lengths of which (**25**: 2.314 Å, **26**: 2.290 Å, **27**: 2.379 Å, **28**: 2.303 Å) are markedly longer than the typical Sn–C single-bond lengths (av. 2.14 Å),[20] have also been synthesized and characterized. Although 6-stannapentafulvene **29** bearing only carbon substituents on the Sn=C moiety was synthesized by Escudié *et al.*,[21] **29** was not structurally characterized due to its ready dimerization at room temperature.

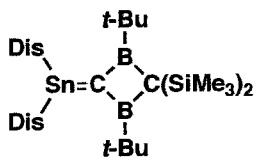

21

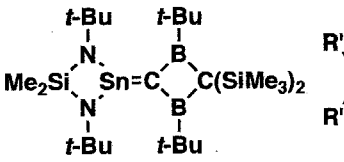

22

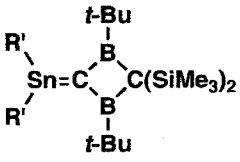

23

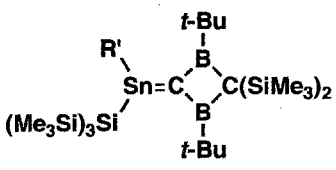

24

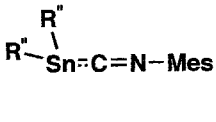

25

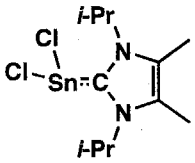

26

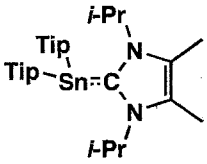

27

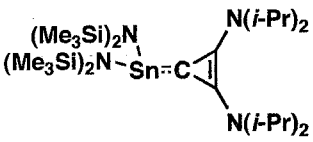

28

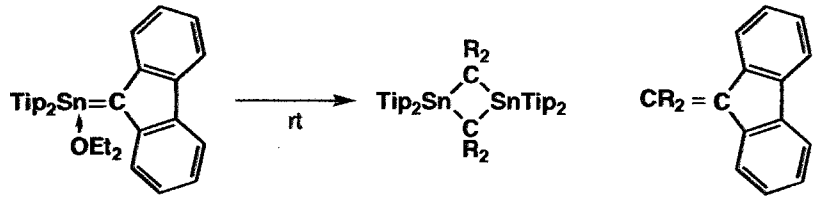

1.2.1.2 Allene Analogues

Tristannaallene The dark blue, air- and moisture-sensitive, thermolabile tristannaallene **30** was prepared by reaction of $Sn[O(t\text{-}Bu)]_2$ or $Sn[N(SiMe_3)_2]_2$ with $(t\text{-}Bu)_3SiNa$ in pentane/benzene at –25 °C.[22] Compound **30** isomerized to give **31** at room temperature ($\tau_{1/2}$ = 9.8 h). According to the result of X-ray structural analyses, the framework of **30** was bent (156°) and the terminal Sn atoms had the pyramidal geometries. The Sn=Sn bonds in **30** (2.68 Å) were approximately equal to the shortest Sn=Sn bond length in **11** [2.6683(10) Å]. In the ^{119}Sn NMR spectrum, two signals at low field (δ 503, 2233, intensity ratio 2:1) were observed in the toluene-d_8 solution. In particular, the latter chemical shift, which was adapted to the central tin atom, was characteristic of those of stannylenes, indicating the bonding situation in **30** could be described by the resonance formulae shown below.

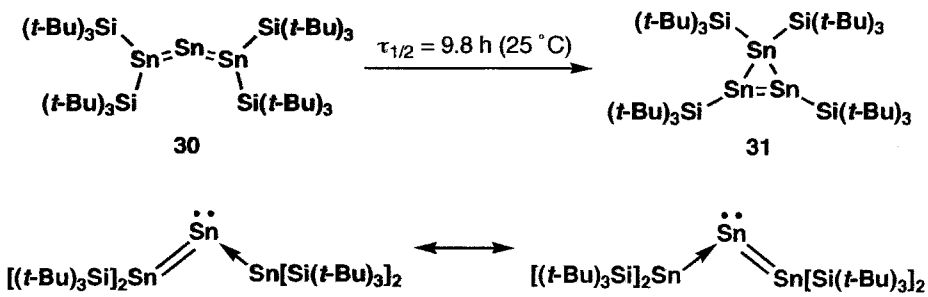

1-Stannaallene Generation of 1-stannaallene **32** was postulated as an intermediate in the synthesis of the first stable distannirane **33** by Escudié in 2004.[23] Because of the probable lability of the tin–carbon double bond, **32** could behave as a stannylene-vinylidene carbene complex as

observed in the related stannaketenimine **25** that behaves as stannylene and isocyanide (in the reactions with trapping agents). Therefore, the generation of the final product of this reaction (**33**) should be most likely interpreted in terms of the [2 + 1] cycloaddition of **32** with the stannylene **34**, which should be generated in an equilibrium amount.

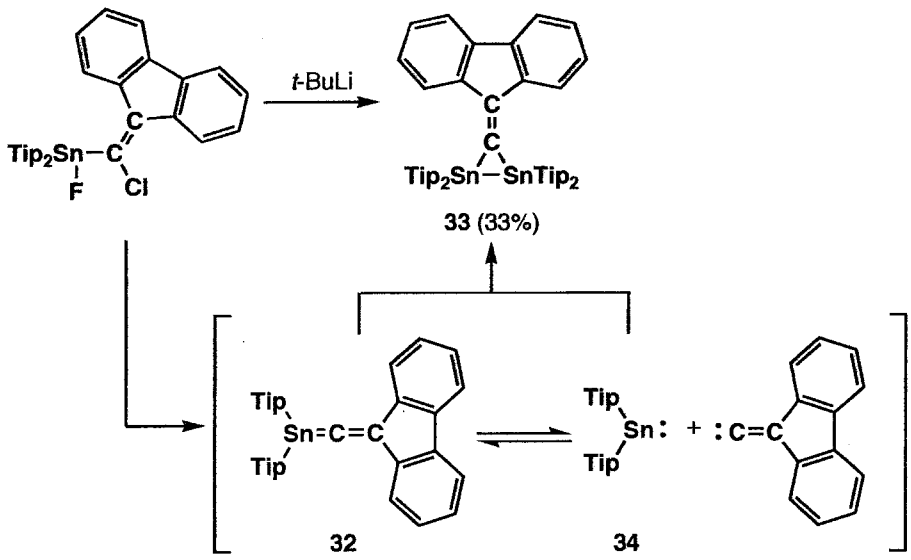

1.2.1.3 Acetylene Analogues

Many experimental and theoretical studies have been devoted to the chemistry of triple-bonded compounds of heavier group 14 elements.[24] Among them, silaisocyanide,[25] silanitrile,[26] silaacetylene,[27] and germaisocyanide[28] have been evidenced as short-lived species by various spectroscopic and trapping experiments. Recently, a series of homonuclear acetylene analogues of heavier group 14 elements, **35**-**38**, have been isolated as stable compounds.[29]

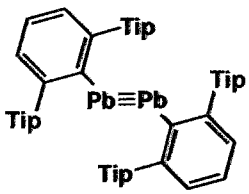

35
Power (2000)

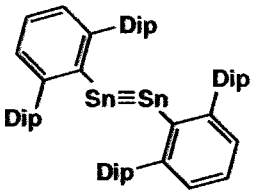

36
Power (2002)

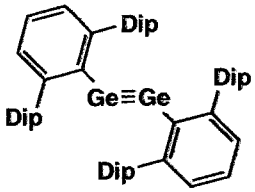

37
Power (2002)

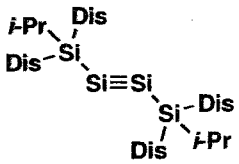

38
Sekiguchi (2005)

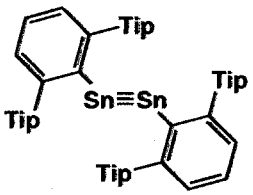

39
Power (2003)

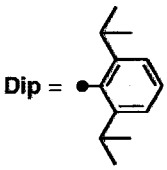

Distannynes (–Sn≡Sn–). Distannynes **36** and **39**, tin-analogues of acetylene, were synthesized by Power and characterized by X-ray crystallographic analysis. The structure of **35** was not linear but bent, and the Sn–Sn bond length, 2.6675(4) Å, is similar to the shortest Sn–Sn distance in the distannene [2.6683(10) Å in **11**]. Unfortunately, the electronic state of the tin atom in **36** and **39** cannot be elucidated in detail, since the ^{119}Sn NMR signals of them have not been detected.

Stannyne (–Sn≡C–). The generation of stannyne **41** by the photolysis of diazomethyl-substituted stannylene **40** was reported by Kira in 2004.[30] The formation of **42** is explained straightforwardly by the intermediacy of stannyne **41** followed by the intramolecular insertion of the carbene moiety of **41** to the proximate methyl C–H bond of the isopropyl group. This result afforded the evidence not only for the generation of **41** but also for its high carbene-like reactivity.

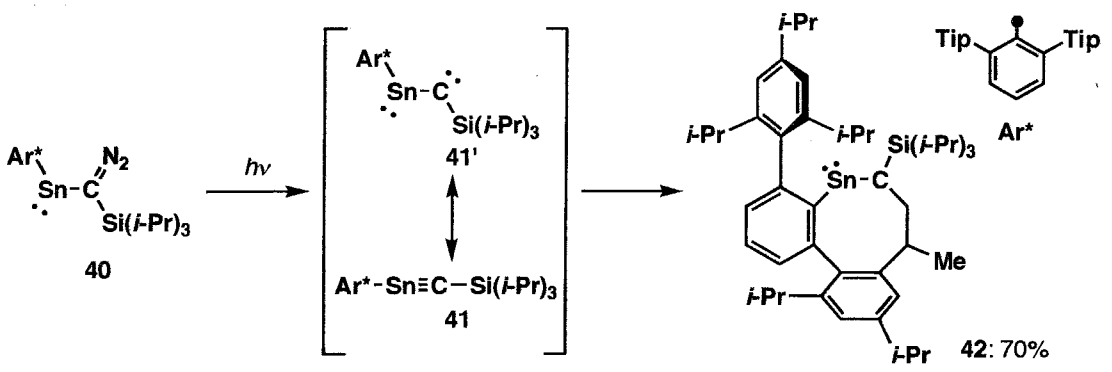

1.2.2 >Sn=Pn– (Pn = Group 15 Elements)

Azastannene (>Sn=N–). Tin-analogues of imines containing a tin–nitrogen double bond are extremely reactive and have been trapped in a variety of reactions. Until now, only two stable azastannenes have been synthesized and characterized by X-ray crystallographic analysis.[31] The structural analysis of **43** shows the short Sn=N bond length of 1.921 Å (Sn–N single bond length: av. 2.05 Å), the planar geometry at tin, and an interligand angle at nitrogen of 120.6(2)°. Although the bond-shortening in **43** implies that this Sn–N bond has a considerable double-bond character, its ^{119}Sn NMR appeared at an extremely high field (–3.4 ppm). It probably results from the inductive effects of the electropositive two nitrogen atoms having two trimethylsilyl groups to the central tin atom. Compound **43** is stable at –30 °C in the crystalline state, but it rearranges within 2 weeks in hexane to give **44** by intramolecular addition of the C–H bond of the isopropyl groups across the Sn=N bond. The Sn–N distance in **45** has the shorter value of 1.905(3) Å.[32]

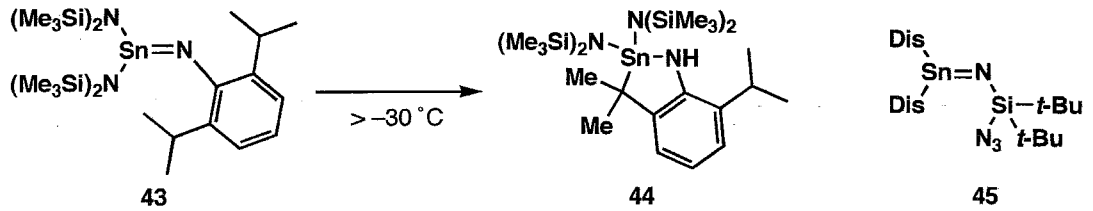

Phosphastannene (>Sn=P–). The first stable phosphastannene **47** was synthesized by dehydrofluorination of the corresponding (fluorostannyl)phosphine **46**.[33] The structure of **47** was unambiguously determined by the NMR spectra. The ^{119}Sn NMR observed at a very low field (658 ppm) is characteristic of a tricoordinated p-π hybridized tin. It is noted that the coupling constants between the phosphorus and tin atoms [^{1}J(P–^{117}Sn) = 2191 Hz, ^{1}J(P–^{119}Sn) = 2295 Hz] are much larger than those of stannylphosphines [for example, ^{1}J(P–^{117}Sn) = 1150 and ^{1}J(P–^{119}Sn) = 1203 Hz for the starting (fluorostannyl)phosphine **46**], indicating the presence of a π-bond between the tin and phosphorus in **47**. The larger coupling constants than those of the single bond have also been observed in the coupling constants of ^{1}J(P–^{29}Si) in the silaphosphene[34] and ^{1}J(P–P) in the diphosphenes.[35] Another stannaphosphene **48** having two Tip groups on the tin atom was synthesized in a similar manner,[36] and it displayed a low-field chemical shift of 500 ppm in the ^{119}Sn NMR spectrum.

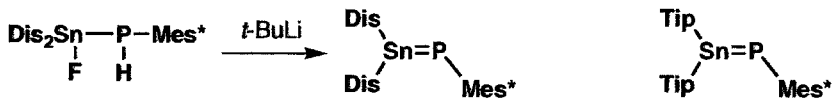

46 **47** **48**

1.2.3 >Sn=Ch (Ch = Group 16 Elements)

Chemistry of heavier element congeners of ketones (*heavy ketones*) has been developed only recently.[37] As for the tin analogues, the kinetically stabilized stannanethiones (Sn=S), stannaneselones (Sn=Se), and stannanetellones (Sn=Te) have been synthesized and characterized, though no stannone (Sn=O) analogue has been isolated as a stable compound so far.

Stannanethiones (**49**[38] and **50**[39]), stannaneselone **51**,[38] and stannanetellones[40] (**52** and **53**) stable at ambient temperature were successfully synthesized for the first time using the combination of Tbt (or Bbt) and *meta*-terphenyl substituents (Ditp or Titp) by Tokitoh and Okazaki. X-Ray crystallographic analyses of **50**, **51**, and **53** were achieved to reveal the

planarity around the tin atoms and the shortening of the Sn=Ch bond lengths in comparison with the corresponding Sn–Ch single-bond lengths. The ^{119}Sn NMR spectrum of **49-53** showed a signal at 282-532 ppm, which is characteristic of the doubly bonded tin derivatives.

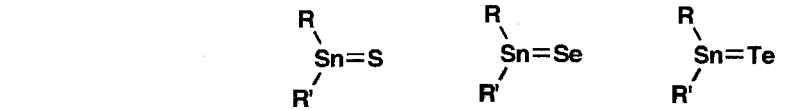

R = Tbt, R' = Ditp	**49**: δ_{Sn} = 531	**51**: δ_{Sn} = 440	**52**: δ_{Sn} = 312
R = Bbt, R' = Titp	**50**: δ_{Sn} = 532	–	**53**: δ_{Sn} = 282

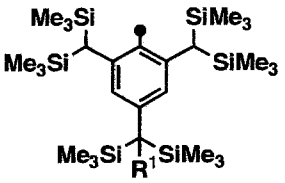

Tbt: R^1 = H
Bbt: R^1 = $SiMe_3$

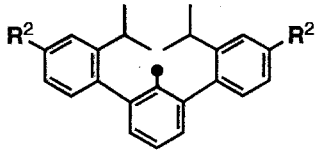

Ditp: R^2 = H
Titp: R^2 = *i*-Pr

1.3 The Purpose of the Present Study

As described above, the chemistry of multiple-bond compounds containing (a) tin atom(s) has the longest history among those of the multiple bonds to the heavier main group elements. However, it developed rapidly in the last decade and is still insufficient to make systematic elucidation of the multiply bonded systems containing (a) tin atom(s).

Especially, all stable stannenes (Sn=C, Section 1.2.1.1) are influenced by the electronic perturbation of the adjacent heteroatom and the nature of the Sn=C double bond could not be discussed in detail despite they are considered as "bridge" compounds between olefins and heavy olefins. In order to study the chemical behaviour of tin–carbon double bond in detail, the author wishes to describe the synthesis and properties of the kinetically stabilized stannenes bearing only carbon substituents in Chapter 2. In Chapter 3, the synthesis and properties of stannaaromatic compounds, which have the formal Sn=C fragments incorporated in aromatic rings, 9-stannaphenantherene and 2-stannanaphthalene, will be reported.

References

1. For a review, see: Gusel'nikov, L. E.; Nametkin, N. S. *Chem. Rev.* **1979**, *6*, 529.
2. (a) Davidson, P. J.; Lappert, M. F. *J. Chem. Soc., Chem. Commun.* **1973**, 317. (b) Goldberg, D. E.; Harris, D. H.; Lappert, M. F. *J. Chem. Soc., Chem. Commun.* **1976**, 261. (c) Goldberg, D. E.; Hitchcock, P. B.; Lappert, M. F.; Thomas, K. M.; Thorne, A. J.; Fjeldberg, T.; Haaland, A.; Schilling, B. E. R. *J. Chem. Soc., Dalton Trans.* **1986**, 2387.
3. Klebach, Th. C.; Lourens, R.; Bickelhaupt, F. *J. Am. Chem. Soc.* **1978**, *100*, 4886.
4. Brook, A. G.; Abdesaken, F.; Gutekunst, B.; Gutekunst, G.; Kallury, R. K. *J. Chem. Soc., Chem. Commun.* **1981**, 191.
5. Yoshifuji, M.; Shima, I.; Inamoto, N.; Hirotsu, K.; Higuchi, T. *J. Am. Chem. Soc.* **1981**, *103*, 4587.
6. West, R.; Fink, M. J.; Michl, J. *Science* **1981**, *214*, 1343.
7. Nakata, N.; Sekiguchi, A. Abstract of the 85th Spring Meeting of the Chemical Socity of Japan, March 26-29, 2005.
8. Nakata, N.; Izumi, R.; Lee, V. Ya.; Ichinohe, M.; Sekiguchi, A. *J. Am. Chem. Soc.* **2004**, *126*, 5058.
9. Desclaux, J. P. *Data Nucl. Data Tables*, **1973**, *12*, 311.
10. (a) Pyykkö, P. *Chem. Rev.* **1988**, *88*, 563. (b) Norman, N. C. In Periodicity and the s- and p-Block Elements; Oxford University Press, New York, 1997.
11. Reviews on distannenes chemistry: (a) Power, P. P. *Chem. Rev.* **1999**, 99, 3463. (b) Klinkhammer, K. W. In The Chemistry of Organic Germanium, Tin and Lead Compounds; Rappoport, Z., Ed.; Wiley: Chichester, 2002; Vol. 2, Part 1, Chapter 4.

12. (a) Masamune, S.; Sita, L. R. *J. Am. Chem. Soc.* **1985**, *107*, 6390. (b) Weidenbruch, M.; Kilian, H.; Peters, K.; von Schnering, H. G.; Marsmann, H. *Chem. Ber.* **1995**, *128*, 983. (c) Klinkhammer, K. W.; Schwarz, W. *Angew. Chem., Int. Ed. Engl.* **1995**, *34*, 1334. (d) Klinkhammer, K. W.; Fassler, T. F.; Grutzmacher, H. *Angew. Chem. Int. Ed.* **1998**, *37*, 124. (e) Sturmann, M.; Saak, W.; Klinkhammer, K. W.; Weidenbruch, M. *Z. Anorg. Allg. Chem.* **1999**, *625*, 1955. (f) Fukawa, T.; Lee, V. Ya.; Nakamoto, M.; Sekiguchi, A. *J. Am. Chem. Soc.* **2004**, *126*, 11758.

13. Chaubon, M.-A.; Escudié, J.; Ranaivonjatovo, H.; Satgé, J. *J. Chem. Soc., Chem. Commun.* **1996**, 2621.

14. (a) Schäfer, A.; Saak, W.; Weidenbruch, M. *Organometallics* **2003**, *22*, 215. (b) Sekiguchi, A.; Izumi, R.; Lee, V. Ya.; Ichinohe, M. *Organometallics* **2003**, *22*, 1483. (c) Lee, V. Ya.; Takanashi, K.; Ichinohe, M.; Sekiguchi, A. *J. Am. Chem. Soc.* **2003**, *125*, 6012.

15. Sekiguchi, A.; Izumi, R.; Lee, V. Ya.; Ichinohe, M. *J. Am. Chem. Soc.* **2002**, *124*, 14822.

16. a) Meyer, H.; Baum, G.; Massa, W.; Berger S.; Berndt, A. *Angew. Chem., Int. Ed. Engl.* **1987**, *26*, 546. b) Berndt, A.; Meyer, H.; Baum, G.; Massa, W.; Berger, S. *Pure Appl. Chem.* **1987**, *59*, 1011. c) Weidenbruch, M.; Kilian, H.; Stürmann, M.; Pohl, S.; Saak, W.; Marsmann, H.; Steiner, D.; Berndt, A. *J. Organomet. Chem.* **1997**, *530*, 255. d) Stürmann, M.; Saak, W.; Weidenbruch, M.; Berndt A.; Sclesclkewitz, D. *Heteroatom Chem.* **1999**, *10*, 554.

17. Grützmacher, H.; Freitag, S.; Herbst-Irmer R.; Scheldrick, G. S. *Angew. Chem., Int. Ed. Engl.* **1992**, *31*, 437.

18. a) Kuhn, N.; Kratz, T.; Bläser D.; Boese, R. *Chem. Ber.* **1995**, *128*, 245. b) Schäfer, A.; Weidenbruch, M.; Saak W.; Pohl, S. *J. Chem. Soc., Chem. Commun.* **1995**, 1157.

19. Schumann, H.; Glanz, M.; Girgsdies, F.; Hahn, F. E.; Tamm M.; Grzegorzewski, A. *Angew. Chem., Int. Ed. Engl.* **1997**, *36*, 2232.

20. Mackay, K. M. in "The Chemistry of Organic Germanium, Tin and Lead Compounds," ed by S. Patai, Wiley, Chichester, U.K., 1995; Vol. 1, Chap. 2.

21. a) Anselme, G.; Ranaivonjatovo, H.; Escudié, J.; Couret C.; Satgé, J. *Organometallics* **1992**, *11*, 2748. b) Anselme, G.; Declercq, J. -P.; Dubourg, A.; Ranaivonjatovo, H.; Escudié J.; Couret, C. *J. Organomet. Chem.* **1993**, *458*, 49. c) For a transient stannene, $[(Me_3Si)_2CH]_2Sn{=}C$(fluorenylidene): Anselme, G.; Couret, C.; Escudié, J.; Richelme S.; Satgé, J. *J. Organomet. Chem.* **1991**, *418*, 321.

22. Wiberg, N.; Lerner, H.-W.; Vasisht, S.-K.; Wagner, S.; Karaghiosoff, K.; Noth, H.; Ponikwar, W. *Eur. J. Inorg. Chem.* **1999**, 1211.

23. Baiget, L,; Ranaivonjatovo, H.; Escudié , J.; Gornitzka, H. *J. Am. Chem. Soc.* **2004**, *126*, 11792.

24. For recent reviews of triply bonded compounds of heavier main group elements, see: (a) Power, P. P. *Chem. Commun.* **2003**, 2091. (b) Weidenbruch, M. *J. Organomet. Chem.* **2002**, *646*, 39. (c) Jutzi, P. *Angew. Chem. Int. Ed.* **2000**, *39*, 3797. (d) Power, P. P. *Chem. Rev.* **1999**, *99*, 3463. (e) Robinson, G. H. *Acc. Chem. Res.* **1999**, *32*, 773.

25. Bock, H.; Dammel, G. *Angew. Chem., Int. Ed. Engl.* **1985**, *24*, 111.

26. Maier, G.; Glatthaar, J. *Angew. Chem., Int. Ed. Engl.* **1994**, *33*, 473.

27. Karni, M.; Apeloig, Y.; Schroder, D.; Zummack, W.; Rabezzana, R.; Schwartz, H. *Angew. Chem., Int. Ed.* **1999**, *38*, 332.

28. Foucat, S.; Pigot, T.; Pfister-Guillouzo, G.; Lavayssiere, H.; Mazieres, S. *Organometallics* **1999**, *18*, 5322.

29. (a) Pu, L.; Twamley, B.; Power, P. P. *J. Am. Chem. Soc.* **2000**, *122*, 3524. (b) Philips, A. D.; Wright, R. J.; Olmstead, M. M.; Power, P. P. *J. Am. Chem. Soc.* **2002**, *124*, 5930. (c) Stender, M.; Phillips, A. D.; Wright, R. J.; Power, P. P. *Angew. Chem., Int. Ed.* **2002**, *41*, 1785. (d) Stender, M.; Phillips, A. D.; Power, P. P. *Chem. Commun.* **2002**, 1312. (e) Sekiguchi, A.; Kinjo, R.; Ichinohe, M. *Science* **2004**, *305*, 1755.

30. Setaka, W.; Hirai, K.; Tomioka, H, Sakamoto, K.; Kira, M. *J. Am. Chem. Soc.* **2004**, 126, 2696.

31. Ossig, G.; Meller, A.; Freitag, S.; Herbst-Irmer, R. *J. Chem. Soc., Chem. Commun.* **1993**, 497.

32. Veith, M.; Rammo, A. *Z. Anorg. Allg. Chem.* **1997**, *623*, 861.

33. Couret, C.; Escudié, J.; Satgé, J.; Raharinirina, A.; Andriamizaka, J. D. *J. Am. Chem. Soc.* **1985**, 107, 8280.

34. Smit, C. N.; Lock, F. M.; Bickelhaupt, F. *Tetrahedron Lett.* **1984**, *25*, 3011.

35. For reviews, see: (a) Cowley, A. H.; *Polyhedron* **1984**, *3*, 389. (b) Cowley, A. H.; *Acc. Chem. Res.* **1984**, *17*, 386.

36. Ranaivonjatovo, H.; Escudié, J.; Couret, C.; Satgé, J. *J. Chem. Soc., Chem. Commun.* **1992**, 1047.

37. For reviews on heavy ketones, see: (a) Tokitoh, N.; Mastuhashi, Y.; Shibata, K.; Mastumoto, T.; Suzuki, H.; Saito, M.; Manmaru, K.; Okazaki, R. *Main Group Metal Chemistry* **1994**, *17*, 55. (b) Tokitoh, N.; Matsumoto, T.; Okazaki, R. *Bull. Chem. Soc. Jpn.* **1999**, *71*, 1665. (c) Okazaki, R.; Tokitoh, N. *Acc. Chem. Res.* **2000**, *33*, 625. (d) Kano, N.; Tokitoh, N.; Okazaki, R. *Journal of Synthetic Organic Chemistry Japan (Yuki Gosei Kagaku Kyokai Shi)* ,**1998**, *56* , 919. (e) Tokitoh, N. *Journal of Synthetic Organic*

Chemistry Japan (Yuki Gosei Kagaku Kyokai Shi), **1994**, *52*, 136. (f) Tokitoh, N.; Okazaki, R. *Adv. Organomet. Chem.* **2001**, *47*, 121.

38. Saito, M.; Tokitoh, N.; Okazaki, R. *J. Am. Chem. Soc.* **2004**, *126*, 15572.

39. Unpublished results.

40. Tajima, T; Sasamori, T; Takeda, N.; Tokitoh, N. Abstract of the 10th Symposium of the Society of Silicon Chemistry, Japan; Oct. 28–29, 2005; p. 46.

Chapter 2

Syntheses and Properties of Tin–carbon Double-Bond Compounds

2.1 Introduction

2.1.1 Dimetallene and Metallene Chemistry

In the past few decades, much attention has been focused on the chemistry of heavier congeners of alkenes, *i.e.*, "metallenes and dimetallenes" (>E=C< and >E=E<: E = Si, Ge, Sn, Pb), and a number of reports have appeared on their syntheses, structures, and properties. A number of stable dimetallenes have been synthesized and characterized so far. The experimental and theoretical studies revealed structures and properties apparently different from olefins (>C=C<). The dominant difference is their *trans*-bent structures in contrast to the planar D_{2h} structures of olefins. Theoretical calculations of several model compounds support such structural features as follows.[1] When the double-bond systems, $R_2E{=}ER_2$, are homolytically cleaved, the resulting two R_2E: units may exist in a triplet or a singlet state. In contrast to the carbon system, the heavier group 14 atoms have low ability to form hybrid orbitals, therefore, they prefer ns^2np^2 valence electronic configuration in their divalent species. Since two electrons remain to be as a singlet pair in the *n*s orbital, the ground state of R_2E: is singlet, unlike the case of R_2C:, the ground state of which is triplet.[2] As a result, severe repulsion between the closed-shell orbitals of two R_2E: units prevents the dimerization between themselves, which lead to the formation of $R_2E{=}ER_2$ in the planar form as shown in Figure 2-1. However, the two R_2E: units can form unique double bonds not only elongated to avoid the repulsion but also in *trans*-bent configuration,[3] where each of R_2E: units donates a lone pair of electrons to an empty p orbital of its bonding partner to form double donor-accepter bonds as shown in Figure 2-1.

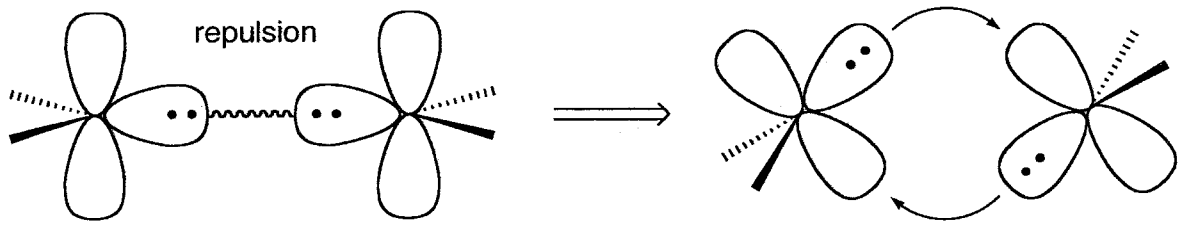

Figure 2-1.

By contrast, in cases of metallenes, their bonding situations are considered to be different from those of dimetallenes because metallenes are formed by the combination of a carbon, which prefers sp^2 hybridization, with a heavier group 14 element, which prefers ns^2np^2 valence electronic configuration. One can hit upon a natural question what types of the geometry metallenes have, *e.g.*, *trans*-bent, or the other form.

2.1.2 Stable Silenes (>Si=C<)

Silenes have been extensively investigated, although only a few stable examples **1**-**6**[4] have been isolated and characterized. Although the X-ray diffraction data of **3** and **4** have not been reported, the silenes **1**, **2**, **5**, and **6** have been reported to show their almost planar geometry around the Si=C bonds and shorter the Si=C bond lengths [1.702(5) (**2**)-1.764(3) (**1**) Å] than the typical Si–C single-bond lengths (ca. 1.87-1.93 Å). Although the ^{29}Si NMR signals of **1**-**5** were observed in the lower field [41.8 (**1**)-144.2 (**2**) ppm] characteristic for the doubly bonded Si atom as compared with those of sp^3 Si atoms, that of **6** was observed in –77.9 ppm, indicating the reversed bond polarity ($Si^{\delta-}=C^{\delta+}$).

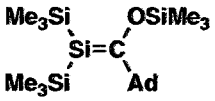

1
Brook (1981)

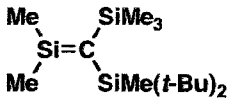

2
Wiberg (1985)

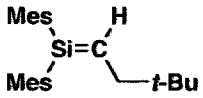

3
Couret (1994)

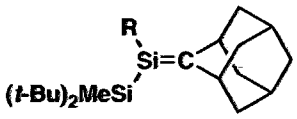

4: R = $SiMe_3$
5: R = $SiMe_2t$-Bu)$_2$
Apeloig (1996)

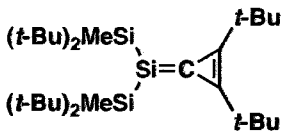

6
Kira (2002)

Allenic compounds involving a Si=C double bond, *i.e.* 1-silaallenes (Si=C=C, **7**-**10**)[5], have been synthesized and characterized by West. The lengths of the Si=C double bonds in **7** and **8** [1.704 and 1.693(3) Å, respectively] are quite short and that of **8** is the shortest distance among those reported for an Si=C double bond to date. The ^{29}Si NMR signals of **7**-**10** were observed in relatively up-field region [13.1 (**8**)-55.1 (**9** and **10**) ppm], indicating the strongly reduced polarity of the Si=C double bond in 1-silaallenes compared to the silenes. Although 1-phospha-3-silaallene **11** (>Si=C=P–) was also synthesized, it underwent ready dimerization above –30 °C.[6]

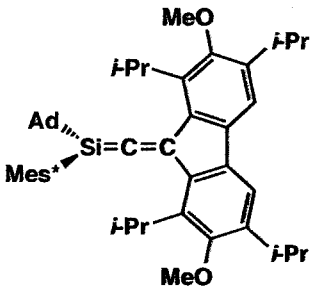

7
West (1993)

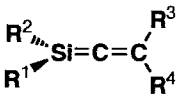

8: R^1 = R^2 = Tip, R^3 = Ph, R^4 = *t*-Bu
9: R^1 = Mes*, R^2 = *t*-Bu, R^3 = Ph, R^4 = *t*-Bu
10: R^1 = Mes*, R^2 = *t*-Bu, R^3 = R^4 = Ph

West (1997)

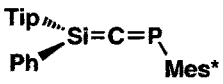

11
stable below –30 °C

Escudié (1999)

2.1.3 Stable Germenes (>Ge=C<)

Since the synthesis of the stable germenes **12**, **17**, and **18** were in 1987,[7] many examples bearing a variety of substituents have been reported.[8] X-Ray crystallographic analyses of **12**, **17**, **20**-**23** have been achieved, showing their almost planar geometries around the Ge=C bonds and

the shorter Ge=C bond [1.771(16) (**20**)-1.858(3) (**23**) Å] in comparison with the typical Ge–C single-bond lengths [1.95-2.00 Å] except **21**. In case of **21**, the Ge=C bond length was 2.085(3) Å, which was longer than the normal Ge–C single bond, and apparent pyramidalization of the Ge atom was observed. These results indicate that **21** actually exhibited the properties of the ylide structure (Ge^{-}–C^{+}) rather than the double bond between the Ge and C atoms due to the 2π-aromatic stabilization.

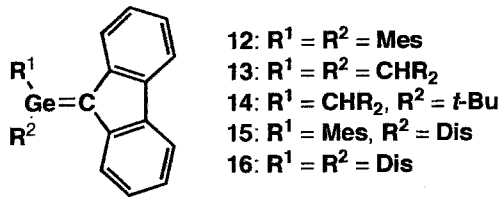

Escudié (1987-)

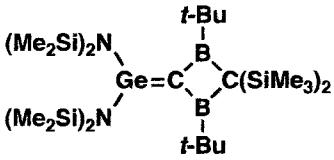

17
Bernt (1987)

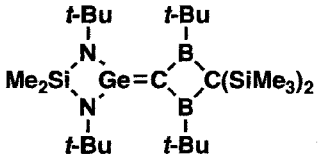

18
Bernt (1987)

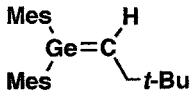

19
Escudié (1992)

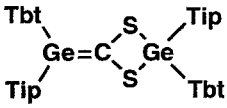

20
Tokitoh (1995)

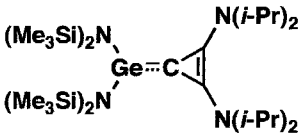

21
Schumann (1997)

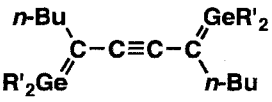

22
Weidenbruch (2000)

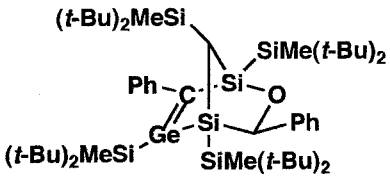

23
Sekiguchi (2002)

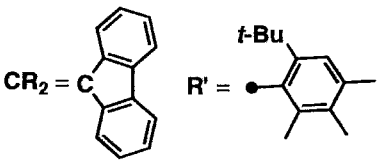

In addition, allenic compounds involving an Ge=C double bond, 1-phospha-3-germaallene (>Ge=C=P–) **24**,[9] 1-germaallenes (Ge=C=C, **25** and **26**)[10], have been synthesized and characterized. The length of the Ge=C double bonds in **25** [1.783(2) Å] is similar to the shortest Ge–C distance [1.771(16) Å in **20**]. Compound **25** show a bent structure at the central carbon atom with the Ge=C=C bond angle (159.2°) along with the pyramidalized Ge atom.

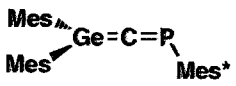

24
Escudié(1996)

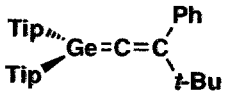

25
West (1998)

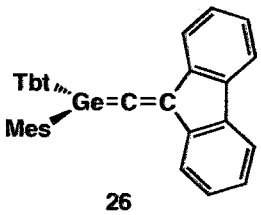

26
Tokitoh (1998)

2.1.4 Stable Stannenes

As described in Section 1.2.1.1, stable stannenes bearing a short tin–carbon bond are limited to the diboryl-substituted ones **27**-**29** reported by Berndt. However, their X-ray crystallographic analysis showed that the environments around the Sn=C bond and the ^{119}Sn NMR signals substantially differ from each other. Although **27** and **29** show the bending structures in the geometry of the substituents (except the Sn atom in **27**), the tin and carbon atoms in **28** have planar environments (Figure 2-2). The ^{119}Sn NMR signals of them are observed at 835 (**27**) and 374 (**28**) ppm.

These compounds are stabilized by not only the steric protection afforded by bulky substituents but also the electronic perturbation. In fact, the shortening of C1–B bond lengths in comparison with typical C–B single bond lengths were observed, indicating the contribution of canonical structures **30** and **30'** (Scheme 2-1).

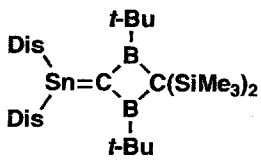

27

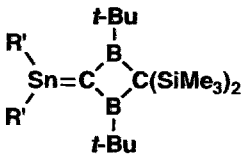

28

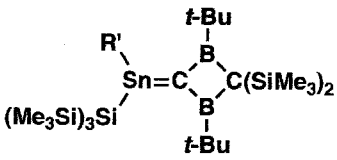

29

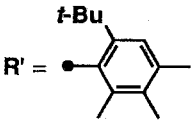

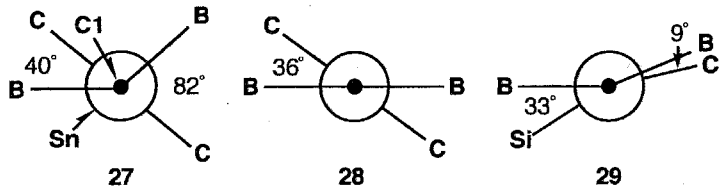

Figure 2-2. Stereo Projections along C1=Sn Bond of **27-29**.

Scheme 2-1.

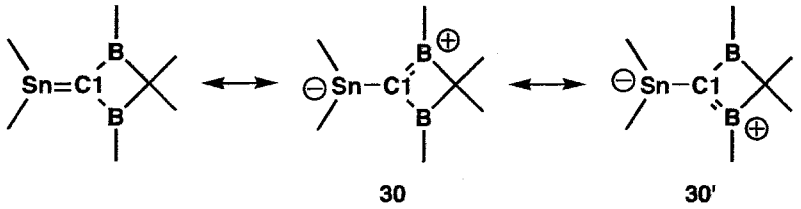

2.2 The Purpose in Chapter 2

The only stable systems, Berndt's stannenes, are inadequate to elucidate the nature of an Sn=C double bond due to the severe electronic perturbation to the central Sn=C moiety. In order to study the chemical behaviour of tin–carbon double bond in detail, the author examined the syntheses of stannenes kinetically stabilized by only carbon substituents, which have less electronic effect than heteroatom substituents.

Although the stannene **31** bearing only carbon substituent was reported by Escudié in 1992, it was known to undergo ready dimerization at room temperature in spite of bearing two Tip groups on the tin atom and **31** was not structurally characterized (Scheme 2-2).

Scheme 2-2.

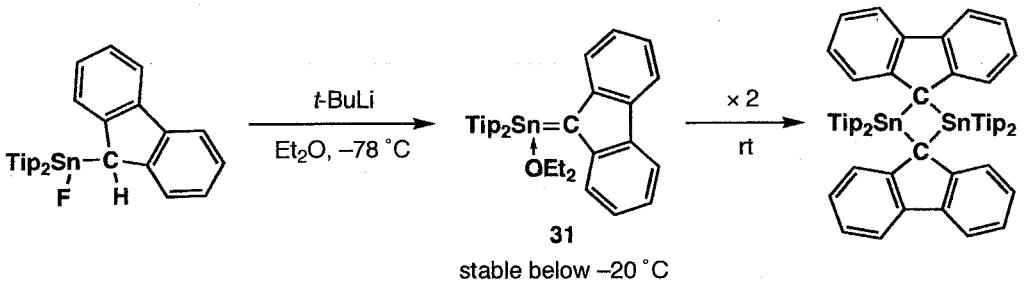

The author believed that the synthesis of stannenes stable at ambient temperature would be accessible by using a Tbt group, which is bulkier than a Tip group and a more effective substituent as a steric protection group. Therefore, the synthesis, structures, and reactivities of stannenes **32** and **33** were investigated in the Chapter 2 in this doctor thesis.

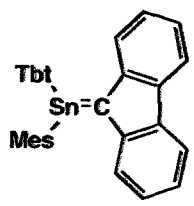

32

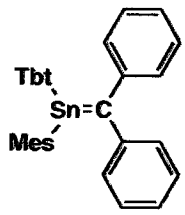

33

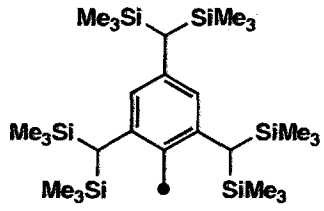

Tbt Group

2.3 Syntheses of the Precursors for 32 and 33

In the light of the reported synthetic method for stannene **31**, the author planned the synthetic strategies for **32** and **33** as shown in Scheme 2-3, *i.e.* the elimination of HX (X = leaving group) from the corresponding halostannanes **34** and **35**, respectively, using an appropriate base.

Scheme 2-3.

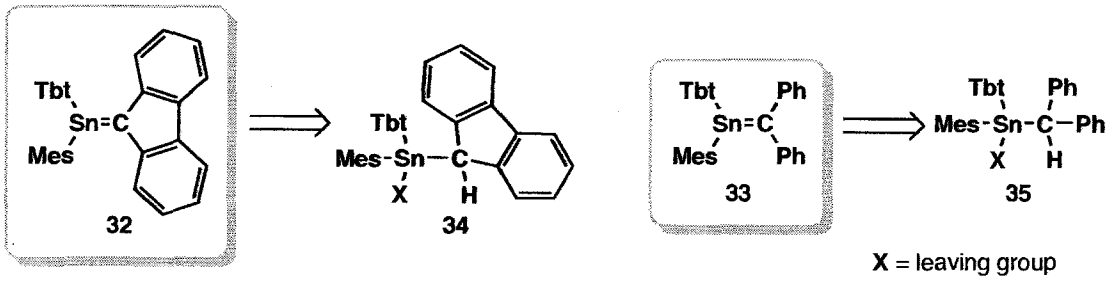

The combination of Tbt and Mes groups was selected as steric protection groups, since the synthesis of Tbt- and Mes-substituted dichlorostannane **36** has already been established as a high-yield process.[11]

Starting from **36**, suitable precursors for **32**, such as chlorostannane **37**, stannanyl triflate **38**, and fluorostannane **39**, were prepared according to Scheme 2-4.

Scheme 2-4.

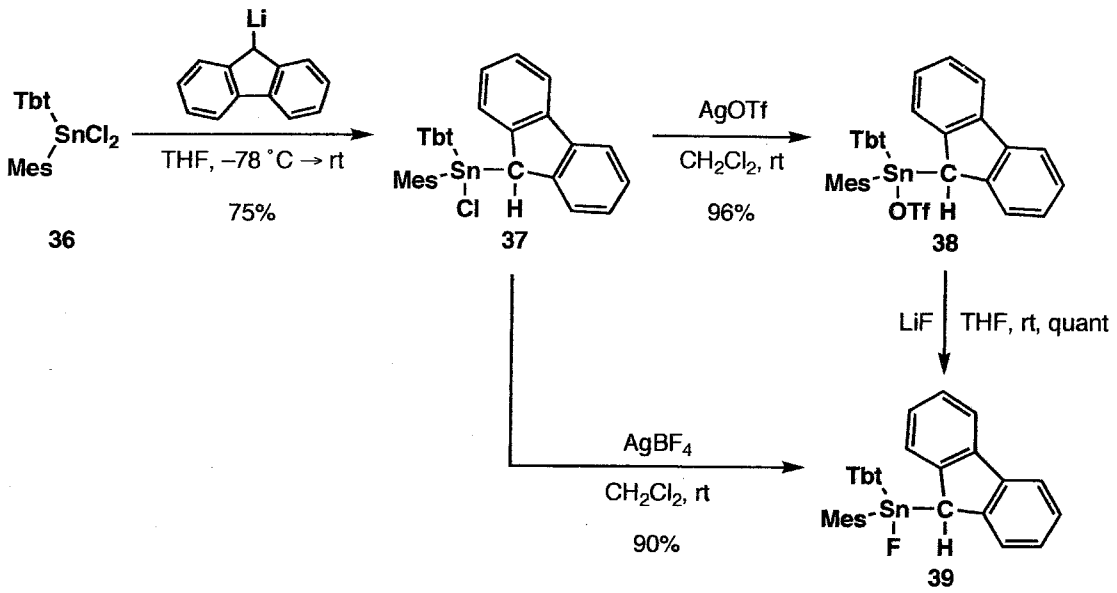

In a similar manner, chlorostannane **42** and fluorostannane **43**, which were expected to be suitable precursors for **33**, were prepared according to Scheme 2-5. Diphenylmethyllithium–THF complex **41** was isolated as orange solid and stable under inert atmosphere.

Scheme 2-5.

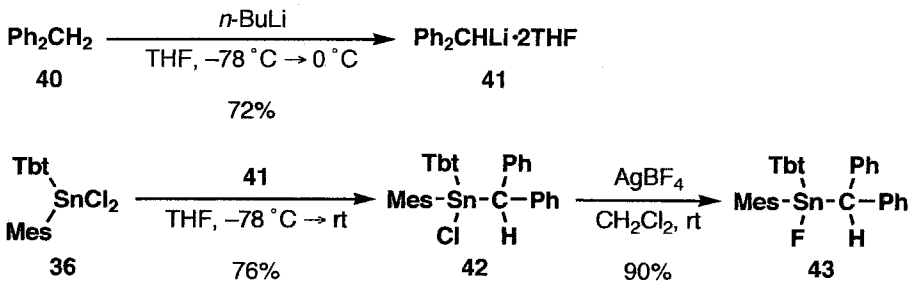

2.4 Synthesis of Stannene 32

2.4.1. Attempted Synthesis of 32 Using Chlorostannane 37 as a Precursor

Initially, synthesis of **32** using chlorostannane **37** as a precursor was attempted. The reaction of **37** with *n*-butyllithium in hexane resulted in the nucleophilic substitution reaction on the tin atom (Scheme 2-6).

Scheme 2-6.

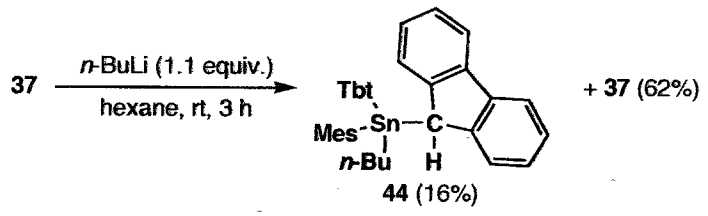

The reaction of **37** with *t*-butyllithium in diethylether at –40 °C, which was examined in order to prevent such nucleophilic substitution reaction, afforded compound X as an orange solid (Scheme 2-7). When the C_6D_6 solution of compound X was exposed to the air and moisture, no hydroxystannane **47**, which should be expected to be obtained by the hydrolysis of the stannene **32**, was observed but quantitative formation of hydrostannane **45** occurred. This result suggested that compound X should not be the expected stannene **32** but hydrostannylbenzyllithium **49** (Scheme 2-8). Indeed, the trapping reaction of compound X using MeI resulted in the formation of the methylfluorenylstannane **46** (19%) together with **45** (38%). The molecular structures of **45** and **46** were determined by X-ray crystallographic analysis (Figures 2-3, 2-4).

Scheme 2-7.

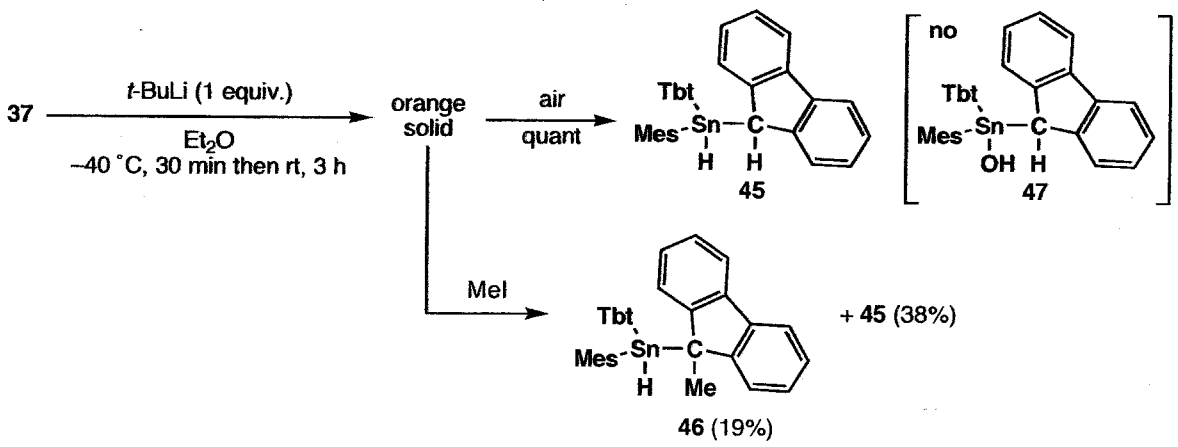

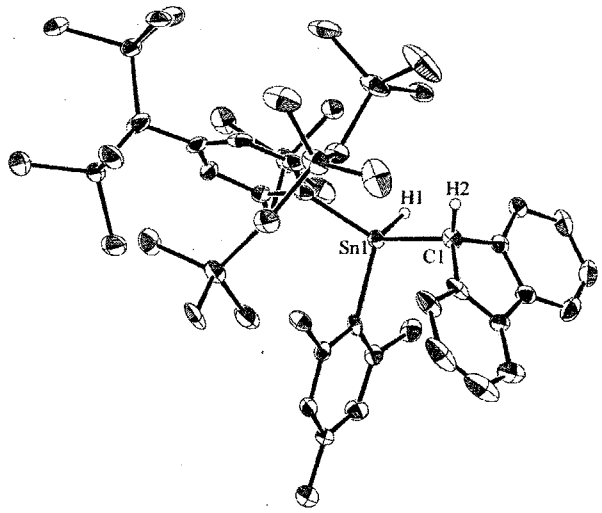

Figure 2-3. X-Ray structure of **45** (ORTEP drawing with 30% probability level). Hydrogen atoms except for those on the central Sn and C atoms were omitted for clarity.

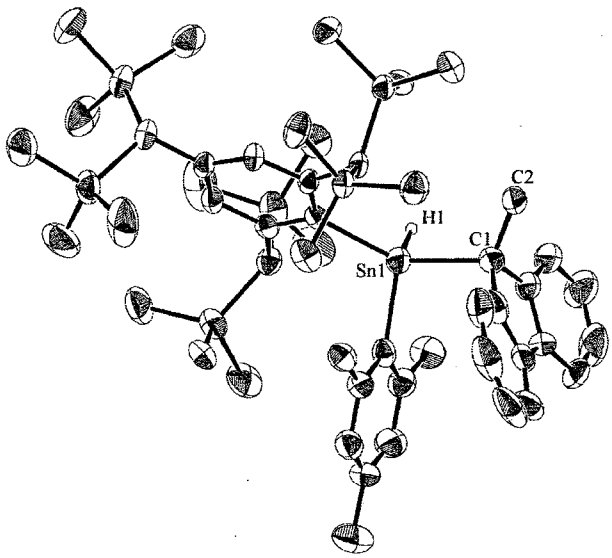

Figure 2-4. X-Ray structure of **46** (ORTEP drawing with 30% probability level). Hydrogen atoms except for that on the central Sn atom were omitted for clarity.

The plausible mechanism for the formation of **45** and **46** is shown in Scheme 2-8. Initially, single electron transfer reaction should proceed to afford stannyl radical **48**, and then the abstraction of a hydrogen atom from the solvent or the resulting compound, which might be

derived from *t*-butyl radical, should proceed to give **45**. The consequent reaction of **45** with *t*-butyllithium occurred to afford **49**.

Scheme 2-8. Mechanism for the reaction of **37** with *t*-BuLi

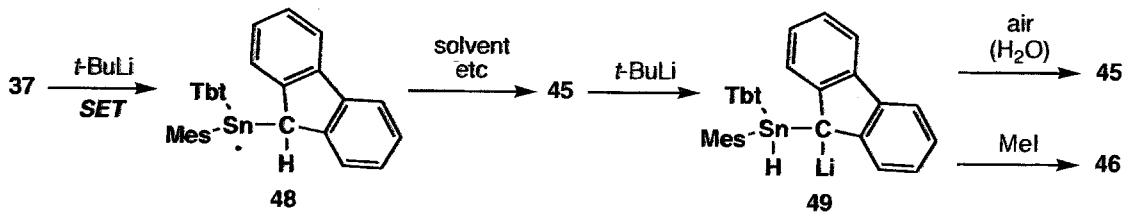

On the other hand, attempted dehydrochlorination reactions shown in Scheme 2-9 were performed under the conditions, resulted in "no-reaction" with the complete recovery of the starting material.

Scheme 2-9.

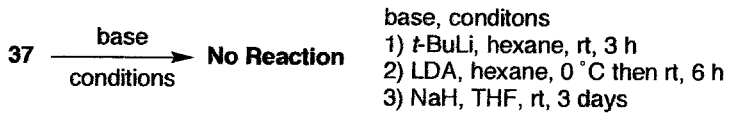

2.4.2. Attempted Synthesis of 32 Using Stannyl Triflate 38 as a Precursor

In the case of the synthesis of 9-silaanthracene **53**, the transformation of a leaving group from a halogen atom (Cl, Br) to a trifluoromethane sulfonyl (-OTf) group was quite effective: the treatment of silyl triflate **52** with LDA afforded **53** in a high yield in contrast to the low conversion in the case of the reactions of chlorosilane **50** or bromosilane **51** with LDA.[12]

Scheme 2-10.

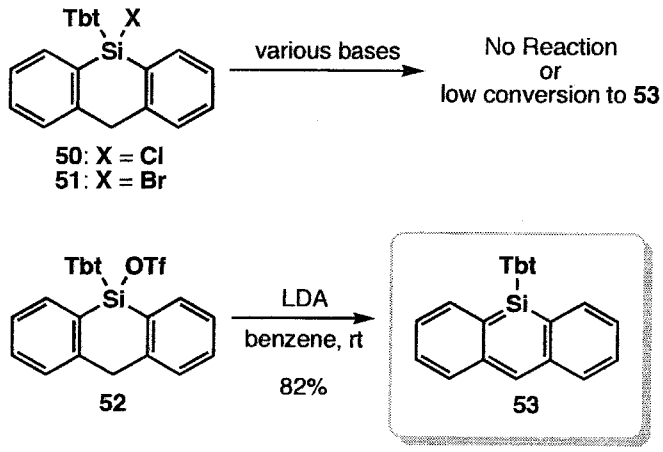

These previous knowledge on the high leaving ability of OTf group naturally prompted the author to examine the reaction of stannyl triflate **38** with a base in the hope of obtaining stannene **32**.

However, the reactions of **38** with lithium amides (LDA and LTMP) resulted in a complicated mixture (Scheme 2-11). Compounds **54**, **55**, and **56** were isolated as the final products in the reaction using LDA. The molecular structure of **54** was determined by X-ray crystallographic analysis (Figure 2-5). It can be concluded that those reactions should not be proper methods for **32**, though the generation of the **55** and **56** might be interpreted in terms of the intermediacy of the stannene **32** (Scheme 2-12, path a).

Scheme 2-11.

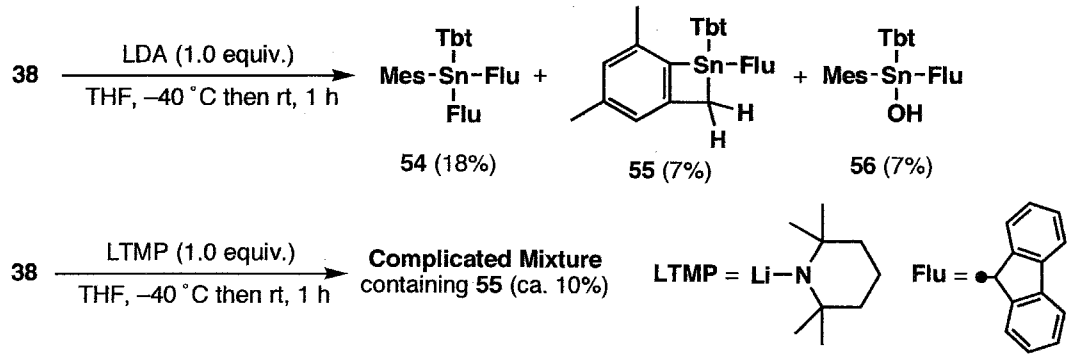

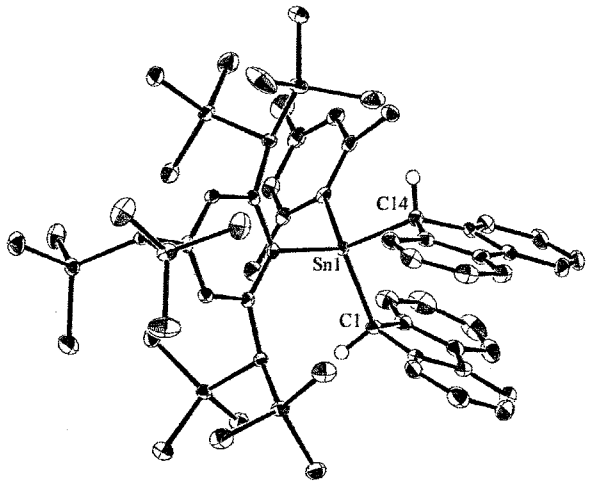

Figure 2-5. X-Ray structure of **54** (ORTEP drawing with 50% probability level). Hydrogen atoms except for that on the C1, C14 atoms and a benzene molecule were omitted for clarity.

Scheme 2-12. Plausible mechanism for the generation of **55** and **56**

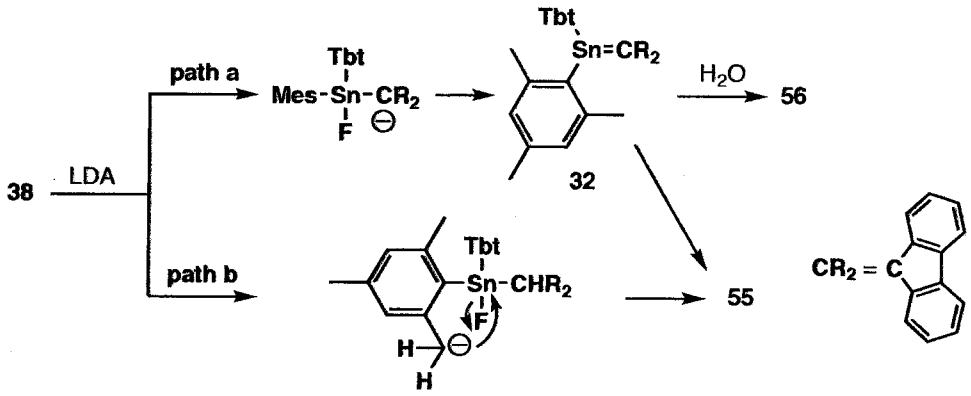

Although the mechanism for the formation of **54**, which has two fluorenyl substituents, is not clear at present, the same compound was obtained in the reaction of **38** with *n*-butyllithium (Scheme 2-13). Probably, the fluorenyl substituent works as a leaving group due to the high stability of the fluorenyl anion, judged by the generation of dibutylstannane **57**. The reaction of **38** with *t*-butyllithium resulted in the formation of **58** by the nucleophilic substitution.

Scheme 2-13.

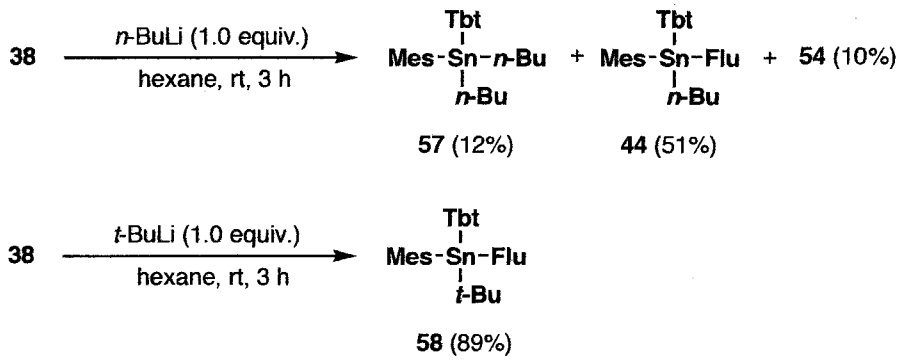

2.4.3. Synthesis of 32 Using Fluorostannane 39 as a Precursor

Finally, stannene **32** was successfully synthesized by the dehydrofluorination of **39** using *t*-butyllithium as a base in Et_2O at –40 °C (Scheme 2-14). Initially, the colour of the reaction mixture turned yellow solution, indicating the formation of the lithiated compound **59**, and then it turned deep violet at room temperature. Removal of LiF and the solvents afforded violet crystals of **32**, the ^1H and ^{13}C NMR spectra of which indicated no coordination of Et_2O in contrast with the case of **31**. Compound **32** was found to be thermally stable under inert atmosphere either in the solid state (mp 167-171 °C, dec.) or in solution (benzene-d_6, at 80 °C in a sealed tube) and highly moisture- and air-sensitive.

Scheme 2-14.

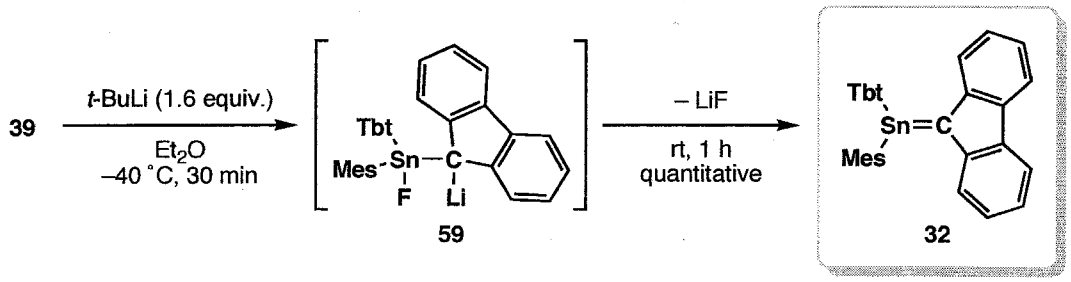

2.5 X-Ray Crystallographic Analysis of Stannene 32

The molecular geometry of **32** was determined by X-ray crystallographic analysis (Figures 2-6, 2-7). The structural parameters of **32** are summarized in Table 2-1 together with the calculated values for the model compounds **60-62** and the real molecule **32**. The bond length of the Sn–C1 bond [2.016(5) Å] is the shortest among those of tin–carbon bonds ever reported. In addition, it is ca. 6% shorter than the typical Sn–C single bond length (ca. 2.14 Å)[13] and close to the observed values for **27-29**. The structural analysis revealed the completely trigonal planar geometry around the Sn1 (359.9°) and C1 (359.9°) atoms. The large twisted angle between the C14-Sn1-C41 plane and the fluorenylidene moiety (28.5°) is probably due to the steric reason, since such twisted structures have already been observed in bifluorenylidene[14] (43°) and Mes_2Ge=C(fluorenylidene) (5.9°).[7a] Although the calculated parameters for **60-62** and **32** are almost similar to those observed for **32**, the twisted angle around the Sn=C unit of **60-62** (7.0-13.5°) is smaller than that of **32** probably due to the less bulkiness of the substituents on the tin atom.

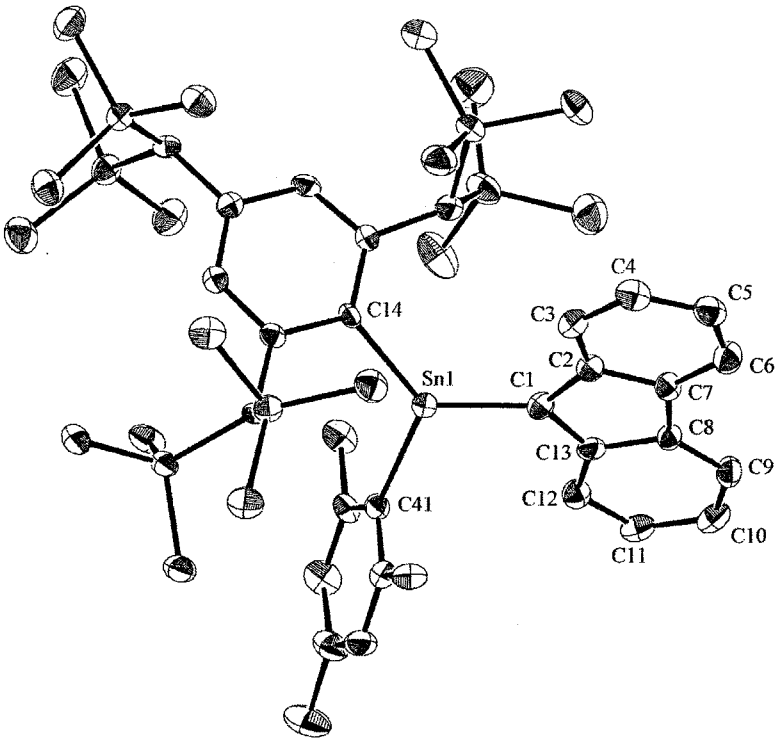

Figure 2-6. X-Ray structure of **32** (ORTEP drawing with 50% probability level). Hydrogen atoms were omitted for clarity.

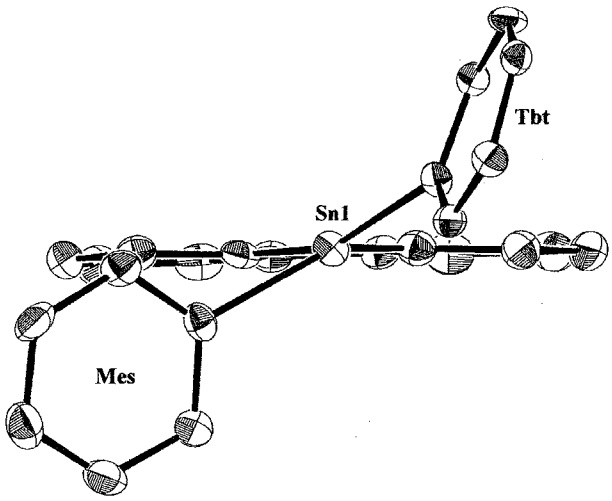

Figure 2-7. ORTEP drawing (50% probability level) of **32** along the Sn1–C1 Bond. Hydrogen atoms and the substituents on the Tbt and Mes groups were omitted for clarity.

Chart 2-1.

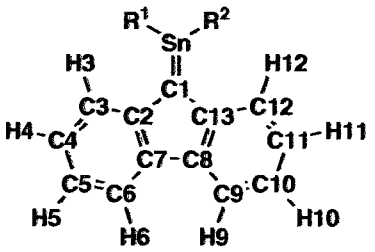

32: R^1 = Tbt, R^2 = Mes
60: R^1 = R^2 = Ph
61: R^1 = R^2 = Dmp
62: R^1 = Bbs, R^2 = Dmp

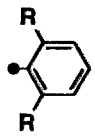

Bbs: R = $CH(SiH_3)_2$
Dmp: R = Me

Table 2-1. Selected bond lengths (Å) and angles (deg) of stannenes

	32 (obsd)	**60** (calcd)[a]	**61** (calcd)[a]	**62** (calcd)[a]	**32** (calcd)[a]
Sn–C1	2.016(5)	1.998	1.997	2.001	2.012
C1–C2	1.452(6)	1.465	1.464	1.463	1.459
C1–C13	1.456(6)	1.465	1.464	1.466	1.469
C2–C7	1.410(6)	1.426	1.427	1.427	1.428
C8–C13	1.425(6)	1.426	1.427	1.427	1.429
C7–C8	1.446(6)	1.457	1.458	1.458	1.454
R^1_{ipso}–Sn–R^2_{ipso}	118.27(17)	110.15	114.18	114.99	115.34
C1–Sn–R^1_{ipso}	127.92(19)	124.92	122.91	124.31	130.73
C1–Sn–R^2_{ipso}	113.67(19)	124.92	122.91	120.59	113.79
C2–C1–C13	106.3(4)	106.19	106.10	106.04	105.80
C2–C1–Sn	128.3(4)	126.93	126.95	127.60	129.15
C13–C1–Sn	125.3(3)	126.93	126.95	126.35	125.04
twisted angle[b]	28.5	13.1	7.0	13.5	24.1

[a] calculated at the B3LYP/6-31G(d) (TZV on Sn) level. [b] Twisted angles between the Sn–R^1_{ipso}–R^2_{ipso}–C1 and Sn–C1–C2–C13 planes.

2.6 Raman Spectra of Stannene 32

In-plane vibration modes for the 6-stannapentafulvene skeleton of **32** were observed by the Raman spectra. A part of the Raman spectrum of **32** was shown in Figure 2-8. The signals at 287 and 674 cm^{-1} were assigned to the skeletal vibrations on the 6-stannapentafulvene plane based on the theoretical calculations. The experimentally observed spectrum showed close

resemblance with the simulated spectrum for **60** as shown in Figure 2-8, indicating that the calculated structure for **60** reproduces the characters of **32** adequately.

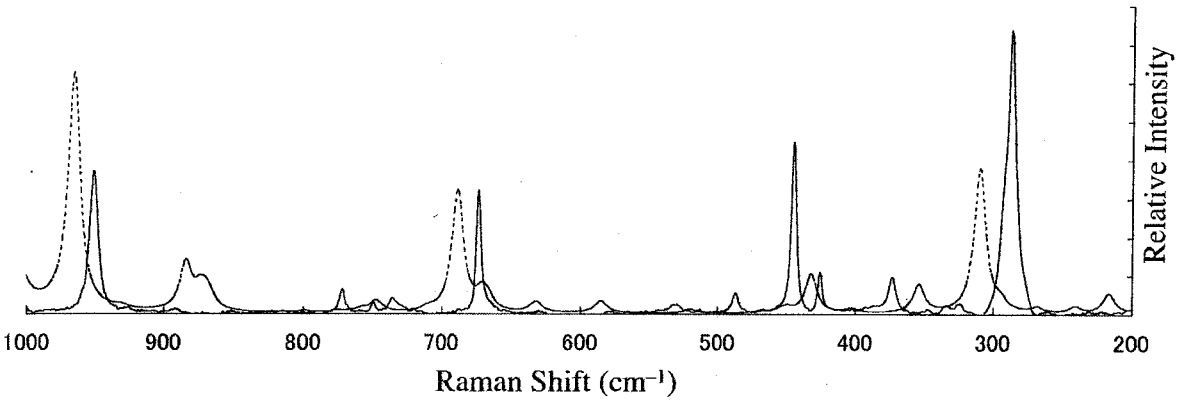

Figure 2-8. Raman spectra of 6-stannapentafulvenes. Solid line: FT-Raman spectrum of **32** measured with the excitation by He-Ne laser (833 nm). Dashed line: Spectrum of **60** simulated by the theoretical calculation at the B3LYP/6-31G(d) [TZ(2d) on Sn] level.

2.7 NMR Spectra of Stannene 32

The ^{119}Sn NMR spectrum of **32** in C_6D_6 showed a signal at 270 ppm, which is characteristic of doubly bonded tin derivatives. This value is slightly upfield-shifted in comparison to that of **31** (288 ppm). The assignments of the ^{1}H, ^{13}C, and ^{119}Sn NMR signals are listed in Table 2-2 along with the calculated values for **60**-**62** and the real molecule **32**. The observed values are in good agreement with the calculated ones except for the case of ^{119}Sn NMR at B3LYP level. At MPW1PW91 level, which was evidenced to be effective for the GIAO calculations for Tip_3Sn^+,[15] the calculated values for **60** (b) and **32** are consistent with the observed ones for **32**. The ^{13}C NMR signal of the Sn=C (144.9 ppm) reasonably appeared in the sp^2 region. It is noteworthy that all the signals of the fluorenylidene unit were observed nonequivalent probably due to the restricted rotation of the Sn–C bond, indicating that doubly bonded structure **32** rather than **32'** (Scheme 2-15) might be dominant in solution.

Table 2-2. Observed and calculated ^{1}H, ^{13}C, and ^{119}Sn NMR chemical shifts (ppm) for stannenes

	32 (obsd)[a]	**60** (calcd)		**61** (calcd)		**62** (calcd)		**32** (calcd)[f]
		a[b]	b[c]	a[b]	b[d]	a[d]	b[e]	
Sn	270	185	259	150	193	167	160	238
H3	7.61	8.22	7.97	7.56	7.73	7.75	7.86	8.29
H12	7.78					7.65	7.73	7.51
H4	7.29	7.11	7.02	6.99	7.24	7.36	7.44	7.49
H11	7.06					7.13	7.23	7.03
H5	7.25	7.18	7.07	7.09	7.31	7.35	7.45	7.48
H10	7.15					7.27	7.37	7.25
H6	7.91	7.94	7.70	7.98	8.00	8.03	8.14	8.30
H9	7.89					8.02	8.13	8.08
C1	144.91	141.16	137.23	146.88	150.60	154.76	150.45	142.42
C2	145.04	147.11	138.76	147.64	151.70	151.02	149.35	148.19
C13	146.39					151.14	149.45	151.48
C3	119.78	120.18	115.27	120.79	125.18	126.20	125.71	127.32
C12	120.18					124.20	123.80	124.62
C4	124.13	120.49	120.06	125.49	129.77	131.33	130.87	128.61
C11	120.59					130.07	129.71	129.75
C5	125.23	125.44	119.06	124.70	127.89	128.97	128.43	126.46
C10	126.64					128.73	128.20	126.60
C6	122.84	125.13	114.90	120.34	123.93	124.38	124.31	124.56
C9	122.99					124.55	124.45	123.33
C7	134.24	136.87	128.88	137.31	141.07	140.65	139.31	139.08
C8	134.40					140.52	139.11	138.68

[a] Measured in benzene-d_6. [b] Calculated at the GIAO-B3LYP/6-311+G(2d,p) (TZV on Sn)//B3LYP/6-31G(d) (LANL2DZ on Sn) level. [c] Calculated at the GIAO-MPW1PW91/6-31G(d) (TZV on Sn)//B3LYP/6-31G(d) (LANL2DZ on Sn) level. [d] Calculated at the GIAO-B3LYP/6-311++G(2d,p) (TZV on Sn)//B3LYP/6-31G(d) (LANL2DZ on Sn) level. [e] Calculated at the GIAO-MPW1PW91/6-311++G(d) (TZV on Sn)//B3LYP/6-31G(d) (LANL2DZ on Sn) level. [f] Calculated at the GIAO-MPW1PW91/6-311+G(d) (TZV on Sn)//B3LYP/6-31G(d) (LANL2DZ on Sn) level.

Scheme 2-15.

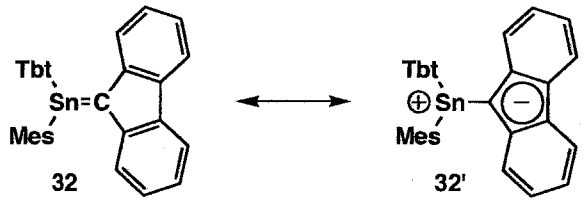

2.8 UV/vis Spectra of Stannene 32

In Figure 2-9 are shown the UV/vis spectrum of stannene **32** in hexane at room temperature. The spectrum showed absorption maximum at 552 nm (ε, 1×10^4), which is slightly red-shifted compared to diethylether-coordinated stannene **31** (542 nm).

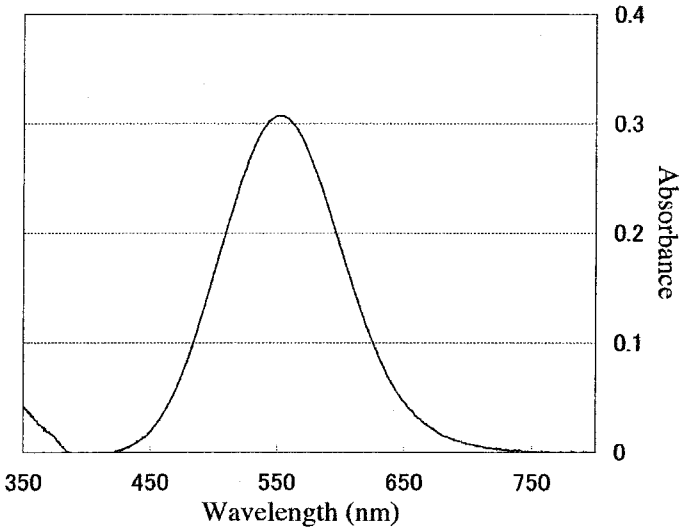

Figure 2-9. UV/vis spectrum of **32** (in hexane, rt).

2.9 Reactivity of Stannene 32

2.9.1 Reaction with Water

The reaction of **32** with water in THF at room temperature afforded the corresponding adduct, hydroxystannane **56**, in 76% yield (Scheme 2-16).

Scheme 2-16.

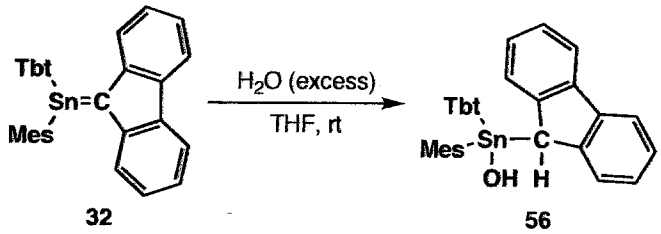

2.9.2 Reaction with 2,3-Dimethyl-1,3-butadiene

Stannene **32** reacts with 2,3-dimethyl-1,3-butadiene at room temperature to afford the [2 + 4] cycloadduct **63** in 51% yield (Scheme 2-17), suggesting that **32** has an Sn=C double-bond character rather than an ionic character (**32'**, Scheme 2-16) from the viewpoints of the chemical reactivity. The molecular structure of **63** was determined by X-ray crystallographic analysis (Figure 2-10).

Scheme 2-17.

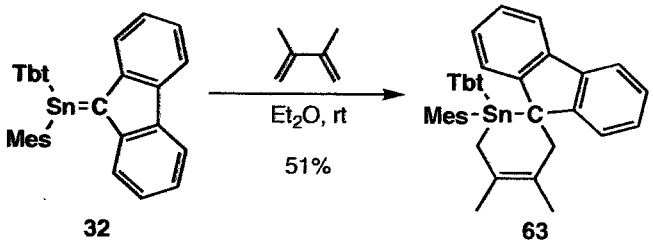

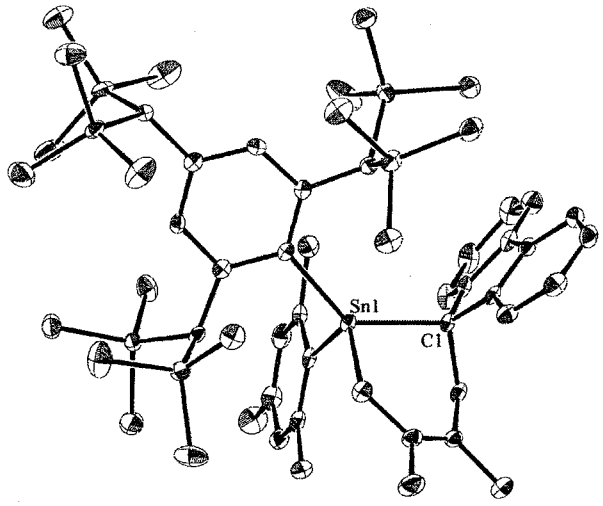

Figure 2-10. X-Ray structure of **63** (ORTEP drawing with 50% probability level). Hydrogen atoms and a benzene molecule were omitted for clarity.

2.9.3 Reaction with Elemental Sulfur

Tbt-substituted sila- and germaaromatics, which have a formal E=C double-bond (E = Si, Ge, respectively), and 1-germaallene **26** were known to react with elemental sulfur giving various cyclic polysulfides. A series of examples containing a Ge atom are shown in Scheme 2-18.

Scheme 2-18.

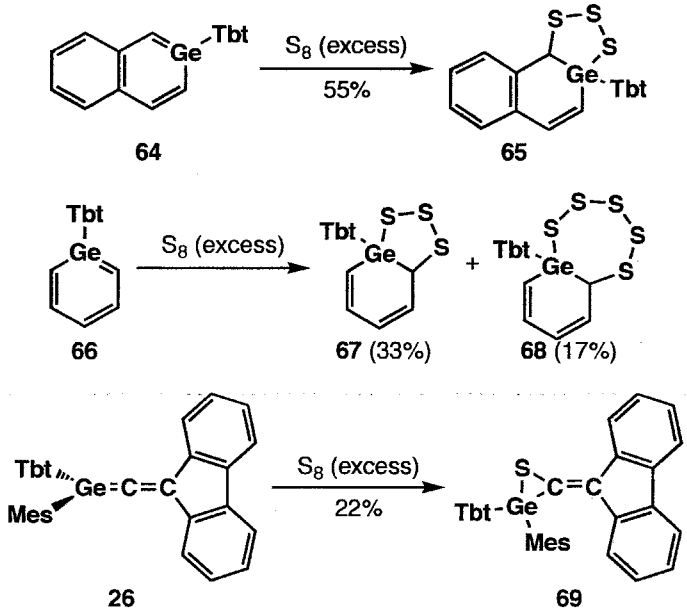

However, the reaction of **32** with elemental sulfur afforded only a complicated mixture containing tetrathiastannolane **70**[16] (22%, Scheme 2-19).

Scheme 2-19.

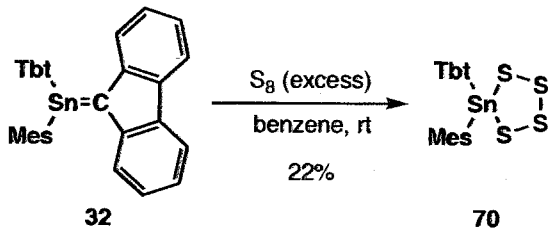

2.9.4 Reaction with *t*-BuLi

The reaction of the stable germene **12** with *t*-butyllithium followed by quenching with methanol was reported to give the hydrogermane **73**. This reaction is explained by a single-electron transfer mechanism via the intermediacy of **71** and **72** (Scheme 2-20).

Scheme 2-20.

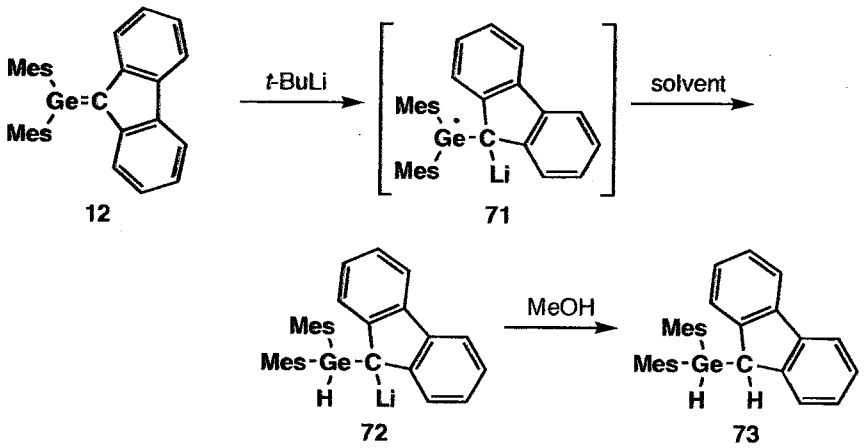

The reaction of stannene **32** with *t*-butyllithium proceeded in a similar way to afford 9-methylfluorenylstannane **46** by quenching with iodomethane in ca. 80% conversion (Scheme 2-21). Compound **46** gradually decomposed during the purification process.

Scheme 2-21.

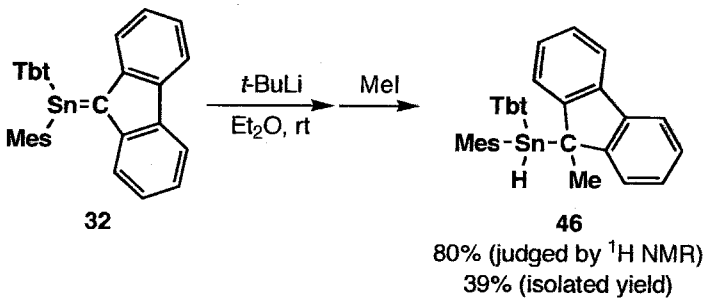

2.9.5 Reaction with Isonitrile

The synthesis of heavier element analogues of cyclopropanes **74-76** has been a great challenge for the last few years. Silicon and germanium heterocycles **74(ab)**, **75(ab)**, and **76(ab)** have been reported.[17] Going down the periodic table, the three-membered heterocycles become more and more unstable due to the large differences between the energies of *n*p and *n*s orbitals. Thus, in the case of tin, all efforts to prepare **74c**[18] have been unsuccessful so far, while the tin-version of **75c**[19] and **76c**[20] have already been synthesized.

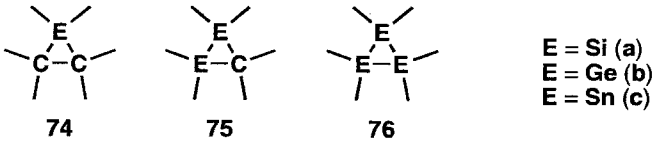

Disilene **77** is known to react with isonitrile **78**, which can work as a carbene, to give disiliranes **79** (Scheme 2-22).[21] A stannene is also considerable to be a synton of stannirane **74c** in the reaction with isonitrile.

Scheme 2-22.

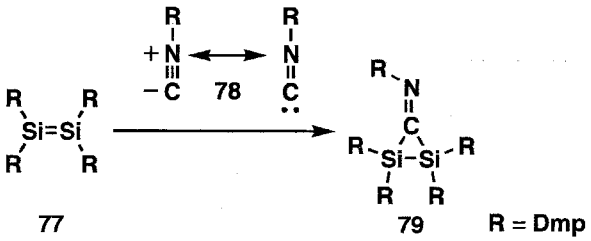

The reaction of **32** with mesityl isocyanide was performed to afford **80** and **81**, and compounds containing a Tbt group were obtained as a complicated mixture (Scheme 2-23). The molecular structure of **80** was confirmed by X-ray crystallographic analysis (Figure 2-11).

Scheme 2-23.

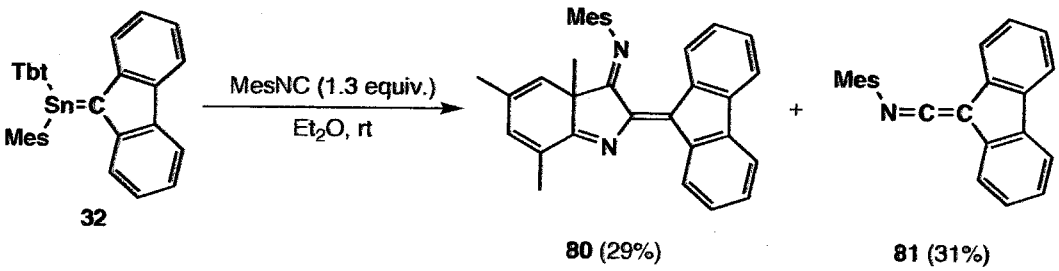

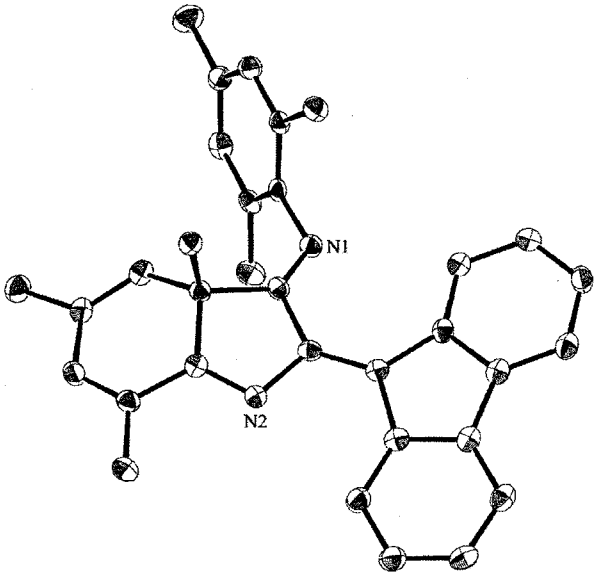

Figure 2-11. X-Ray structure of **80** (ORTEP drawing with 50% probability level). Hydrogen atoms were omitted for clarity.

The generation of **80** and **81** should be most likely interpreted in terms of the intermediacy of stannirane **82** (Scheme 2-24). Due to the highly stained skeleton of **82**, the bond cleavage should occur to generate stannylene **83** and ketenimine **81**. Stannylene **83** should decompose to give a complicated mixture and **81** reacted with misityl isocyanide once again with the [4+1] cycloaddition fashion to afford the final product **80**.

Scheme 2-24.

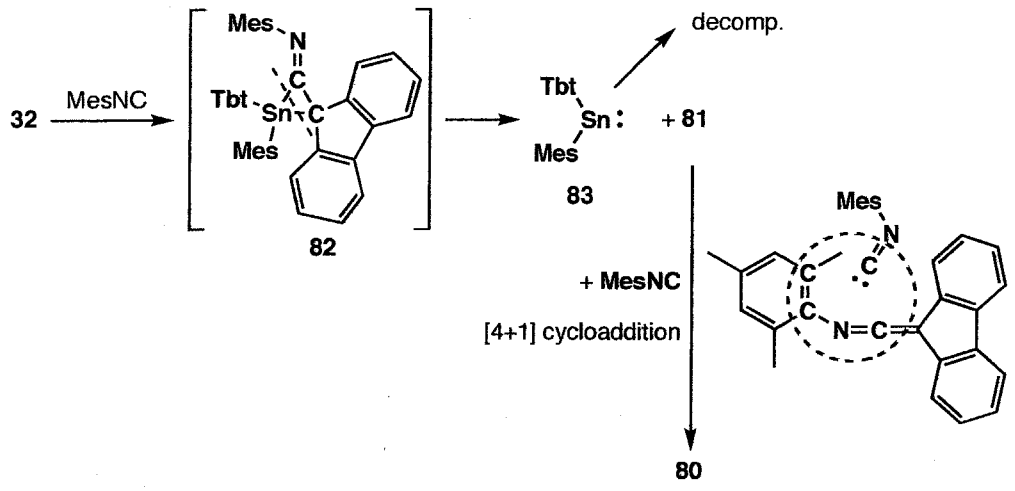

2.9.6 Reaction with 2,4,6-Tri(*t*-butyl)benzonitrile Oxide

2,4,6-Tri(*t*-butyl)benzonitrile oxide reacted with **32** as a 1,3-dipolar reagent at room temperature to give the [2 + 3] cycloadduct **84** in 24% yield (Scheme 2-25). However, adduct **84** underwent gradual decomposition under air to afford **85**. The molecular structure of **85** was determined by X-ray crystallographic analysis (Figure 2-12).

Scheme 2-25.

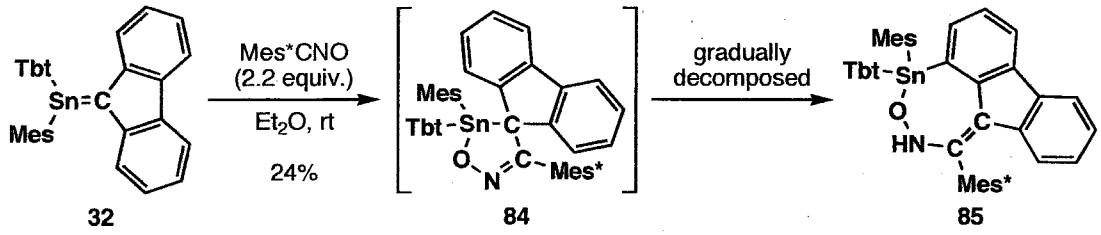

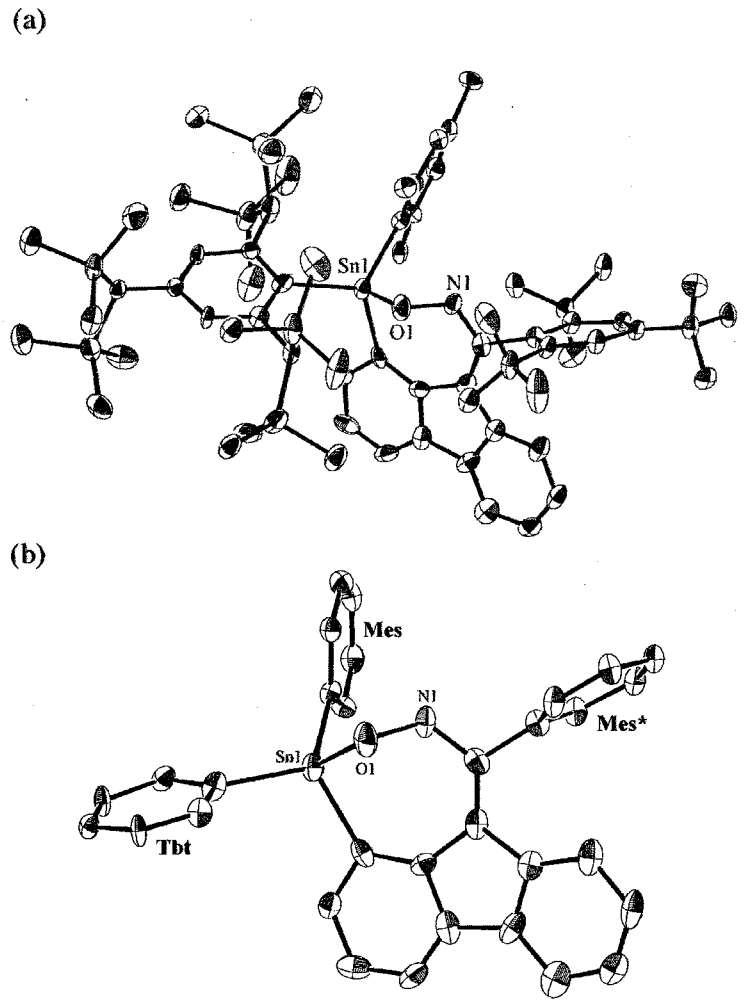

Figure 2-12. X-Ray structure of **85** (ORTEP drawing with 50% probability level). (a) Hydrogen atoms and a chloroform molecule were omitted for clarity. (b) Hydrogen atoms, a chloroform molecule, and the substituents on Tbt, Mes, and Mes* groups were omitted for clarity.

The isomerization from **84** to **85** was explained as described in Scheme 2-26. Probably, protonation on the nitrogen atom was the initial step.

Scheme 2-26.

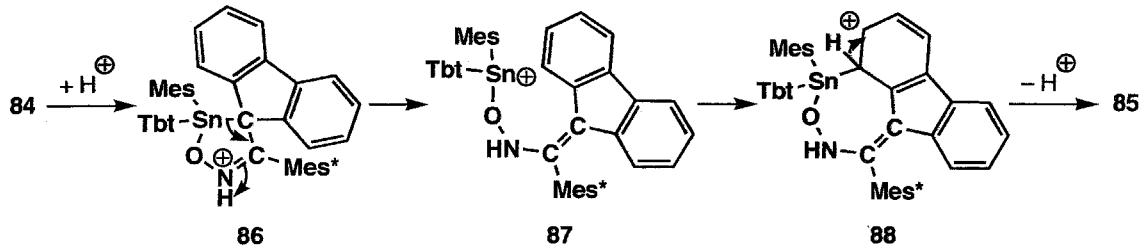

2.10 Attempted Synthesis of Stannene 33

The successful results in the 6-stannapentafulvene systems **32** naturally prompted the author to extend this chemistry to diphenyl-substituted stannene **33**.

However, the reactions of chlorostannane **42** or fluorostannane **43** with *t*-butyllithium did not afford the expected stannene **33** (Scheme 2-27). In the case of using fluorostannane **43** as a precursor, stannabutabenzene **89** and hydrostannane **90** were obtained in low yields. The molecular structure of **89** was determined by X-ray crystallographic analysis (Figure 2-13).

Scheme 2-27.

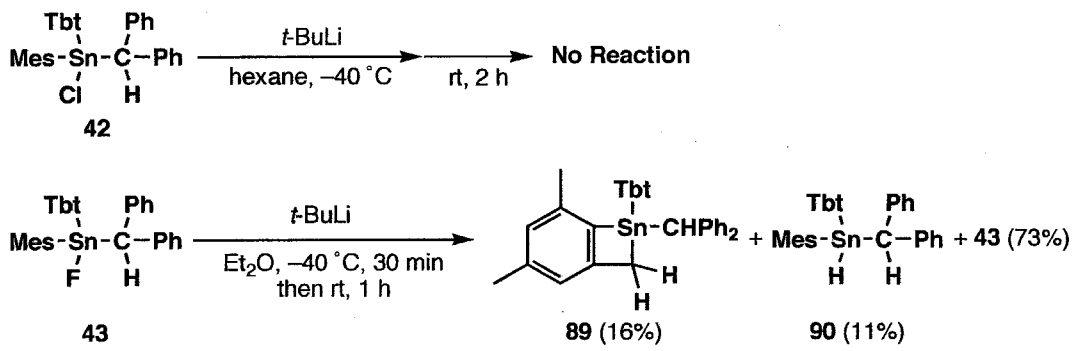

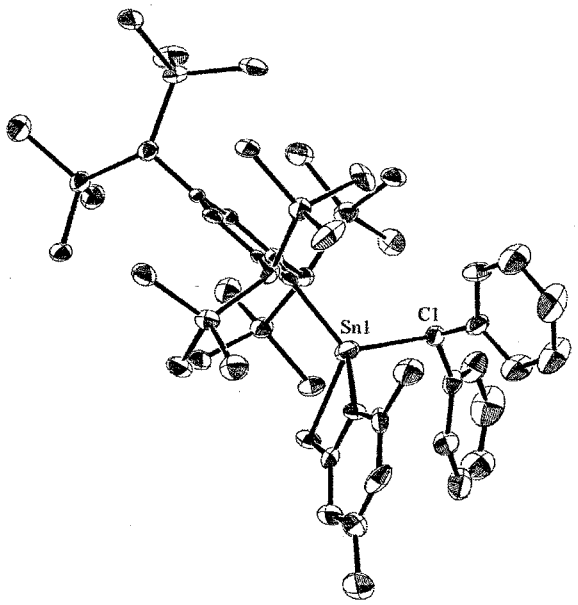

Figure 2-13. X-Ray structure of **89** (ORTEP drawing with 30% probability level). Hydrogen atoms were omitted for clarity.

Although compounds **89** and **90** might be formed *via* stannene **33** (Scheme 2-28, path a), the reaction mechanism should be ambiguous at present, since a similar reaction of **96** with *t*-butyllithium was reported by Weidenbruch, suggesting benzyllithium intermediate **97**.[22]

Scheme 2-28.

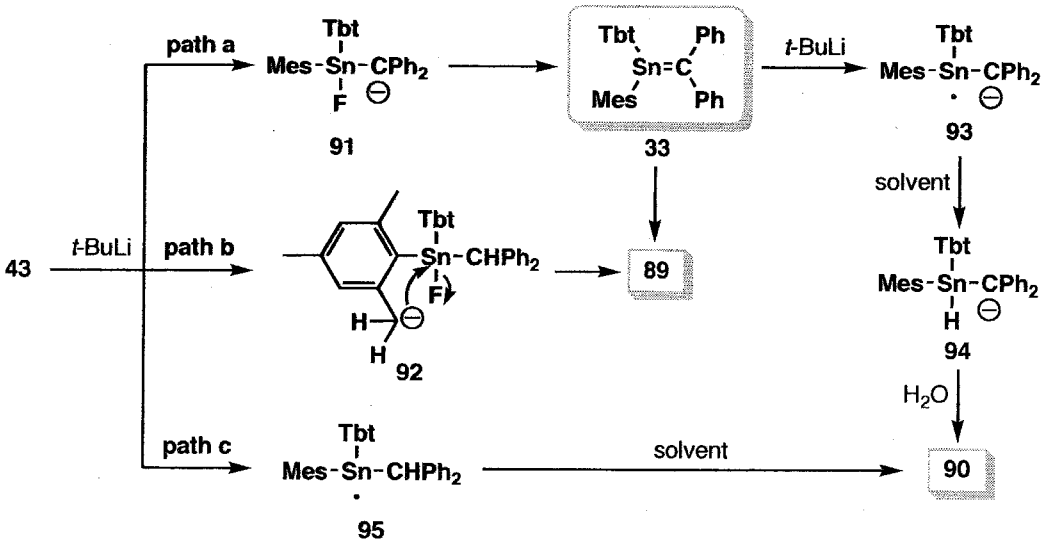

Scheme 2-29.

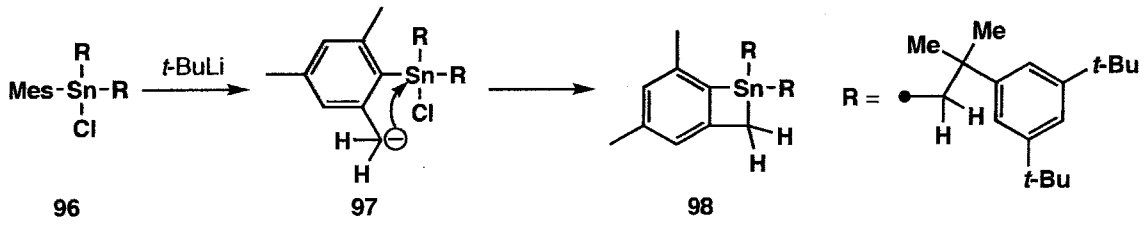

2.11 Conclusion

In summary, the author succeeded in the synthesis and X-ray crystallographic analysis of stannene **32** stable at ambient temperature for the first time. Judging from the NMR spectra, molecular structure, and reactivities, **32** has a sufficient Sn=C double-bond character. These results demonstrate a possibility of the forming π-bond between tin and carbon atoms, when it is kinetically well stabilized.

Table 2-3. Crystal data for compounds **45**, **46**, and [**54**·C_6H_6].

	45	**46**	[**54**·C_6H_6]
Empirical formula	$C_{49}H_{80}Si_6Sn$	$C_{50}H_{82}Si_6Sn$	$C_{62}H_{88}Si_6Sn{\cdot}C_6H_6$
Formula weight	956.36	970.39	1198.66
Temperature (K)	103(2)	203(2)	103(2)
Crystal color	colorless	colorless	colorless
Crystal dimensions	0.10 × 0.10 × 0.05	0.20 × 0.20 × 0.10	0.20 × 0.10 × 0.10
Crystal system	monoclinic	triclinic	monoclinic
Space group	$P2_1/a$ (#14)	$P\bar{1}$ (#2)	$P2_1/n$ (#14)
Lattice parameters			
a (Å)	22.7974(5)	13.0528(10)	12.325(5)
b (Å)	9.3195(2)	14.1037(10)	22.818(5)
c (Å)	26.1196(7)	17.1682(15)	23.880(5)
α (°)	90	68.190(4)	90
β (°)	105.2014(17)	73.214(3)	103.291(5)
γ (°)	90	75.586(4)	90
V (Å^3)	5355.2(2)	2773.4(4)	6536(3)
Z	4	2	4
D_{calc} (g·cm^{-3})	1.186	1.162	1.218
μ (mm^{-1})	0.641	0.620	0.539
θ range (°)	2.21 to 25.00	2.35 to 25.00	1.97 to 25.00
Independent reflections	8597	7970	11501
R_{int}	0.1060	0.0543	0.0262
Completeness to θ (%)	91.2	81.6	99.9
Restraints	0	0	0
No. of parameters	537	540	737
Goodness of fit	1.002	1.019	1.077
Final R indices [$I>2\sigma(I)$]	$R_1 = 0.0540$	$R_1 = 0.0707$	$R_1 = 0.0284$
	$wR_2 = 0.0938$	$wR_2 = 0.1517$	$wR_2 = 0.0622$
R indices (all data)	$R_1 = 0.0540$	$R_1 = 0.1537$	$R_1 = 0.0338$
	$wR_2 = 0.0938$	$wR_2 = 0.1961$	$wR_2 = 0.0655$
Largest diff. peak (e·Å^3)	0.757	1.453	0.595
Largest diff. hole (e·Å^3)	–1.047	–0.650	–0.222

Table 2-4. Crystal data for compounds **32**, [**63**·0.5C_6H_6], and **80**.

	32	[**63**·0.5C_6H_6]	**80**
Empirical formula	$C_{49}H_{78}Si_6Sn$	$C_{55}H_{88}Si_6Sn{\cdot}0.5C_6H_6$	$C_{33}H_{30}N_2$
Formula weight	953.34	1075.54	454.59
Temperature (K)	103(2)	103(2)	103(2)
Crystal color	purple	colorless	red
Crystal dimensions	0.20 × 0.20 × 0.20	0.20 × 0.20 × 0.10	0.20 × 0.20 × 0.05
Crystal system	monoclinic	triclinic	monoclinic
Space group	$C2/c$ (#15)	$P\bar{1}$ (#2)	$P2_1/n$ (#14)
Lattice parameters			
a (Å)	21.0447(6)	12.347(2)	10.274(3)
b (Å)	13.5070(5)	13.0052(18)	11.261(3)
c (Å)	38.1717(13)	20.418(4)	21.652(6)
α (°)	90	71.537(7)	90
β (°)	96.1949(12)	81.570(7)	102.608(4)
γ (°)	90	74.856(7)	90
V (Å^3)	10787.0(6)	2994.7(8)	6536(3)
Z	8	2	4
D_{calc} (g·cm^{-3})	1.175	1.193	1.235
μ (mm^{-1})	0.636	0.581	0.072
θ range (°)	3.02 to 25.00	2.29 to 25.00	2.43 to 25.00
Independent reflections	9441	10339	4290
R_{int}	0.0843	0.0250	0.0586
Completeness to θ (%)	99.6	97.8	99.7
Restraints	0	18	0
No. of parameters	526	667	322
Goodness of fit	1.001	1.068	1.106
Final R indices [$I>2\sigma(I)$]	$R_1 = 0.0488$	$R_1 = 0.0350$	$R_1 = 0.0622$
	$wR_2 = 0.0927$	$wR_2 = 0.0713$	$wR_2 = 0.1223$
R indices (all data)	$R_1 = 0.1027$	$R_1 = 0.0431$	$R_1 = 0.0917$
	$wR_2 = 0.1065$	$wR_2 = 0.0750$	$wR_2 = 0.1378$
Largest diff. peak (e·Å^3)	0.726	0.549	0.264
Largest diff. hole (e·Å^3)	–0.644	–0.384	–0.246

Table 2-5. Crystal data for compounds [**85**·$CHCl_3$] and **89**.

	[**85**·$CHCl_3$]	**89**
Empirical formula	$C_{68}H_{107}NOSi_6Sn{\cdot}CHCl_3$	$C_{49}H_{80}Si_6Sn$
Formula weight	1361.14	956.36
Temperature (K)	103(2)	103(2)
Crystal color	yellow	colorless
Crystal dimensions	0.20 × 0.20 × 0.10	0.30 × 0.20 × 0.05
Crystal system	triclinic	triclinic
Space group	$P\bar{1}$ (#2)	$P\bar{1}$ (#2)
Lattice parameters		
a (Å)	13.4321(9)	10.7365(15)
b (Å)	16.0559(16)	11.2638(11)
c (Å)	18.7404(16)	23.474(3)
α (°)	69.697(4)	92.252(4)
β (°)	78.716(3)	90.717(5)
γ (°)	83.316(3)	107.155(11)
V (Å^3)	3712.1(5)	2709.6(6)
Z	2	2
D_{calc} (g·cm^{-3})	1.218	1.172
μ (mm^{-1})	0.588	0.634
θ range (°)	2.29 to 25.00	2.86 to 25.00
Independent reflections	10024	7212
R_{int}	0.0880	0.0786
Completeness to θ (%)	76.6	75.4
Restraints	114	0
No. of parameters	797	525
Goodness of fit	1.136	1.002
Final R indices [I>2σ(I)]	R_1 = 0.0939	R_1 = 0.0797
	wR_2 = 0.1986	wR_2 = 0.1672
R indices (all data)	R_1 = 0.1938	R_1 = 0.1669
	wR_2 = 0.2521	wR_2 = 0.2046
Largest diff. peak (e·Å^3)	0.960	3.079
Largest diff. hole (e·Å^3)	–1.185	–0.955

Experimental Section

General procedure. All experiments were performed under an argon atmosphere unless otherwise noted. Solvents used for the reactions were purified by The Ultimate Solvent System (GlassContour Company).[23] ^{1}H NMR (300 MHz), ^{13}C NMR (76 MHz), and ^{119}Sn NMR (111 MHz) spectra were measured in $CDCl_3$ or C_6D_6 with a JEOL JNM-AL300 spectrometer. In ^{1}H NMR, signals due to $CHCl_3$ (7.25 ppm) and C_6D_5H (7.15 ppm) were used as references, and those due to $CDCl_3$ (77 ppm) and C_6D_6 (128 ppm) were used in ^{13}C NMR. ^{119}Sn NMR was measured with NNE technique using $SnMe_4$ as an external standard. Multiplicity of signals in ^{13}C NMR spectra was determined by DEPT technique. High-resolution mass spectral data were obtained on a JEOL JMS-SX102GC/MS spectrometer. WCC (wet column chromatography) was performed on Wakogel C-200. PTLC (preparative thin-layer chromatography) was performed with Merck Kieselgel 60 PF254 (Art. No. 7747). GPLC (gel permeation liquid chromatography) was performed on an LC-908 (Japan Analytical Industry Co., Ltd.) equipped with JAIGEL 1H and 2H columns (eluent: chloroform or toluene). All melting points were determined on a Yanaco micro melting point apparatus and were uncorrected. Elemental analyses were carried out at the Microanalytical Laboratory of the Institute for Chemical Research, Kyoto University. All theoretical calculations were carried out using the Gaussian 98 or 03 programs.[24,25]

Preparation of 37. To a THF (4 mL) solution of fluorene (102 mg, 0.614 mmol) was added *n*-butyllithium (1.5 M in hexane, 0.340 mL, 0.510 mmol) at –78 °C. After stirring at the same temperature for 1 h, THF (4 mL) solution of Tbt(Mes)$SnCl_2$ **36** (353 mg, 0.410 mmol) was added to the mixture. After stirring for 3 h at –78 °C, the reaction mixture was warmed to room temperature and stirred for 12 h at the same temperature. After removal of the solvent, hexane

was added to the residue. The resulting suspension was filtered through Celite®, and the solvent was removed. The residue was separated by GPLC ($CHCl_3$) to afford **37** (304 mg, 0.307 mmol, 75%). **37**: colorless crystals, mp 223-224 °C (dec.); ^{1}H NMR (300 MHz, C_6D_6, 25 °C): δ 0.02 (s, 9H), 0.17 (s, 18H), 0.21 (s, 9H), 0.24 (s, 18H), 1.56 (s, 1H), 1.86 (s, 3H), 2.00 (s, 6H), 2.48 (s, 1H), 2.91 (s, 1H), 5.21 (s, 1H), 6.46 (s, 2H), 6.69 (br s, 1H), 6.84 (br s, 1H), 7.03-7.22 (m, 5H), 7.66-7.70 (m, 2H), 8.64 (d, ^3J= 7.8 Hz, 1H); ^{13}C NMR (75 MHz, $CDCl_3$, 25 °C): δ 0.90 (q), 1.15 (q), 1.76 (q), 2.16 (q), 20.86 (q), 26.18 (q), 29.52 (d), 30.50 (d), 30.73 (d), 48.18 (d), 119.36 (d), 119.45 (d), 123.74 (d), 125.18 (d), 125.80 (d), 126.02 (d), 126.22 (d), 126.32 (d), 126.58 (d), 128.56 (d), 128.65 (d), 137.21 (s), 139.82 (s), 140.89 (s), 141.16 (s), 142.43 (s), 142.76 (s), 143.09 (s), 144.90 (s), 145.59 (s), 152.24 (s), 152.64 (s); ^{119}Sn NMR (111 MHz, $CDCl_3$, 25 °C): δ –35.2; Anal. Calcd for $C_{49}H_{79}ClSi_6Sn$: C, 59.40; H, 8.04. Found: C, 59.16; H, 8.06.

Preparation of 38. A CH_2Cl_2 (3 mL) solution of **37** (109 mg, 0.110 mmol) and AgOTf (40.4 mg, 0.157 mmol) was stirred for 3 h at room temperature. After removal of the solvent, the reaction mixture was taken into a glovebox filled with argon. Hexane was added to the residue and the resulting suspension was filtered through Celite®. The solvent was removed to afford **38** (115 mg, 0.104 mmol, 95%). **38**: colorless crystals, ^{1}H NMR (300 MHz, C_6D_6, 70 °C): δ 0.03 (s, 18H), 0.16 (s, 18H), 0.23 (s, 18H), 1.60 (s, 1H), 1.86 (s, 3H), 2.04 (br s, 6H), 2.25 (br s, 2H), 5.36 (s, 1H), 6.56 (s, 2H), 6.71 (d, ^3J = 7.5 Hz, 1H), 6.79 (br s, 2H), 7.10-7.32 (m, 4H), 7.65-7.67 (m, 2H), 8.58 (d, ^3J= 7.5 Hz, 1H); ^{13}C NMR (75 MHz, C_6D_6, 25 °C): δ 1.19 (q), 1.23 (q), 1.48 (q), 1.94 (q), 2.06 (q), 20.84 (q), 26.26 (d), 29.67 (d), 31.44 (q), 31.73 (d), 51.20 (d), 119.82 (q, $^1J_{CF}$= 321 Hz), 119.83 (d), 120.47 (d), 124.87 (d), 126.55 (d), 126.79 (d), 127.08 (d), 127.11(d), 127.28 (d), 127.83 (d), 129.26 (d), 129.96 (d), 139.25 (s), 140.69 (s), 141.75 (s×2), 142.14 (s), 143.36 (s),

143.55 (s), 144.60 (s), 147.14 (s), 152.59 (s), 152.92 (s); ^{19}F NMR (283 MHz, C_6D_6, 25 °C): δ –74.9.

Preparation of 39 from 37. A CH_2Cl_2 (18 mL) solution of **37** (203 mg, 0.204 mmol) and $AgBF_4$ (ca. 150 mg, 0.77 mmol) was stirred for 1 h at room temperature. After removal of the solvent, hexane was added to the residue. The resulting suspension was filtered through Celite®, and the solvent was removed. The residue was separated by WCC ($CHCl_3$) to afford **39** (183 mg, 0.188 mmol, 92%). **39**: colorless crystals, mp 264-266 °C (dec.); ^{1}H NMR (300 MHz, $CDCl_3$, 25 °C): δ –0.02 (s, 18H), –0.01 (s, 9H), 0.03 (s, 9H), 0.09 (s, 18H), 1.39 (s, 1H), 1.73 (s, 6H), 1.88 (br s, 1H), 1.97 (br s, 1H), 2.08 (s, 3H), 4.90 (s, 1H), 6.45 (br s, 1H), 6.49 (s, 2H), 6.57 (br s, 1H), 7.13 (dd, ^3J= 7.5 Hz, ^3J= 7.5 Hz 1H), 7.22-7.32 (m, 3H), 7.49 (d, ^3J= 7.5 Hz, 1H), 7.71-7.73 (m, 2H), 7.94 (d, ^3J= 6.9 Hz, 1H); ^{13}C NMR (75 MHz, $CDCl_3$, 25 °C): δ 0.76 (q), 0.84 (q), 1.02 (q), 1.13 (q), 1.51 (q), 20.85 (q), 25.23 (q), 25.29 (q), 30.65 (d), 31.11 (d), 31.49 (d), 49.74 (d, $^2J_{CF}$= 9.3 Hz), 119.42 (d), 119.72 (d), 122.62 (d), 124.95 (d), 125.60 (d), 125.74 (d), 125.85 (d), 125.95 (d), 126.37 (d), 127.48 (d), 128.10 (d), 138.93 (s, $^2J_{CF}$= 54 Hz), 139.21 (s), 139.95 (s), 140.72 (s), 143.32 (s), 143.47 (s, $^2J_{CF}$= 33 Hz), 143.64 (s), 144.27 (s), 145.68 (s), 151.49 (s), 152.02 (s); ^{19}F NMR (283 MHz, $CDCl_3$, 25 °C): δ –177.1 [$^1J_{SnF}$ = 2340 Hz (^{117}Sn), 2450 Hz (^{119}Sn)]; ^{119}Sn NMR (111 MHz, $CDCl_3$, 25 °C): δ –50.5 ($^1J_{SnF}$ = 2450 Hz); Anal. Calcd for $C_{49}H_{79}FSi_6Sn$: C, 60.40; H, 8.17. Found: C, 60.51; H, 8.17.

Preparation of 39 from 38. In a glovebox filled with argon, a THF (2 mL) solution of **38** (179 mg, 0:160 mmol) and LiF (36.3 mg, 1.40 mmol) was stirred for 12 h at room temperature. After removal of the solvent, hexane was added to the residue. The resulting suspension was filtered

through Celite®, and the solvent was removed. The residue was separated by WCC ($CHCl_3$) to afford **39** (125 mg, 0.128 mmol, 80%).

Preperation of diphenylmethyllithium–THF complex 41. To a THF (8 mL) solution of diphenylmethane **40** (863 mg, 5.13 mmol) was added *n*-butyllithium (1.5 M in hexane, 3.3 mL, 5.0 mmol) at –78 °C. After stirring at 0 °C for 3 h, the solvent was removed in vacuo. The reaction mixture was taken into a glovebox filled with argon, and washed with hexane to afford **41** as yellow powder (1.17 g, 3.67 mmol, 72%). **41**: yellow powder, ^{1}H NMR (300 MHz, C_6D_6, 25 °C): δ 1.20-1.25 (m, 8H, thf), 3.12-3.16 (m, 8H, thf), 4.45 (s, 1H, bzl-H), 6.46-6.52 (m, 2H), 7.15-7.18 (m, 8H).

Preparation of 42. To a THF (8 mL) solution of **41** (237 mg, 0.745 mmol) was added THF (18 mL) solution of **36** (543 mg, 0.621 mmol) was added to the mixture at –78 °C. After stirring for 1.5 h at the same temperature, the reaction mixture was warmed to room temperature and stirred for 10 h at the same temperature. After removal of the solvent, hexane was added to the residue. The resulting suspension was filtered through Celite®, and the solvent was removed. The residue was separated by GPLC ($CHCl_3$) to afford **42** (468 mg, 0.471 mmol, 76%). **42**: colorless crystals, mp 181-183 °C (dec.); ^{1}H NMR (300 MHz, $CDCl_3$, 25 °C): δ –0.19 (s, 9H), –0.14 (s, 9H), 0.03 (s, 9H), 0.04 (s, 9H), 0.05 (s, 9H), 0.06 (s, 9H), 1.33 (s, 1H), 1.63 (s, 1H), 1.68 (s, 1H), 2.17 (s, 6H), 2.22 (s, 3H), 4.51 (s, 1H), 6.35 (br s, 1H), 6.46 (br s, 1H), 6.67 (s, 2H), 6.94-6.98 (m, 3H), 7.09-7.16 (m, 3H), 7.22-7.24 (m, 2H), 7.52-7.55 (m, 2H); ^{13}C NMR (75 MHz, $CDCl_3$, 25 °C): δ 0.68 (q), 0.81 (q), 0.93 (q), 1.01 (q), 1.88 (q), 20.97 (q), 26.19 (q), 30.44 (d), 31.67 (d), 31.99 (d), 55.56 (d), 122.51 (d), 125.70 (d), 126.16 (d), 127.60 (d), 127.96 (d), 128.29 (d), 128.80 (d), 128.98 (d), 130.17 (d), 139.15 (s), 139.52 (s), 141.22 (s), 142.24 (s), 142.76 (s), 144.23 (s),

144.76 (s), 150.15 (s), 150.90 (s); ^{119}Sn NMR (111 MHz, $CDCl_3$, 25 °C): δ –53.2; Anal. Calcd for $C_{49}H_{81}ClSi_6Sn$: C, 59.28; H, 8.22. Found: C, 59.03; H, 8.11.

Preparation of 43. A CH_2Cl_2 (3 mL) solution of **42** (64.0 mg, 0.0645 mmol) and $AgBF_4$ (ca. 50 mg, 0.26 mmol) was stirred for 1 h at room temperature. After removal of the solvent, hexane was added to the residue. The resulting suspension was filtered through Celite®, and the solvent was removed. The residue was separated by WCC ($CHCl_3$) to afford **43** (56.6 mg, 0.0580 mmol, 90%). **43**: colorless crystals, ^{1}H NMR (300 MHz, $CDCl_3$, 25 °C): δ –0.19 (s, 9H), –0.15 (s, 9H), 0.00 (s, 9H), 0.02 (s, 9H), 0.03 (s, 9H), 0.05 (s, 9H), 1.33 (s, 1H), 1.54 (br s, 1H), 1.61 (br s, 1H), 2.08 (s, 6H), 2.21 (s, 3H), 4.52 (d, $^3J_{HF}$ = 4.2 Hz, 1H), 6.35 (br s, 1H), 6.47 (br s, 1H), 6.66 (s, 2H), 6.95-7.03 (m, 3H), 7.11-7.16 (m, 3H), 7.22-7.27 (m, 2H), 7.48-7.50 (m, 2H); ^{19}F NMR (283 MHz, $CDCl_3$, 25 °C): δ –187.0 [$^1J_{SnF}$ = 2420 Hz (^{117}Sn), 2540 Hz (^{119}Sn)].

Reaction of 37 with *n*-butyllithium. To a hexane (4 mL) solution of **37** (62.5 mg, 0.0631 mmol) was added *n*-butyllithium (0.43 M in hexane, 0.160 mL, 0.0690 mmol) at room temperature. The reaction mixture was stirred for 3 h at the same temperature, and then MeOH (1.0 mL) was added. After removal of the solvents, hexane was added to the residue and the mixture was filtered with Celite®. After removal of the solvent, the residue was separated by PTLC (Et_2O/hexane = 1/9) to afford **44** (10.0 mg, 0.00988 mmol, 16%) and **37** (39.0 mg, 0.0394, 62%). **44**: colorless crystals, ^{1}H NMR (300 MHz, C_6D_6, 25 °C): δ 0.02 (s, 9H), 0.12 (s, 9H), 0.16 (s, 9H), 0.22 (s, 9H), 0.26 (s, 9H), 0.28 (s, 9H), 0.84 (t, ^3J = 7.1 Hz, terminal-<u>Me</u> of Bu), 1.10-1.37 (m, 4H, -C<u>H</u>$_2$- of Bu), 1.58 (s, 1H), 1.59-1.83 (m, 2H, -C<u>H</u>$_2$- of Bu), 2.01 (s, 3H), 2.11 (s, 6H+1H), 2.34 (br s, 1H), 4.95 (s, 1H), 6.65 (s, 2H), 6.68 (br s, 1H), 6.80 (br s, 1H), 6.85-6.87 (m, 1H), 7.17-7.29 (m, 4H), 7.74-7.81 (m, 3H).

Reaction of 37 with *t*-butyllithium (exposure to the air). In a glovebox filled with argon, *t*-butyllithium (2.3 M in pentane, 0.0070 mL, 0.016 mmol) was added to a diethylether (1 mL) solution of **37** (13.9 mg, 0.0140 mmol) at –40 °C. The reaction mixture was stirred for 0.5 h at the same temperature, and then for 3 h at room temperature. After removal of the solvents, C_6D_6 solution of the residue was placed in a 5 mm ϕ NMR tube. The tube was evacuated and sealed and ^{1}H NMR spectrum was measured. The ^{1}H NMR spectrum showed signals probably assignable to **45** and **49** (ca 1:2). After exposure to the air of this solution, ^{1}H NMR spectrum was measured. The NMR signals were assignable only to **45**. **45**: colorless crystals, ^{1}H NMR (300 MHz, C_6D_6, 25 °C): δ 0.11 (s, 9H), 0.13 (s, 9H), 0.20 (s, 18H), 0.32 (s, 18H), 1.51 (s, 1H), 1.86 (s, 3H), 1.98 (s, 6H), 2.12 (br s, 1H), 2.20 (br s, 1H), 5.15 (s, 1H), 6.42 (s, 2H), 6.69 (br s, 1H), 6.78 (br s, 1H), 7.02-7.28 (m, 4H), 7.35 (s, 1H, Sn-H), 7.48-7.50 (m, 1H), 7.61-7.65 (m, 1H), 7.91-7.98 (m, 1H).

X-Ray crystallographic analysis of 45. Crystal data for **45** are shown in Table 2-3. Colorless and needle-like single crystals of **45** were grown by the slow evaporation of its hexane solution. The intensity data were collected on a Rigaku/MSC Mercury CCD diffractometer with graphite monochromated MoKα radiation (λ = 0.71069 Å) to $2\theta_{max}$ = 50° at 103 K. The structure was solved by Patterson methods (DIRDIF-99.2[26]) and refined by full-matrix least-squares procedures on F^2 for all reflections (SHELXL-97[27]). Two trimethylsilyl groups of the $CH(SiMe_3)_2$ groups at *para*-position of the Tbt group were disordered. The occupancies of the disordered parts were refined (0.75:0.25). All hydrogen atoms except Sn–H were placed using AFIX instructions, while all the other atoms were refined anisotropically except for six carbon atoms, which were in the minor part of the disordered trimethylsilyl groups and refined isotropically.

Reaction of 37 with *t*-butyllithium (trapping experiment by MeI). In a glovebox filled with argon, *t*-butyllithium (2.3 M in pentane, 0.036 mL, 0.083 mmol) was added to a diethylether (6 mL) solution of **37** (74.8 mg, 0.0755 mmol) at –40 °C. The reaction mixture was stirred for 0.5 h at the same temperature, and then for 3 h at room temperature. After removal of the solvents, iodomethane (0.5 mL) was added to the benzene solution of the residue. After removal of the solvent, the residue was separated by PTLC (hexane) to afford **46** (13.9 mg, 0.0143 mmol, 19%) and **45** (27.6 mg, 0.0288 mmol, 38%). **46**: colorless crystals, mp 104-108 °C (dec.); ^{1}H NMR (300 MHz, C_6D_6, 60 °C): δ 0.01 (s, 18H), 0.14 (s, 9H), 0.16 (s, 9H), 0.25 (s, 18H), 1.45 (s, 1H), 1.75 (br s, 1H), 1.83 (br s, 1H), 1.99 (s, 6H), 2.05 (s, 3H), 2.10 (s, 3H), 6.55 (s, 2H), 6.64 (br s, 2H), 7.11-7.18 (m, 4H), 7.46 (s, 1H, Sn-H), 7.49-7.60 (m, 3H), 7.78 (d, ^3J = 7.7 Hz, 1H); ^{119}Sn NMR (111 MHz, C_6D_6, 25 °C): δ –151.9.

X-Ray crystallographic analysis of 46. Crystal data for **46** are shown in Table 2-3. Colorless and prismatic single crystals of **46** were grown by the slow evaporation of its hexane solution. The intensity data were collected on a Rigaku/MSC Mercury CCD diffractometer with graphite monochromated MoKα radiation (λ = 0.71069 Å) to $2\theta_{max}$ = 50° at 203 K. The structure was solved by Patterson methods (DIRDIF-99.2[26]) and refined by full-matrix least-squares procedures on F^2 for all reflections (SHELXL-97[27]). All hydrogen atoms except Sn–H were placed using AFIX instructions, while all the other atoms were refined anisotropically.

Reaction of 37 with *t*-butyllithium in hexane. To a hexane (4 mL) solution of **37** (60.5 mg, 0.0611 mmol) was added *t*-butyllithium (0.47 M in hexane, 0.140 mL, 0.0660 mmol) at room temperature. The reaction mixture was stirred for 3 h at the same temperature, and then MeOH (1.0 mL) was added. After removal of the solvents, hexane was added to the residue and the

mixture was filtered with Celite®. The solvent was removed to afford only **37** judging from the ^{1}H NMR spectrum.

Reaction of 37 with LDA. To a hexane (4 mL) solution of **37** (40.6 mg, 0.0410 mmol) was added lithium diisopropylamide (2.0 M in heptane/THF/ethylbenzene, 0.020 mL, 0.040 mmol) at 0 °C. The reaction mixture was stirred for 6 h at the same temperature, and then MeOH (1.0 mL) was added. After removal of the solvents, hexane was added to the residue and the mixture was filtered with Celite®. The solvent was removed to afford only **37** (39.9 mg, 0.0403 mmol, 98%).

Reaction of 37 with NaH. In a glovebox filled with argon, THF (3 mL) solution of **37** (59.8 mg, 0.0604 mmol) and sodium hydride (4.2 mg, 0.18 mmol) was stirred for 3 days at room temperature. The reaction mixture was quenched by MeOD (1.0 mL), and the solvents were removed. Hexane was added to the residue and the mixture was filtered with Celite®. The solvent was removed to afford only **37** (55.5 mg, 0.0561 mmol, 93%; D content: 0%).

Reaction of 38 with LDA. In a glovebox filled with argon, lithium diisopropylamide (2.0 M in heptane/THF/ethylbenzene, 0.035 mL, 0.070 mmol) was added to a THF (2 mL) solution of **38** (77.5 mg, 0.0692 mmol) at –40 °C. The reaction mixture was stirred for 1 h at room temperature. After removal of the solvent, hexane was added to the residue. The resulting suspension was filtered through Celite®, and the solvent was removed. A C_6D_6 solution of the residue was placed in a 5 mm ϕ NMR tube, and the tube was evacuated and sealed. After the measurement of ^{1}H NMR spectrum (complicated mixture), the sealed tube was opened in a glovebox, MesCNO (28.3 mg, 0.177 mmol) was added to the solution at room temperature. The reaction mixture was stirred for 3 h at the same temperature, and the solvent was removed. The residue was separated

by GPLC (toluene) and PTLC ($CHCl_3$/hexane = 10/1) to afford **54** (13.9 mg, 0.0124 mmol, 18%), **55** (4.3 mg, 0.0045 mmol, 7%) and **56** (4.4 mg, 0.0045 mmol, 7%). **54**: colorless crystals, ^{1}H NMR (300 MHz, C_6D_6, 25 °C): δ 0.09 (s, 18H), 0.20 (s, 18H), 0.28 (s, 18H), 1.64 (s, 1H), 2.17 (s, 3H), 2.51 (s, 1H), 2.53 (s, 1H), 2.73 (s, 6H), 4.90 (s, 2H), 6.74 (s, 1H), 6.77 (s, 2H), 6.81 (s, 1H), 6.88-7.34 (m, 16H). **55**: colorless crystals, ^{1}H NMR (300 MHz, C_6D_6, 25 °C): δ 0.04 (s, 9H), 0.16 (s, 9H), 0.19 (s, 9H), 0.21 (s, 9H), 0.32 (s, 9H), 0.34 (s, 9H), 1.48 (s, 3H), 1.52 (s, 1H), 1.85 (s, 3H), 2.09 (br s, 1H), 2.17 (br s, 1H), 2.89 (d, ^2J = 14.4 Hz, 1H), 2.99 (d, ^2J = 14.4 Hz, 1H), 5.15 (s, 1H), 6.37 (s, 1H), 6.52 (s, 1H), 6.69 (s, 1H), 6.79 (s, 1H), 7.01-7.34 (m, 4H), 7.52 (d, ^3J= 7.7 Hz, 1H), 7.71 (d, ^3J= 7.3 Hz, 1H), 7.85-7.88 (m, 2H). **56**: colorless crystals, mp 246-248 °C (dec.); ^{1}H NMR (300 MHz, $CDCl_3$, 25 °C): δ –0.09 (s, 9H), –0.06 (s, 9H), 0.07 (s, 18H), 0.09 (s, 18H), 0.59 (s, 1H, O<u>H</u>), 1.39 (s, 1H), 1.67 (s, 6H), 2.06 (s, 3H+2H), 4.90 (s, 1H), 6.39 (s, 2H), 6.43 (br s, 1H), 6.55 (br s, 1H), 7.06 (dd, ^3J= 7.2 Hz, ^3J= 7.2 Hz, 1H), 7.13 (dd, ^3J= 7.2 Hz, ^3J= 7.2 Hz, 1H), 7.27-7.32 (m, 2H), 7.48 (d, ^3J= 7.5 Hz, 1H), 7.57 (d, ^3J= 7.5 Hz, 1H), 7.73 (dd, ^3J= 4.4 Hz, ^3J= 4.4 Hz, 1H), 7.85 (dd, ^3J= 4.2 Hz, ^3J= 4.2 Hz, 1H); ^{13}C NMR (75 MHz, $CDCl_3$, 25 °C): δ 0.78 (q), 0.86 (q), 0.90 (q), 1.11 (q), 1.52 (q), 1.81 (q), 20.83 (q), 25.73 (q), 30.48 (d), 31.37 (d), 31.66 (d), 50.13 (d), 119.54 (d), 120.01 (d), 122.57 (d), 124.01 (d), 124.78 (d), 125.06 (d), 125.30 (d), 125.52 (d), 125.97 (d), 127.40 (d), 127.74 (d), 138.25 (s), 138.48 (s), 139.79 (s), 140.04 (s), 140.34 (s), 143.72 (s), 144.39 (s), 144.72 (s), 144.75 (s), 150.69 (s), 151.18 (s); ^{119}Sn NMR (111 MHz, $CDCl_3$, 25 °C): δ –87.5; High resolution FAB-MS *m/z* calcd for $C_{49}H_{80}OSi_6{}^{120}Sn$: 972.3847, found: 972.3842. Anal. Calcd for $C_{49}H_{80}OSi_6Sn{\cdot}1.5H_2O$: C, 58.89; H, 8.37. Found: C, 58.95; H, 8.29.

X-Ray crystallographic analysis of [54·C_6H_6]. Crystal data for [**54**·C_6H_6] are shown in Table 2-3. Colorless and prismatic single crystals of [**54**·C_6H_6] were grown by the slow evaporation of its

benzene solution. The intensity data were collected on a Rigaku/MSC Mercury CCD diffractometer with graphite monochromated MoKα radiation (λ = 0.71069 Å) to $2\theta_{max}$ = 50° at 103 K. The structure was solved by Patterson methods (DIRDIF-99.2[26]) and refined by full-matrix least-squares procedures on F^2 for all reflections (SHELXL-97[27]). All hydrogen atoms were placed using AFIX instructions, while all the other atoms were refined anisotropically.

Reaction of 38 with LTMP. In a glovebox filled with argon, lithium tetramethylpiperidide [freshly prepared by tetramethylpiperidine (12.0 mg, 0.0850 mmol) and *n*-butyllithium (1.5 M in hexane, 0.051 mL, 0.077 mmol) in THF (0.5 mL)] was added to a THF (2 mL) solution of **38** (77.3 mg, 0.0690 mmol) at –40 °C. The reaction mixture was stirred for 1 h at room temperature. After removal of the solvent, hexane was added to the residue. The resulting suspension was filtered through Celite®, and the solvent was removed. A C_6D_6 solution of the residue was placed in a 5 mm ϕ NMR tube, and the tube was evacuated and sealed. After the measurement of ^{1}H NMR spectrum (complicated mixture), the sealed tube was opened in a glovebox, MesCNO (28.0 mg, 0.174 mmol) was added to the solution at room temperature. The reaction mixture was stirred for 3 h at the same temperature, and the solvent was removed to afford complicated mixture. The residue was separated by GPLC (toluene) to give the fraction containing **55** mainly (9.7 mg, 0.010 mmol, 15%, if pure). The other products could not be isolated and identified.

Reaction of 38 with *n*-butyllithium. In a glovebox filled with argon, *n*-butyllithium (1.5 M in hexane, 0.050 mL, 0.075 mmol) was added to a hexane (6 mL) solution of **38** (86.4 mg, 0.0771 mmol) at room temperature. The reaction mixture was stirred for 3 h at room temperature. After removal of the solvent, hexane was added to the residue. The resulting suspension was filtered through Celite®, and the solvent was removed. A C_6D_6 solution of the residue was placed in a 5

mm ϕ NMR tube. The tube was evacuated and sealed. After the measurement of ^{1}H NMR spectrum (suggesting the generation of *n*-Bu adducts), the sealed tube was opened. After removal of the solvent, the residue was separated by GPLC ($CHCl_3$) and PTLC (hexane) to afford **44** (39.7 mg, 0.0392 mmol, 51%), **54** (9.0 mg, 0.0080 mmol, 10%), and **57** (8.7 mg, 0.0096 mmol, 12%). **57**: colorless crystals, ^{1}H NMR (300 MHz, C_6D_6, 25 °C): δ 0.18 (s, 18H), 0.19 (s, 18H), 0.23 (s, 18H), 0.94 (t, ^3J= 7.3 Hz, 6H, terminal-Me of Bu), 1.37-1.70 (m, 12H, -CH_2- of Bu), 1.47 (s, 1H), 1.95 (br s, 1H), 2.06 (br s, 1H), 2.14 (s, 3H), 2.59 (s, 6H), 6.56 (br s, 1H), 6.68 (br s, 1H), 6.81 (s, 2H).

Reaction of 38 with *t*-butyllithium. In a glovebox filled with argon, *t*-butyllithium (2.6 M in hexane, 0.025 mL, 0.065 mmol) was added to a hexane (6 mL) solution of **38** (73.2 mg, 0.0653 mmol) at room temperature. The reaction mixture was stirred for 3 h at room temperature. After removal of the solvent, hexane was added to the residue. The resulting suspension was filtered through Celite®, and the solvent was removed. A C_6D_6 solution of the residue was placed in a 5 mm ϕ NMR tube. The tube was evacuated and sealed. After the measurement of ^{1}H NMR spectrum (suggesting the generation of **58**), the sealed tube was opened. After removal of the solvent, the residue was separated by PTLC (hexane) to afford **58** (58.7 mg, 0.0580 mmol, 89%). **58**: colorless crystals, mp 133-136 °C (dec.); ^{1}H NMR (300 MHz, C_6D_6, 25 °C): δ 0.25 (s, 18H), 0.34 (s, 9H), 0.38 (s, 9H), 0.43 (s, 9H), 0.44 (s, 9H), 1.28 (s, *t*-Bu), 1.71 (s, 1H), 1.96 (s, 1H), 2.29 (s, 1H), 2.40 (br s, 6H), 2.48 (s, 3H), 5.15 (s, 1H), 6.86 (br s, 2H), 6.99 (s, 2H), 7.10-7.15 (m, 1H), 7.34-7.57 (m, 3H), 7.72-7.96 (m, 2H), 8.00-8.06 (m, 2H).

Synthesis of 32. To a solution of **39** (36.0 mg, 0.0369 mmol) in dry Et_2O (6 mL) placed in a glovebox filled with argon was added *t*-butyllithium (1.0 M hexane solution, 0.060 mL, 0.060

mmol) at –40 °C. The reaction mixture was stirred for 0.5 h at the same temperature and for 1 h while being warmed up to room temperature. After removal of the solvents, dry hexane was added to the residue and the mixture was filtered with Celite®. The filtrate was evaporated to afford **32** in a pure form as purple crystalline solids (35.2 mg, 0.0369 mmol, quant.). **32**: purple crystalline solids; mp 167–171 °C (dec.); ^{1}H NMR (300 MHz, C_6D_6, 25 °C): δ –0.02 (s, 9H), 0.02 (s, 9H), 0.12 (s, 18H), 0.18 (s, 9H), 0.26 (s, 9H), 1.56 (s, 1H), 1.91 (s, 1H), 2.06 (s, 1H), 2.10 (s, 3H), 2.59 (br s, 3H), 2.66 (s, 3H), 6.73 (br s, 1H), 6.84 (br s, 1H + 2H), 7.06 (ddd, ^3J = 8 Hz, ^3J = 8 Hz, ^4J = 2 Hz, 1H), 7.15 (dd, ^3J = 8 Hz, ^3J = 8 Hz, 1H), 7.25 (ddd, ^3J = 7 Hz, ^3J = 6 Hz, ^4J = 2 Hz, 1H), 7.29 (ddd, ^3J = 7 Hz, ^3J = 7 Hz, ^4J = 2 Hz, 1H), 7.61 (dd, ^3J = 7 Hz, ^4J = 2 Hz, 1H), 7.78 (d, ^3J = 8 Hz, 1H), 7.89 (dd, ^3J = 8 Hz, ^4J = 2 Hz, 1H), 7.91 (dd, ^3J = 6 Hz, ^4J = 2 Hz, 1H); ^{13}C NMR (75 MHz, C_6D_6, 25 °C): δ 1.07 (q), 1.20 (q), 1.45 (q), 1.65 (q), 21.13 (q), 27.62 (q), 28.63 (q), 31.25 (d), 35.96 (d), 37.59 (d), 119.78 (d), 120.18 (d), 120.59 (d), 122.84 (d), 122.99 (d), 123.20 (d), 124.13 (d), 125.23 (d), 125.64 (d), 128.29 (d), 129.12 (d), 129.40 (d), 134.24 (s), 134.40 (s), 140.61 (s), 142.75 (s), 143.35 (s), 143.62 (s), 144.91 (s), 145.04 (s), 145.87 (s), 146.39 (s), 150.73 (s), 151.33 (s); ^{119}Sn NMR (111 MHz, C_6D_6, 25 °C): δ 270; UV/vis (hexane, rt) 552 nm (ε 1×10^4); High resolution FAB-MS *m/z* calcd for $C_{49}H_{79}Si_6{}^{120}Sn$ [(M+H)$^+$]: 955.3827, found: 955.3851.

X-Ray crystallographic analysis of 32. Crystal data for **32** are shown in Table 2-4. Purple and prismatic single crystals of **32** were grown by the slow evaporation of its hexane solution in a glovebox filled with argon. The intensity data were collected on a Rigaku/MSC Mercury CCD diffractometer with graphite monochromated MoKα radiation (λ = 0.71069 Å) to $2\theta_{max}$ = 50° at 103 K. The structure was solved by Patterson methods (DIRDIF-99.2[26]) and refined by full-

matrix least-squares procedures on F^2 for all reflections (SHELXL-97[27]). All hydrogen atoms were placed using AFIX instructions, while all the other atoms were refined anisotropically.

Measurement of UV/vis spectrum of 32. In a glovebox filled with argon, **32** (0.3 mg, 3×10^7 mol) was dissolved in hexane (1 mL, dried over K mirror and distilled by trap-to-trap distillation). This solution (3×10^4 M) was put into UV cell (pathlength 1 mm), and UV/vis spectrum was measured with JASCO Ubest-50 UV/vis spectrometer at room temperature.

Measurement of Raman spectrum of 32. In a glovebox filled with argon, **32** was powdered and put into a glass capillary. The capillary was evacuated and sealed. FT-Raman spectrum was measured with the excitation by He-Ne laser (833 nm) at room temperature in the solid state with Spex 1877 Triplemate and EG&G PARC 1421 intensified photodiode array detector by Prof. Furukawa at Waseda University.

Reaction of 32 with water. To a THF (1 mL) solution of **32** (16.6 mg, 0.0174 mmol) was added H_2O (0.3 mL) at room temperature. After addition of an aqueous solution (sat.) of NH_4Cl, the mixture was extracted with Et_2O. After removal of the solvent, the residue was separated by PTLC ($CHCl_3$/hexane = 1/5) to afford **56** (12.9 mg, 0.0133 mmol, 76%).

Reaction of 32 with 2,3-dimethyl-1,3-butadiene. To a THF (2 mL) solution of **32** (75.4 mg, 0.0790 mmol) was added 2,3-dimethyl-1,3-butadiene (0.4 mL) at room temperature. After removal of the solvent, hexane was added to the residue. The resulting suspension was filtered through Celite®, and the solvent was removed. The residue was separated by PTLC (hexane) to afford **63** (41.9 mg, 0.0404 mmol, 51%). **63**: colorless crystals, mp 180-183 °C (dec.); ^{1}H NMR

(300 MHz, C_6D_6, 50 °C): δ –0.06 (s, 18H), 0.12 (s, 18H), 0.15 (s, 9H), 0.21 (s, 9H), 1.36 (s, 3H), 1.41 (s, 1H), 1.77 (s, 3H), 2.00 [(s, 3H+1H) + (d, 1H, ^2J = 18.3 Hz)], 2.15 (s, 3H+1H), 2.54 (d, 1H, ^2J = 17.6 Hz), 2.71 [(s, 3H) + (d, 1H, ^2J = 17.6 Hz)], 3.16 (d, 1H, ^2J = 18.3 Hz), 6.52 (br s, 1H), 6.63 (br s, 1H), 6.71 (br s, 1H), 6.90 (br s, 1H), 6.83-7.28 (m, 5H), 7.74-7.81 (m, 2H), 7.90 (m, 1H), ^{13}C NMR (75 MHz, C_6D_6, 50 °C): δ 1.06 (q), 1.27 (q), 1.58 (q), 1.92 (q), 2.37 (q), 2.56 (q), 20.99 (q), 23.51 (q), 24.88 (q), 27.23 (q), 28.55 (t), 29.49 (d), 30.67 (q), 32.33 (d), 33.24 (d), 46.45 (t), 53.53 (s), 120.64 (d), 120.95 (d), 123.17 (d), 124.64 (d), 125.65 (d), 126.25 (d), 126.47 (d), 126.92 (d), 128.58 (d), 128.75 (d), 128.84 (d), 129.14 (s×2), 129.55 (d), 130.11 (s), 138.91 (s), 139.44 (s), 140.57 (s), 140.89 (s), 141.85 (s), 143.19 (s), 145.61 (s), 146.99 (s), 151.28 (s×2), 152.14 (s); ^{119}Sn NMR (111 MHz, C_6D_6, 50 °C): δ –113.1; High resolution FAB-MS *m/z* calcd for $C_{55}H_{88}Si_6{}^{120}Sn$ [M^+]: 1036.4524, found: 1036.4559. Anal. Calcd for $C_{55}H_{88}Si_6Sn{\cdot}0.5C_6H_6$: C, 64.77; H, 8.53. Found: C, 64.47; H, 8.52.

X-Ray crystallographic analysis of [63·0.5(C_6H_6)]. Crystal data for [**63**·0.5(C_6H_6)] are shown in Table 2-4. Colorless and prismatic single crystals of [**63**·0.5(C_6H_6)] were grown by the slow evaporation of its benzene solution. The intensity data were collected on a Rigaku/MSC Mercury CCD diffractometer with graphite monochromated MoKα radiation (λ = 0.71069 Å) to $2\theta_{max}$ = 50° at 103 K. The structure was solved by Patterson methods (DIRDIF-99.2[26]) and refined by full-matrix least-squares procedures on F^2 for all reflections (SHELXL-97[27]). Two trimethylsilyl groups of the $CH(SiMe_3)_2$ groups at *para*-position of the Tbt group were disordered. The occupancies of the disordered parts were refined (0.77:0.23). The U_{ij} values of the disordered trimethylsilyl groups were resrained using SIMU instructions. All hydrogen atoms were placed using AFIX instructions, while all the other atoms were refined anisotropically.

Reaction of 32 with elemental sulfur. In a glovebox filled with argon, elemental sulfur (S_8, 35.8 mg, 1.12 mmol as S) was added to a benzene (2 mL) solution of **32** [prepared from **34** (52.2 mg, 0.0536 mmol) and *t*-butyllithium (2.3 M in pentane, 0.0255 mL, 0.0589 mmol)] at room temperature. The reaction mixture was stirred for 12 h at the same temperature. After removal of the solvent, the residue was separated by GPLC (toluene) and PTLC ($CHCl_3$/hexane = 1/5) to afford **70**[16] (10.9 mg, 0.0119 mmol, 22% from **34**).

Reaction of 32 with *t*-butyllithium. In a glovebox filled with argon, *t*-butyllithium (2.3 M in pentane, 0.0145 mL, 0.0334 mmol) was added to a diethylether (2 mL) solution of **32** [prepared from **34** (29.7 mg, 0.0305 mmol) and *t*-butyllithium (2.3 M in pentane, 0.0145 mL, 0.0334 mmol)] at –40 °C. The raection was quenched by iodomethane (0.5 mL) at room temperature. After removal of the solvent, the residue was separated by PTLC (hexane) to afford **46** (11.4 mg, 0.0117 mmol, 39% from **34**).

Reaction of 32 with mesityl isocyanide. In a glovebox filled with argon, mesityl isocyanide (7.5 mg, 0.052 mmol) was added to a diethylether (2 mL) solution of **32** [prepared from **34** (39.3 mg, 0.0403 mmol) and *t*-butyllithium (0.95 M in hexane, 0.043 mL, 0.041 mmol)] at room temperature. The reaction mixture was stirred for 15 h at room temperature. After removal of the solvent, the residue was separated by GPLC ($CHCl_3$) to afford **80** (5.2 mg, 0.0117 mmol, 29% from **34**) and **81** (3.7 mg, 0.0124 mmol, 31% from **34**). **80**: red crystals, mp 138-141 °C (dec.); ^{1}H NMR (300 MHz, $CDCl_3$, 25 °C): δ 1.21 (s, 3H), 1.67 (s, 3H), 1.91 (s, 3H), 2.23 (s, 3H), 2.28 (s, 3H), 2.34 (s, 3H), 5.22 (s, 1H), 6.25 (s, 1H), 6.88 (s, 1H), 6.96 (s, 1H), 7.13-7.19 (m, 1H), 7.29-7.36 (m, 3H), 7.68-7.70 (m, 2H), 9.06-9.08 (m, 1H), 9.47 (d, ^3J = 8.0 Hz, 1H). **81**: yellow

powder, ^{1}H NMR (300 MHz, $CDCl_3$, 25 °C): δ 2.32 (s, 3H), 2.46 (s, 6H), 6.97 (s, 2H), 7.27-7.37 (m, 4H), 7.59-7.62 (m, 2H), 7.91-7.94 (m, 2H), LRMS (EI): *m/z* 309 (M^+), 294 [$(M–Me)^+$].

X-Ray crystallographic analysis of 80. Crystal data for **80** are shown in Table 2-4. Red and prismatic single crystals of **80** were grown by the slow evaporation of its benzene solution. The intensity data were collected on a Rigaku/MSC Mercury CCD diffractometer with graphite monochromated MoKα radiation (λ = 0.71070 Å) to $2\theta_{max}$ = 50° at 103 K. The structure was solved by a direct method (SHELXS-97[27]) and refined by full-matrix least-squares procedures on F^2 for all reflections (SHELXL-97[27]). All hydrogen atoms were placed using AFIX instructions, while all the other atoms were refined anisotropically.

Reaction of 32 with 2,4,6-tri(*t*-butyl)benzonitrile oxide. In a glovebox filled with argon, 2,4,6-tri(*t*-butyl)benzonitrile oxide (29.0 mg, 0.101 mmol) was added to a diethylether (8 mL) solution of **32** [prepared from **34** (55.3 mg, 0.0568 mmol) and *t*-butyllithium (2.3 M in pentane, 0.027 mL, 0.062 mmol)] at room temperature. The reaction mixture was stirred for 12 h at room temperature. After removal of the solvent, the residue was separated by GPLC (toluene) to afford **84** (17.1 mg, 0.0138 mmol, 24% from **34**). Compound **84** underwent slow decomposition afford to **85**. **84**: colorless powder, ^{1}H NMR (300 MHz, C_6D_6, 25 °C): δ –0.11 (s, 9H), –0.07 (s, 9H), 0.19 (s, 18H), 0.35 (s, 9H), 0.37 (s, 9H), 0.89 (s, 9H), 1.30 (s, 9H), 1.41 (s, 1H), 1.71 (s, 9H), 2.06 (s, 3H+1H), 2.16 (s, 1H), 2.44 (s, 3H), 2.51 (s, 3H), 6.34 (d, ^3J = 8.3 Hz, 1H), 6.90-7.93 (13H, not assignable). **85**: yellow crystals, δ –0.14 (s, 9H), 0.19 (s, 9H), 0.20 (s, 9H), 0.23 (s, 9H), 0.41 (s, 18H), 1.13 (s, 9H), 1.33 (s, 9H+1H), 1.41 (s, 9H), 1.57 (s, 1H), 1.91 (s, 1H), 2.05 (s, 3H), 2.22 (s, 3H), 2.57 (s, 3H), 5.66 (s, 1H, N<u>H</u>), 6.19 (d, ^3J = 8.1 Hz, 1H), 6.59 (s, 1H, Tbt-arom.), 6.69 (s, 1H, Tbt-arom.), 6.74-7.88 (10H, not assignable).

X-Ray crystallographic analysis of [85·$CHCl_3$]. Crystal data for [**85**·$CHCl_3$] are shown in Table 2-5. Yellow and prismatic single crystals of [**85**·$CHCl_3$] were grown by the slow evaporation of its $CHCl_3/CH_3CN$ solution. The intensity data were collected on a Rigaku/MSC Mercury CCD diffractometer with graphite monochromated MoKα radiation (λ = 0.71069 Å) to $2\theta_{max}$ = 50° at 103 K. The structure was solved by Patterson methods (DIRDIF-99.2[26]) and refined by full-matrix least-squares procedures on F^2 for all reflections (SHELXL-97[27]). The chloroform molecule was disordered, and the occupancies of the disordered parts were refined (0.78:0.22). The U_{ij} values of the disordered chloroform molecules were restrained using SIMU instructions. The six C–Cl bonds of the chloroform molecules (major and minor) were restrained to have the typical C–Cl distance (1.7 Å) using DFIX instructions. All hydrogen atoms were placed using AFIX instructions, while all the other atoms were refined anisotropically.

Reaction of 42 with *t*-butyllithium. In a glovebox filled with argon, *t*-butyllithium (0.95 M in hexane, 0.051 mL, 0.048 mmol) was added to a hexane (4 mL) solution of **42** (47.7 mg, 0.0480 mmol) at –40 °C. The reaction mixture was stirred for 2 h at the same temperature. After removal of the solvents, hexane was added to the residue and the mixture was filtered with Celite®. The solvent was removed to afford only **42** judging from the ^{1}H NMR spectram.

Reaction of 43 with *t*-butyllithium. In a glovebox filled with argon, *t*-butyllithium (0.95 M in hexane, 0.063 mL, 0.060 mmol) was added to a diethylether (4 mL) solution of **43** (58.3 mg, 0.0597 mmol) at –40 °C. The reaction mixture was stirred for 0.5 h at the same temperature and for 1 h while being warmed up to room temperature. After removal of the solvent, hexane and benzene were added to the residue. The resulting suspension was filtered through Celite®, and the solvents was removed. A C_6D_6 solution of the residue was placed in a 5 mm ϕ NMR tube.

The tube was evacuated and sealed. After measurement of ^{1}H NMR spectrum, the sealed tube was opened. After removal of the solvent, the residue was separated by PTLC ($CHCl_3$/hexane = 1/4) to afford **89** (9.1 mg, 0.0095 mmol, 16%), **90** (6.2 mg, 0.065 mmol, 11%), and **43** (42.5 mg, 0.0435 mmol, 73%). **89**: colorless crystals, mp 181-184 °C (dec.); ^{1}H NMR (300 MHz, $CDCl_3$, 25 °C): δ –0.11 (s, 9H), –0.02 (s, 18H), 0.00 (s, 9H), 0.04 (s, 9H), 0.05 (s, 9H), 1.33 (s, 1H), 1.68 (s, 1H), 1.69 (s, 1H), 1.72 (s, 3H), 2.11 (d, ^3J = 14.5 Hz, 1H), 2.22 (s, 3H), 2.38 (d, ^3J = 14.5 Hz, 1H), 4.69 (s, 1H), 6.37 (s, 1H), 6.50 (s, 2H), 6.80 (s, 1H), 7.04-7.23 (m, 10H). **90**: colorless crystals, mp 172-176 °C (dec.); ^{1}H NMR (300 MHz, $CDCl_3$, 25 °C): δ –0.20 (s, 9H), –0.16 (s, 9H), 0.14 (s, 9H), 0.22 (s, 9H), 0.34 (s, 9H), 0.51 (s, 9H), 1.30 (s, 1H), 1.62 (s, 1H), 1.67 (s, 1H), 2.13 (s, 6H), 2.21 (s, 3H), 4.49 (s, 1H), 6.34 (s, 1H), 6.44 (s, 1H), 6.66 (s, 2H), 6.93-6.96 (m, 3H), 7.07-7.25 (m, 5H), 7.36 (s, 1H, Sn-H), 7.50-7.53 (m, 2H).

X-Ray crystallographic analysis of 89. Crystal data for **89** are shown in Table 2-5. Colorless and prismatic single crystals of **89** were grown by the slow evaporation of its $CHCl_3$ solution. The intensity data were collected on a Rigaku/MSC Mercury CCD diffractometer with graphite monochromated MoKα radiation (λ = 0.71069 Å) to $2\theta_{max}$ = 50° at 103 K. The structure was solved by Patterson methods (DIRDIF-99.2[26]) and refined by full-matrix least-squares procedures on F^2 for all reflections (SHELXL-97[27]). All hydrogen atoms were placed using AFIX instructions, while all the other atoms were refined anisotropically.

References

1. (a) Jacobsen, H.; Ziegler, T. *J. Am. Chem. Soc.* **1994**, *116*, 3667. (b) Dobbs, K. D.; Hehre, W. J. *Organometallics* **1986**, *5*, 2057. (c) Grützmacher, H.; Fässler, T. F. *Chem. Eur. J.* **2000**, *6*, 2317.
2. Apeloig, Y.; Pauncz, R.; Karni, M.; West, R.; Steiner, W.; Chapman, D. *Organometallics* **2003**, *22*, 3250.
3. Karni, M.; Apeloig, Y. *J. Am. Chem. Soc.* **1990**, *112*, 8589.
4. (a) Brook, A. G.; Abdesaken, F.; Gutekunst, B.; Gutekunst, G.; Kallury, R. K. *J. Chem. Soc., Chem. Commun.* **1981**, 191. (b) Wiberg, N.; Wagner, G.; Müller, G. *Angew. Chem., Int. Ed. Engl.* **1985**, *24*, 229. (c) Delpon-Lacaze, G., Couret, C. *J. Organomet. Chem.* **1994**, *480*, C4. (d) Apeloig, Y.; Bendikov, M.; Yuzefovich, M.; Nakash, M.; Bravo-Zhivotovskii, D. *J. Am. Chem. Soc.* **1996**, *118*, 12228. (e) Sakamoto, K.; Ogasawara, J.; Kon, Y.; Sunagawa, T.; Kabuto, C.; Kira, M. *Angew. Chem. Int. Ed.* **2002**, *41*, 1402.
5. (a) Miracle, G. E.; Ball, J. L.; Powell, D. R.; West, R. *J. Am. Chem. Soc.* **1993**, *115*, 11598. (b) Trommer, M.; Miracle, G. E.; eichler, B. E.; Powell, D. R.; West, R. *Organometallics* **1997**, *16*, 5737.
6 Rigon, L.; Ranaivonjatovo, H.; Escudié. J.; Dubourg, A.; Declercq, J.-P. *Chem Eur. J.* **1999**, *5*, 774.
7. (a) Couret, C.; Escudié, J.; Satgé, J.; Lazraq, M. *J. Am. Chem. Soc.* **1987**, *109*, 4411. (b) Meyer, H.; Baum, G.; Massa, W.; Berndt, A. *Angew. Chem., Int. Ed. Engl.* **1987**, *21*, 221. (c) Berndt, A.; Meyer, H.; Baum, G.; Massa, W.; Berger, S. *Pure Appl. Chem.* **1987**, *59*, 1011.

8. (a) Couret, C.; Escudié, J.; Delpon-Lacaze, G.; Satgé, J. *Organometallics* **1992**, *11*, 3176. (b) Lazraq, M.; Couret, C.; Escudié, J.; Satgé, J.; Soufiaoui, M. *Polyhedron* **1991**, *10*, 1153. (c) Anselme, G.; Escudié, J.; Couret, C.; Satgé, J. *J. Organomet. Chem.* **1991**, *403*, 93. (d) Tokitoh, N.; Kishikawa, K.; Okazaki, R. *J. Chem. Soc., Chem. Commun.* **1995**, 1425. (e) Schumann, H.; Glanz, M.; Girgsdies, F.; Ekkehardt Hahn, F.; Tamm, M.; Grzegorzewski, A. *Angew. Chem., Int. Ed.* **1997**, *36*, 2232. (f) Meiners, F.; Saak, W.; Weidenbruch, M. *Organometallics* **2000**, *19*, 2835. (g) Lee, V. Ya.; Ichinohe, M.; Sekiguchi, A. *J. Am. Chem. Soc.* **2002**, *124*, 9962.

9. Ramdane, H.; Ranaivonjatovo, H.; Escudié. J. *Organometallics* **1996**, *15*, 3070.

10. (a) Eichler, B. E.; Powell, D. R.; West, R. *Organometallics* **1998**, *17*, 2147. (b) Eichler, B. E.; Powell, D. R.; West, R. *Organometallics* **1999**, *18*, 540.

11. Matsuhashi, Y.; Tokitoh, N.; Okazaki, R.; Goto, M.; Nagase, S. *Organometallics* **1993**, *12*, 1351.

12. Takeda, N.; Shinohara, A.; Tokitoh, N. *Organometallics* **2002**, *21*, 256.

13. Mackay, K. M. in "The Chemistry of Organic Germanium, Tin and Lead Compounds," ed by Patai, S. Wiley, Chichester, U.K., 1995; Vol. 1, Chap. 2.

14. a) Bailey N. A.; Hull, S. E. *Acta Cryst.* **1978**, *B34*, 3289. b) Lee J.-S.; Nyburg, S. C. *Acta Cryst.* **1985**, *C41*, 560.

15. Lambert, J. B.; Lin, L.; Keinan S.; Müller, T. *J. Am. Chem. Soc.* **2003**, *125*, 6022.

16. Matsuhashi, Y.; Tokitoh, N.; Okazaki, R.; Goto, M.; Nagase, S. *Organometallics* **1993**, *12*, 1351.

17. For reviews on small heterocycles of group 14 elements, see: (a) Kabe, Y.; Ando, W. *Adv. Strain Org. Chem.* **1993**, *3*, 59. (b) Ando, W.; Kabe, Y.; Nami, C. *Main Group Met. Chem.*

1994, *17*, 209. (c) Weidenbruch, M. *Chem. Rev.* **1995**, *95*, 1479. (d) Ando, W.; Kabe, Y. In *The Chemistry of Organic Silicon Compounds*; Rappoport, Z., Apeloig, Y., Eds.; Wiley: Chichester, U.K., **1988**; Vol. 2, Part 3, Chapter 42.

18. A stannirene Sn–C=C has been synthesized by cycloaddition between a stannylene and an alkyne: Sita, L. R.; Bickerstaff, R. D. *J. Am. Chem. Soc.* **1988**, *110*, 5208.

19. Baiget, L,; Ranaivonjatovo, H.; Escudié , J.; Gornitzka, H. *J. Am. Chem. Soc.* **2004**, *126*, 11792.

20. (a) Masamune, S.; Sita, L. *J. Am. Chem. Soc.* **1985**, *107*, 6390. (b) Sita, L. R.; Kinoshita, I. *Organometallics* **1990**, *9*, 2865. (c) Fu, J.; Neumann, W. P. *J. Organomet. Chem.* **1984**, *272*, C5.

21. Yokelson, H. B.; Millevolte, A. J.; Haller, K. J.; West, R. *J. Chem. Soc., Chem. Commun.* **1987**, 1605

22. Weidenbruch, M.; Schäfers, K.; Schlaefke, J.; Peters, J. S.; von Schnering, H. G. *J. Organomet. Chem.* **1991**, *15*, 343.

23. Pangborn, A. B.; Giardello, M. A.; Grubbs, R. H.; Rosen, R. K.; Timmers F. J. *Organometallics* **1996**, *15*, 1518.

24. Gaussian 98: Frisch, M. J.; Trucks, G. W.; Schlegel, H. B.; Scuseria, G. E.; Robb, M. A.; Cheeseman, J. R.; Zakrzewski, V. G.; Montgomery, Jr., J. A.; Stratmann, R. E.; Burant, J. C.; Dapprich, S.; Millam, J. M.; Daniels, A. D.; Kudin, K. N.; Strain, M. C.; Farkas, O.; Tomasi, J.; Barone, V.; Cossi, M.; Cammi, R.; Mennucci, B.; Pomelli, C.; Adamo, C.; Clifford, S.; Ochterski, J.; Petersson, G. A.; Ayala, P. Y.; Cui, Q.; Morokuma, K.; Malick, D. K.; Rabuck, A. D.; Raghavachari, K.; Foresman, J. B.; Cioslowski, J.; Ortiz, J. V.; Stefanov, B. B.; Liu, G.; Liashenko, A.; Piskorz, P.; Komaromi, I.; Gomperts, R.; Martin,

R. L.; Fox, D. J.; Keith, T.; Al-Laham, M. A.; Peng, C. Y.; Nanayakkara, A.; Gonzalez, C.; Challacombe, M.; Gill, P. M. W.; Johnson, B.; Chen, W.; Wong, M. W.; Andres, J. L.; Head-Gordon, M.; Replogle, E. S.; Pople, J. A. Gaussian 98; Gaussian, Inc.: Pittsburgh, PA, 1998.

25. Gaussian 03: Frisch, M. J.; Trucks, G. W.; Schlegel, H. B.; Scuseria, G. E.; Robb, M. A.; Cheeseman, J. R.; Montgomery, Jr., J. A.; Vreven, T.; Kudin, K. N.; Burant, J. C.; Millam, J. M.; Iyengar, S. S.; Tomasi, J.; Barone, V.; Mennucci, B.; Cossi, M.; Scalmani, G.; Rega, N.; Petersson, G. A.; Nakatsuji, H.; Hada, M.; Ehara, M.; Toyota, K.; Fukuda, R.; Hasegawa, J.; Ishida, M.; Nakajima, T.; Honda, Y.; Kitao, O.; Nakai, H.; Klene, M.; Li, X.; Knox, J. E.; Hratchian, H. P.; Cross, J. B.; Adamo, C.; Jaramillo, J.; Gomperts, R.; Stratmann, R. E.; Yazyev, O.; Austin, A. J.; Cammi, R.; Pomelli, C.; Ochterski, J. W.; Ayala, P. Y.; Morokuma, K.; Voth, G. A.; Salvador, P.; Dannenberg, J. J.; Zakrzewski, V. G.; Dapprich, S.; Daniels, A. D.; Strain, M. C.; Farkas, O.; Malick, D. K.; Rabuck, A. D.; Raghavachari, K.; Foresman, J. B.; Ortiz, J. V.; Cui, Q.; Baboul, A. G.; Clifford, S.; Cioslowski, J.; Stefanov, B. B.; Liu, G.; Liashenko, A.; Piskorz, P.; Komaromi, I.; Martin, R. L.; Fox, D. J.; Keith, T.; Al-Laham, M. A.; Peng, C. Y.; Nanayakkara, A.; Challacombe, M.; Gill, P. M. W.; Johnson, B.; Chen, W.; Wong, M. W.; Gonzalez, C.; Pople, J. A. Gaussian, Inc., Pittsburgh PA, 2003.

26. Beurskens, P. T.; Beurskens, G.; de Gelder, R.; Garcia-Granda, S.; Gould, R. O.; Israel, R.; Smits, J. M. M. *The DIRDIF–99.2 program system, Crystallography Laboratory*; University of Nijmegen: The Netherlands, 1999.

27. Sheldrick, G. M. *SHELX-97, Program for the Refinement of Crystal Structures*; University of Göttingen: Göttingen, Germany, 1997.

Chapter 3

Syntheses and Properties of Stannaaromatic Compounds

3.1 Introduction

3.1.1 Aromatic Compounds

Aromatic compounds, *i.e.*, [4*n*+2]π electron ring systems, are widely studied from the viewpoints of not only the fundamental chemistry but also the application towards organic synthesis and material science.[1] The history of aromatic compounds began with the isolation of benzene by Faraday in 1825.[2]

benzene

Cyclic conjugation of π-bonds causes the special features of aromatic compounds as follows:

1. Chemical behavior

Aromatic compounds undergo electrophilic substitution reactions more easily than addition reactions due to the effect of the resonance stabilization.

2. Structural features

Aromatic ring is planar and bond lengths in the aromatic ring become intermediate between those of C–C double and single bonds due to the delocalization of the π-electrons.

3. Energetic features

Stability of the aromatic ring is much enhanced than that without aromaticity.

4. Magnetic features

Aromatic compounds have large ring current effect and unique magnetic features such as anomalous chemical shifts, large magnetic anisotropy, and diamagnetic susceptibility exaltation.

These features are called one simple word, *aromaticity*. However, aromaticity has many criteria due to its variety of features, and evaluation of aromaticity is still a conventional problem.[3] Thus, all (chemical, structural, energetic, and magnetic) criteria must be used to estimate the *aromaticity*.

3.1.2 Heteraromatic Compounds

In the chemistry of aromatic compounds, heteraaromatic compounds such as pyridine, in which one carbon atom of benzene is replaced with a nitrogen atom, has been well known for a long time and their structure and properties have been extensively investigated.

pyridine

phosphabenzene

Since phosphabenzene, phosphorus analogue of pyridine, has been synthesized in 1966,[4] much attention has been focused on aromatic systems containing a heavy atom. Structural analyses of phosphabenzenes revealed that the P–C bond lengths in the ring are in the middle between those of P–C double and single bonds, and the C–C bond lengths of the ring are similar to that of parent benzene, indicating the delocalization of the π electrons on the phosphabenzene rings.

Aromatic systems containing a heavier group 15 element, *i.e.*, arsenic, antimony, and bismuth, have also been studied.[5] Although these compounds were synthesized as stable species and turned out to have aromatic character, they were found to be less stable on going from As to Bi.

arsabenzene

stibabenzene

bismabenzene

Furthermore, boratabenzenes, isoelectronic species of benzene and pyridine, have also been extensively investigated for 30 years.[6] Aromatic characters of boratabenzenes, which are an anionic aromatic ring with 6π-electrons, have been elucidated by structural analyses and complexations with transition metals.[7] Gallatabenzene and its complex were reported in 1995,[8] and it was revealed to have aromaticity similarly.

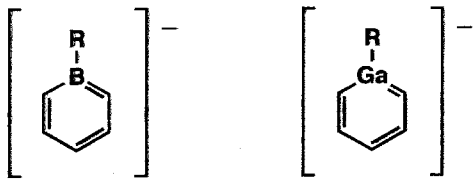

boratabenzenes gallatabenzenes

3.1.3 Stable Sila- or Germaaromatic Compounds

The chemistry of metallaaromatic compounds of heavier group 14 elements, *i.e.*, heavier congeners of the cyclic conjugated systems with $[4n+2]\pi$ electrons, showed a marked development only in the past decade. However, the examples for the isolation of stable systems are limited to those containing Si or Ge atom.[9,10]

3.1.3.1 Ionic Species

Cyclopentadienide Analogues. It is well known that cyclopentadienide ion is an aromatic species with a five-membered 6π electron ring system. The compounds in which one carbon atom of cyclopentadienide ion is replaced by a silicon or a germanium atom are have been well investigated. Metallole dianions (**1**), monoanions (**2**), 1-metallaindenide dianions (**3**), 1-germaindenide anions (**4**), and 9-silafluorenide anion (**5**), were successfully synthesized and characterized.[11,12,13]

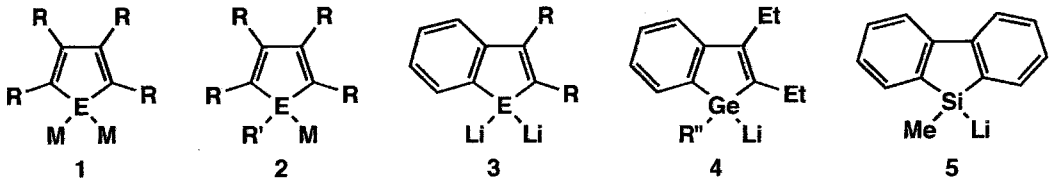

E = Si, Ge
M = Li, Na, K

These species are thermally stable and some of them are structurally characterized by X-ray crystallographic analyses. Although the dianion species (**1**, **3**) have η^5-η^5 or η^1-η^5 interaction mode (Chart 3-1), the endocyclic C–C bond lengths are almost same in the all cases, indicating their π-delocalized structures. On the other hand, all of the monoanion species, which are structurally determined by X-ray crystallographic analysis, feature the localized anion rather than delocalized structure (Chart 3-1).

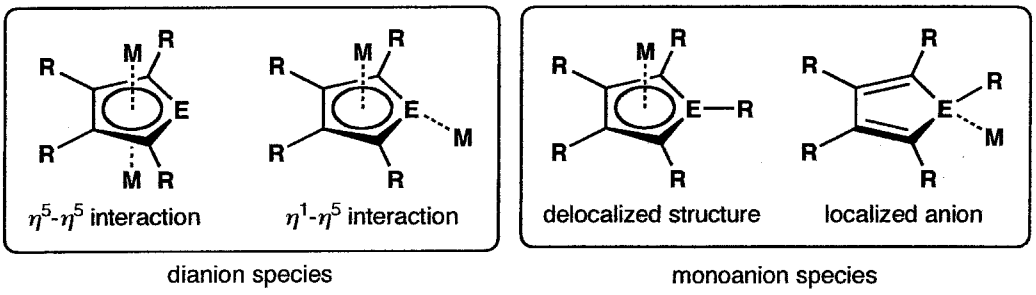

Chart 3-1.

Quite recently, 1,2-disila-3-germacyclopentadienides (**6**, **7**), which contain two silicon atoms and one germanium atom in one cyclopentadienide ring, were reported.[14] The X-ray analysis of **7** revealed a delocalized aromatic cyclopentadienide-type structure with the diagnostic 5-coordination of the Li^+ cation to the five-membered ring.

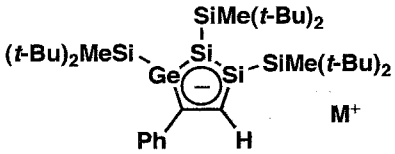

6: M = K
7: M = Li

Some examples of transition metal complexes **8**-**13**, incorporating metallole units as ligands, have also been reported to have an aromatic character.[15,16]

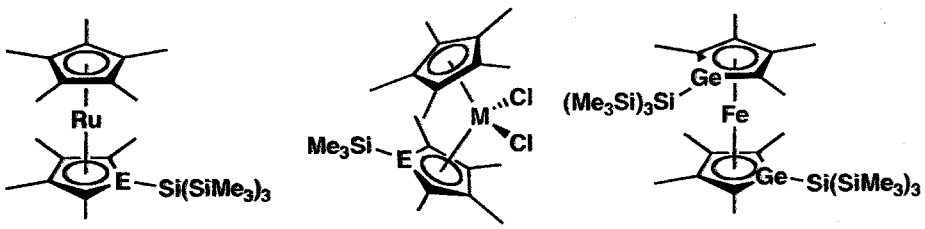

8: E = Si
9: E = Ge

10: E = Si, M = Hf
11: E = Si, M = Zr
12: E = Ge, M = Hf

13

Cyclopropenylium Cation Analogues The cyclopropenium cation possessing a Hückel-type 2π-electron system is the smallest aromatic compound. The germanium analogue **15** was reported in 1997[17] and silicon analogues **14a**-**c** were done in 2005[18] by Sekiguchi.

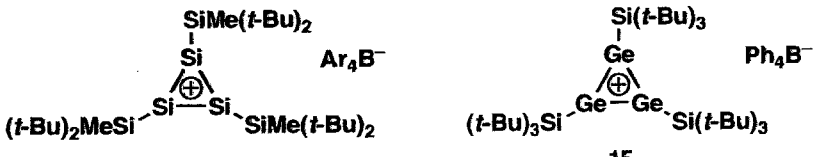

14 **15**

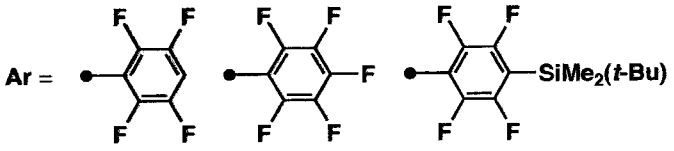

a **b** **c**

According to the X-ray crystallographic analyses of **14c** and **15**, their three-membered rings form an equilateral triangle similar to the carbon analogues, *i.e.*, cyclopropenium cation. The bond lengths of the Si–Si in **14c** and the Ge–Ge in **15** are intermediate between the corresponding double-bond and single-bond lengths.

3.1.3.2 Cyclic Diaminosilylenes and Germylenes

Metallylenes are one of the most important intermediates in the chemistry of group 14 elements. Although metallylenes have been known as highly reactive, unstable species, cyclic

diaminosilylene and germylene **16**, **17** were successfully isolated.[19,20] These compounds are extremely stable, and the unsaturated metallylenes **16** were more stable than the saturated ones **17**. For example, silylene **16a** can be distilled at 94 °C without decomposition in contrast to the fact that silylene **17a** slowly decomposes at room temperature in the solid state.

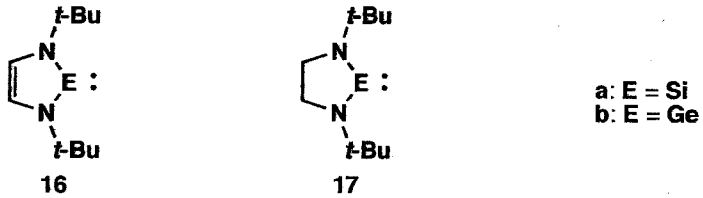

These facts indicated the existence of 6π-aromatic stabilization effect in unsaturated metallylenes **16**, confirmed by further experimental and theoretical investigations. Although the stabilization of metallylenes **16** was dominantly achieved by electron donation from lone pairs of nitrogen atoms to the empty p orbital of silicon, additional stabilization by cyclic delocalization of 6π electrons (two lone pairs on the nitrogen atoms and C=C π electrons) exists in the five-membered ring of unsaturated diaminometallylenes **16** (Figure 3-1). Metallylenes **16** can be regarded as aromatic systems, but they are special cases of aromaticity and very different from common aromatic compounds.

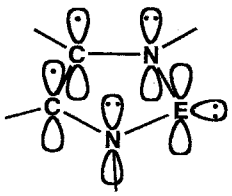

Figure 3-1.

3.1.3.3 Neutral Sila- and Germaaromatic Compounds

Although no synthesis and isolation of neutral sila- and germaaromatic compounds had been reported until very recently due to their extremely high reactivity, sila- and germaaromatic

compounds, to which only one substituent can be introduced on its reactive silicon center, were also synthesized as stable crystalline compounds by taking advantage of this Tbt group.

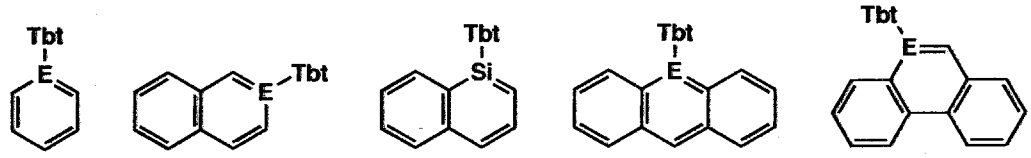

E = Si	18	20	22	23	25
E = Ge	19	21		24	26

Thus, the syntheses of neutral sila- and germaaromatic compounds **18-26** were achieved, and such stable examples of metallaaromatics enabled us to make the systematic elucidations for their aromaticity.[21]

Their aromaticity was evaluated on the basis of NMR, UV/vis and Raman spectroscopic analyses. The molecular structures of them (except **22**) were finally determined by X-ray crystallographic analyses, which revealed the planar geometries of the rings containing an Si or a Ge atom. The lengths of the endocyclic E–C bonds were intermediate between the corresponding double-bond and single-bond lengths, and those for the two endocyclic E–C bonds in the benzene analogues **18** or **19** were found to be essentially equal to each other, indicating their delocalized π-electrons. These results suggested that sila- and germaaromatic compounds **18-26** feature high aromaticity comparable to the parent aromatic compounds.

3.1.4 Stannaaromatic Compounds

As described above, sila- and germaaromatic compounds are widely investigated. However, the syntheses of stannaaromatic compounds were limited to some stannole anions **27-30** by Saito *et al.*[22]

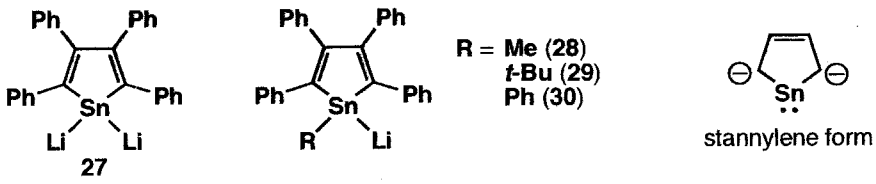

The X-ray crystallographic analysis of **27** revealed its η^5-η^5 interaction mode (Chart 3-1) and the planarity of the stannole ring. The lengths of C–C bonds in the stannole ring were almost equal to each other, and the negative charges are considerably delocalized on the ring. The ^{119}Sn NMR signal for **27** appeared at a relatively low field (δ =163.3), reflecting the strong contribution of a resonance structure along with stannylene character.

Although these results indicate that **27** forms 6π-electron system, they should be classified as special stannaaromatic compounds with negative charges.

3.2 The Purpose in Chapter 3

In view of the recent progress in the chemistry of sila- and germaaromatic compounds, the synthesis of stannaaromatic compounds is of great interest from the standpoint of systematic elucidation of the properties of metallaaromatic systems of heavier group 14 elements. Although some stannole anions and dianions, *i.e.*, ionic stannaaromatic compounds,have been synthesized as stable compounds and fully characterized (Section 3.1.4), neutral stannaaromatic compounds are still elusive and their properties have not been disclosed yet so far. The main reason for the lack of neutral stannaaromatic compounds is probably due to the difficulty in their synthesis and isolation responsible for the extremely high reactivity of Sn–C double bonds.

The successful results in the tetraarylstannene (Chapter 2) and neutral sila- and germaaromatic compound (3.1.3.3) using a Tbt group naturally prompted the author to extend this chemistry to stannaaromatic compounds. As one of the main project in this doctor thesis, the synthesis, structures, and reactivities of 9-stannaphenantherene **31** and 2-stannanaphthalene **32** were investigated in the Chapter 3.

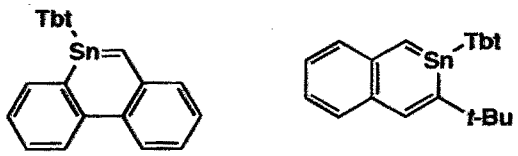

31 32

3.3 Generation of 9-Stannaphenanthrenes

3.3.1 Syntheses of the Precursors

9,10-Dihydro-9-stannaphenanthrenes **33** bearing a leaving group on the tin atom were considered to be suitable precursors of **31**.

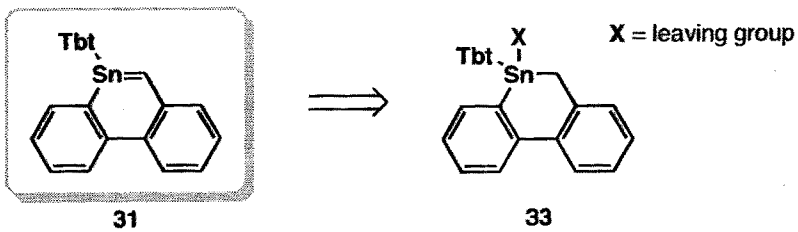

31 33

Initially, the formation of a 9,10-dihydro-9-stannaphenanthrene skeleton was examined by the coupling reaction of **34** with $TbtSnCl_3$ (**35**) using Mg metal followed by the reduction with $LiAlH_4$ (Scheme 3-1). Although Tbt-substituted 9,10-dihydro-9-stannaphenanthrene **36** could be isolated, this reaction suffers from the low-yield process and low reproducibility.

Scheme 3-1.

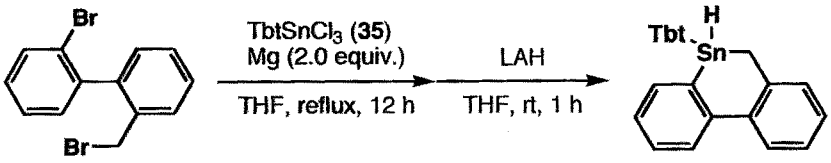

34 36 (up to 17%)

Next, the stepwise synthesis of 9,10-dihydro-9-stannaphenanthrene skeleton was examined and bromostannnane **42** and chlorostannane **43** were prepared according to Scheme 3-2. Since a considerable amount of the bromostannane was formed in the first stannylation step due to the ready halogen-exchange reactions with MgBrCl, the initially generated halostannanes **38** were

subjected to the $LiAlH_4$ reduction followed by the re-chlorination with CCl_4 with the intension of transforming into the corresponding dichlorostannanes **40** in a pure form.

Scheme 3-2.

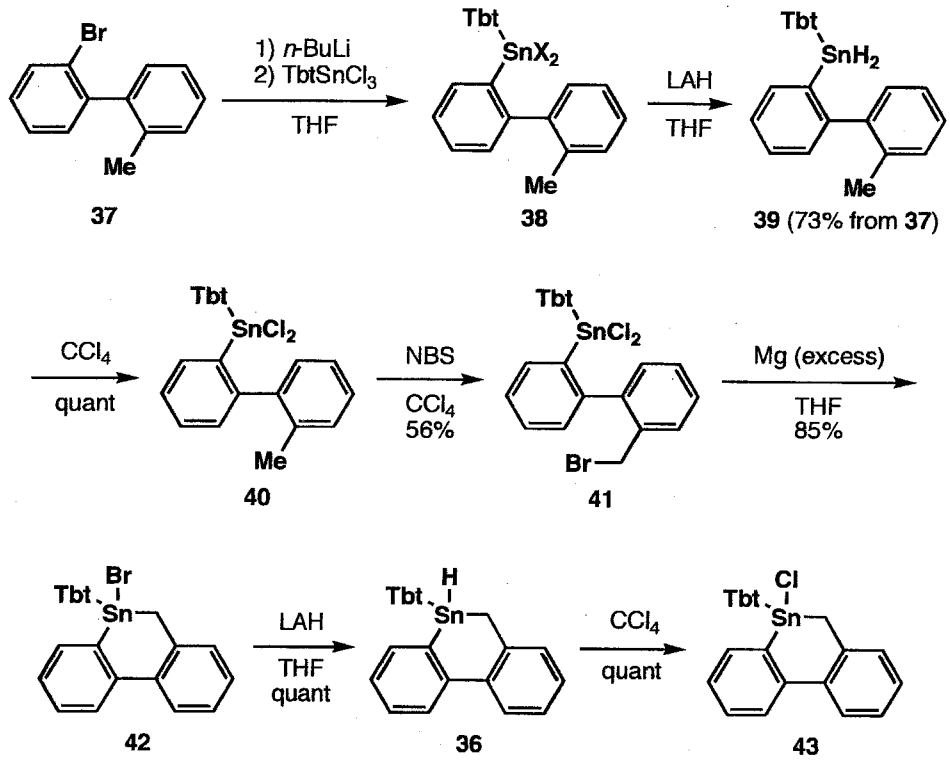

3.3.2 Generation of 9-Stannaphenanthrene 31

Synthesis of **31** was attempted by the dehydrochlorination of **43** with various kinds of bases [lithium hexamethyldisilazide (LHMDS), 1,8-diazabicyclo[5.4.0]undec-7-ene (DBU), and *tert*-butyl lithium]. Although these reactions did not proceed (Scheme 3-3), the reaction of **43** with lithium diisopropylamide (LDA) resulted in the formation of aminostannane **44** as judged by the ^1H NMR spectrum (Scheme 3-4). Compound **44** could not be isolated and fully characterized, and exposure of the C_6D_6 solution of **44** to the air afforded hydroxystannane **45** almost quantitatively. Although compound **45** was also unstable species probably due to the

oligomerization by the dehydration reaction in solution, the structure was determined by X-ray crystallographic analysis (Figure 3-2).

Scheme 3-3.

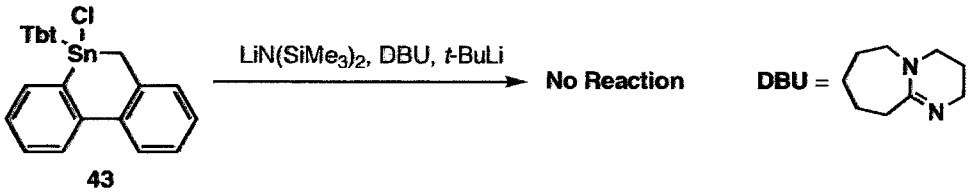

Scheme 3-4.

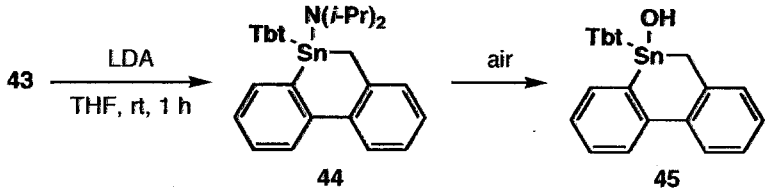

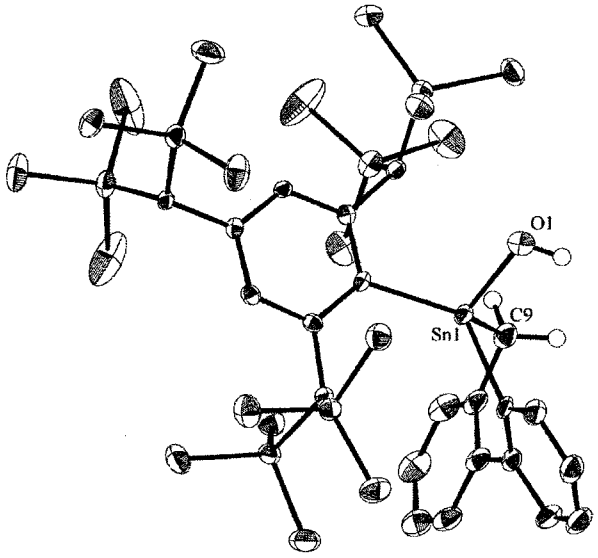

Figure 3-2. X-Ray structure of **45** (ORTEP drawing with 50% probability level). Hydrogen atoms except for those on the O1 and C9 atoms and the other molecule of the crystallographically non-identical molecules were omitted for clarity.

To inhibit such nucleophilic substitution reaction, the reaction with lithium 2,2,6,6-tetramethylpiperidide (LTMP) as a base was performed. The reaction of **43** with LTMP at room

temperature resulted in the stereoselective formation of *cis*-[2+2] dimer **46** (46%) of 9-stannaphenanthrene **31** (Scheme 3-5). The molecular structure of **46** was unambiguously determined by X-ray crystallographic analysis (Figure 3-3).

Scheme 3-5.

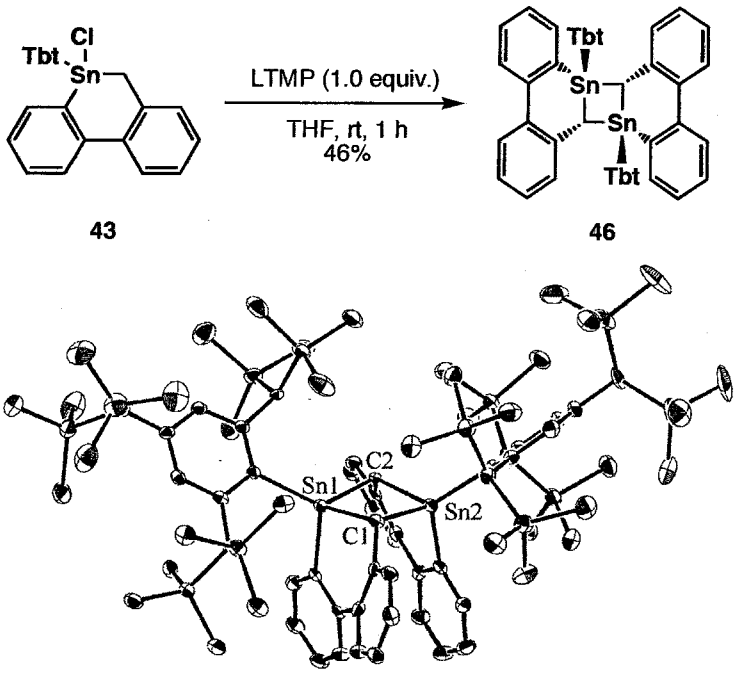

Figure 3-3. X-Ray structure of **46** (ORTEP drawing with 50% probability level). Hydrogen atoms a benzene molecule were omitted for clarity.

3.3.3 Trapping Experiments of 9-Stannaphenanthrene 31

Since the formation of **46** suggested the generation of **31** as a transient species, the trapping experiments at low temperature were examined. To the reaction mixture of **43** and LTMP were added MeOD, Mes*CNO [Mes* = 2,4,6-tri(*tert*-butyl)phenyl], and 2,3-dimethyl-1,3-butadiene as trapping reagents at –78 °C to give the corresponding adducts **47-*d*** (almost quantitative as estimated by ^{1}H NMR), **48** (43% isolated yield), and **49** (67% isolated yield), respectively (Scheme 3-6). Compound **47-*d*** was moisture-sensitive and could not be isolated as a pure

compound because of the difficulty in the separation from 2,2,6,6-tetramethylpiperidine, which is the inevitable byproduct of this reaction. The molecular structure of **47-*d*** was determined by the comparison with that of pure **47**, which was prepared by the reaction of **43** with LiOMe in THF. The molecular structures of **48** and **49** were confirmed with the ^{1}H, ^{13}C, and ^{119}Sn NMR and mass spectral data, and were finally established by X-ray crystallographic analysis (Figures 3-4, 3-5). Since 2,3-dimethyl-1,3-butadiene is inert to anionic species such as 9-chloro-10-lithio-9-Tbt-9,10-dihydro-9-stannaphenanthrene **50**, which is an alternative intermediate in the reactions of **43** with LTMP giving **46**, **47-*d***, and **48**, the formation of a [2+4] cycloadduct **49** from **43** indicates that the reaction of **43** with LTMP affords not an anionic intermediate but a neutral stannaphenanthrene **31**.

These results strongly indicate that **31** exists as a monomer in a THF solution at –78 °C. The thermal instability of **31** is in sharp contrast to the high stability of Tbt-substituted 9-sila- and germaphenanthrene (**25**, **26**), which are stable at 100 °C in C_6D_6.

Scheme 3-6.

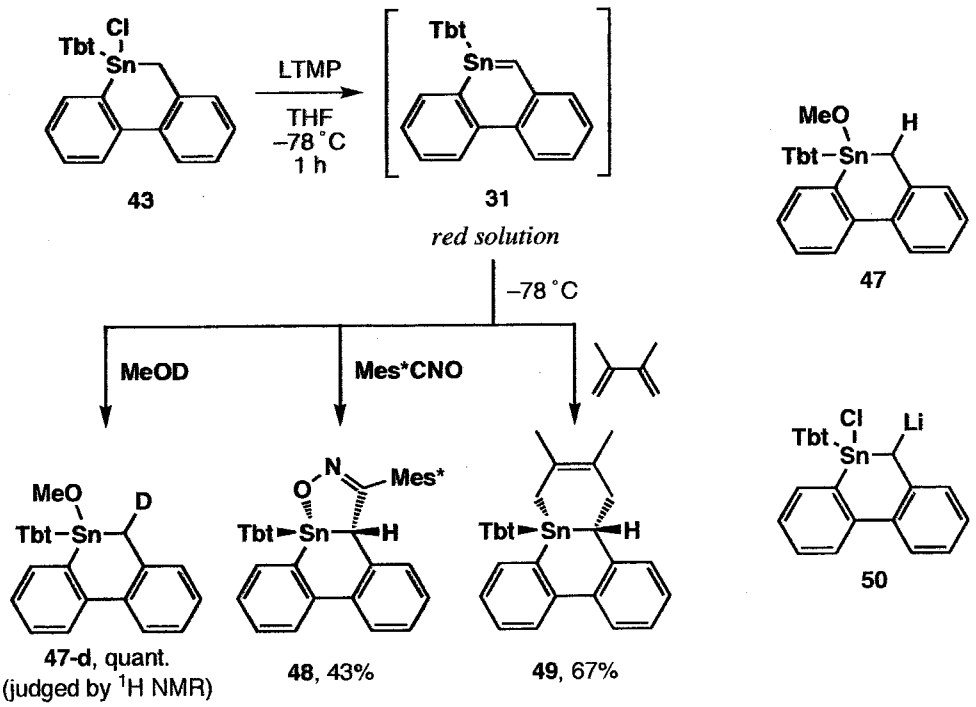

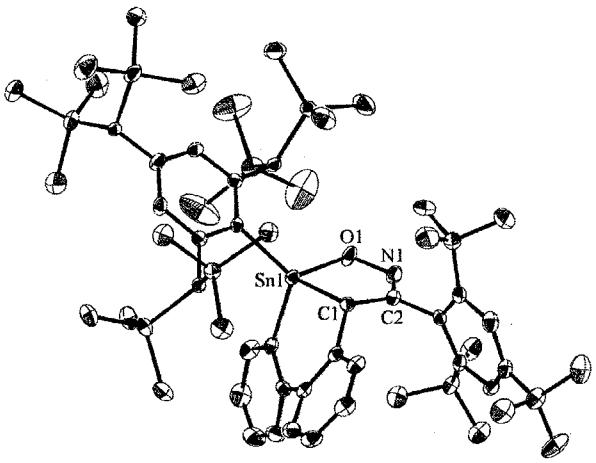

Figure 3-4. X-Ray structure of **48** (ORTEP drawing with 50% probability level). Hydrogen atoms were omitted for clarity.

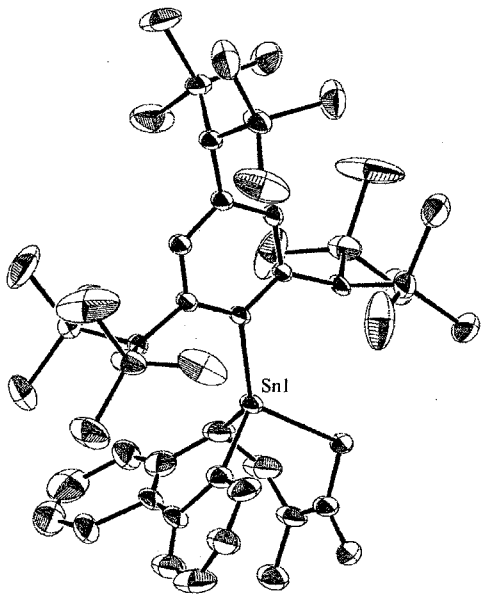

Figure 3-5. X-Ray structure of **49** (ORTEP drawing with 30% probability level). Hydrogen atoms were omitted for clarity.

3.3.4 Attempted Synthesis of 9-Tbt-10-Ph-9-stannaphenanthrene 51

If an additional substituent can be introduced in 10-position, dimerization of 9-stannaphenanthrene may be prevented (Figure 3-6) due to the steric repulsion. Therefore, synthesis of **51** bearing phenyl group on 10-position was attempted.

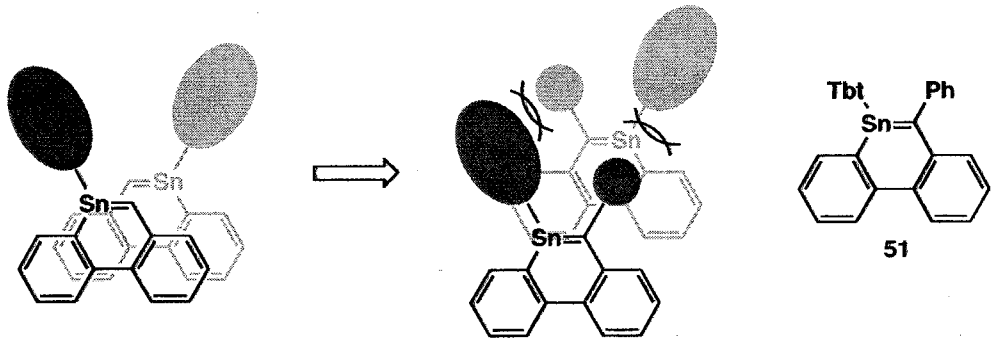

Figure 3-6.

Synthetic strategy for **51** was similar to that for **31**, and the suitable precursors **59**, **60**, and **61** were prepared according to Scheme 3-7. Molecular structure of **59** was finally determined by the X-ray crystallographic analysis (Figure 3-7).

Scheme 3-7.

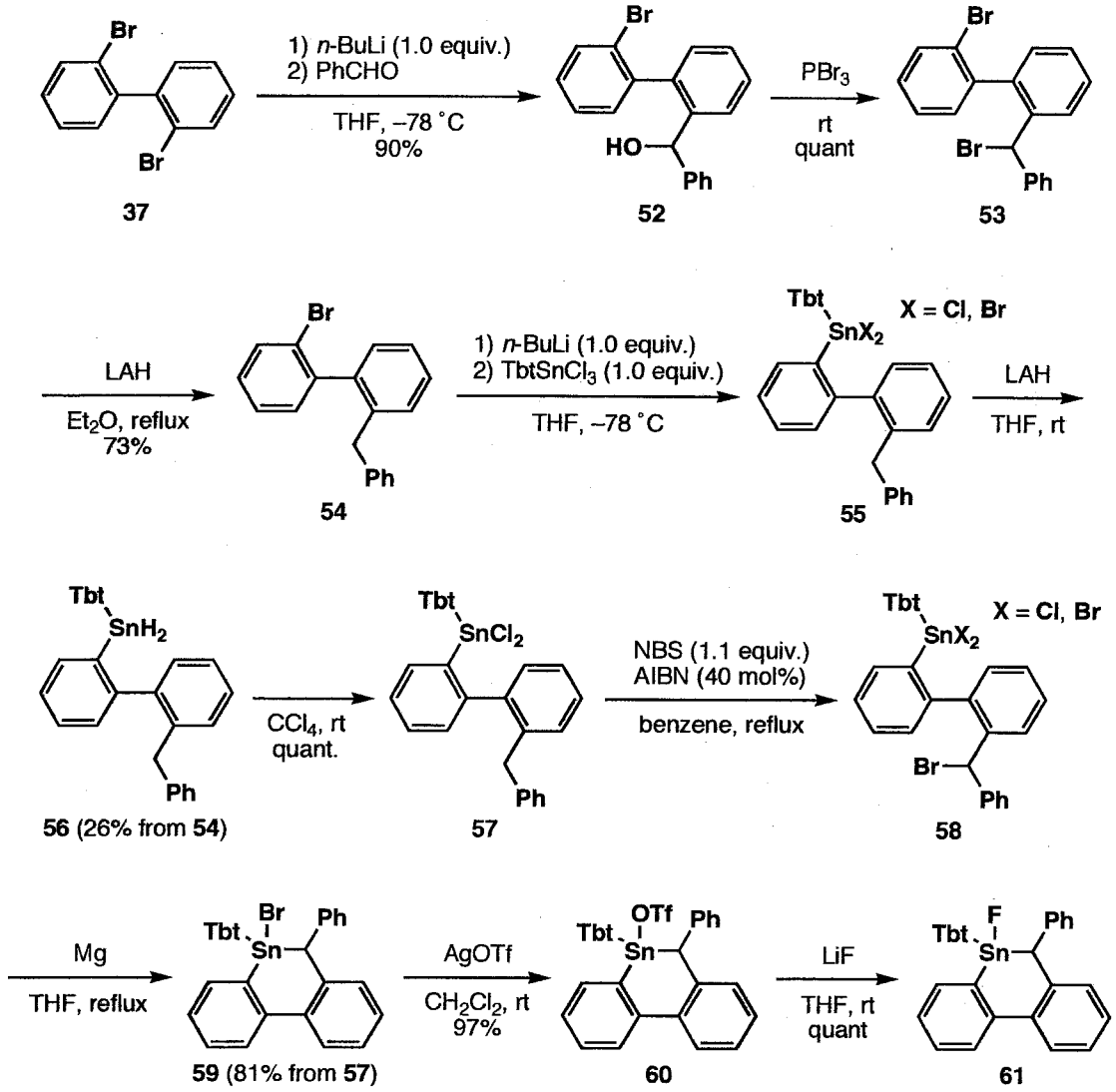
Br
Br
37
1) n-BuLi (1.0 equiv.)
2) PhCHO
THF, –78 °C
90%
Br
HO
Ph
52
PBr3
rt
quant
Br
Br
Ph
53
LAH
Et2O, reflux
73%
Br
Ph
54
1) n-BuLi (1.0 equiv.)
2) TbtSnCl3 (1.0 equiv.)
THF, –78 °C
Tbt
SnX2
X = Cl, Br
Ph
55
LAH
THF, rt
Tbt
SnH2
Ph
56 (26% from 54)
CCl4, rt
quant.
Tbt
SnCl2
Ph
57
NBS (1.1 equiv.)
AIBN (40 mol%)
benzene, reflux
Tbt
SnX2
X = Cl, Br
Br
Ph
58
Mg
THF, reflux
Tbt
Br
Sn
Ph
59 (81% from 57)
AgOTf
CH2Cl2, rt
97%
Tbt
OTf
Sn
Ph
60
LiF
THF, rt
quant
Tbt
F
Sn
Ph
61

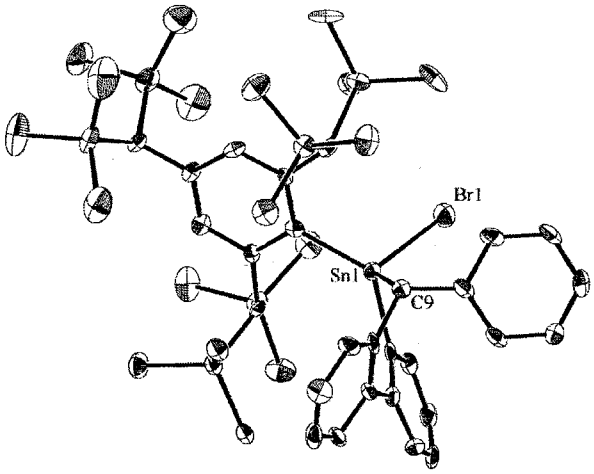

Figure 3-7. X-Ray structure of **59** (ORTEP drawing with 50% probability level). Hydrogen atoms and a chloroform molecule were omitted for clarity.

The reaction of bromostannane **59** with LDA did not proceed (Scheme 3-8) probably due to the steric reason of the Br atom. However, the reaction of fluorostannane **61** with LDA was performed to afford aminostannane **62** (Scheme 3-9).

Scheme 3-8.

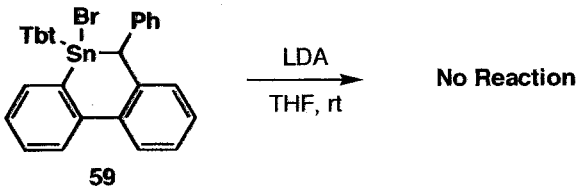

Scheme 3-9.

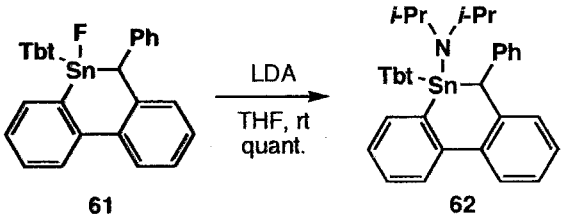

Similarly, the reaction of **61** with *t*-butyllithium gave *t*-butylstannane **63** (Scheme 3-10), indicating the steric hindrance around the proton in the 10-position.

Scheme 3-10.

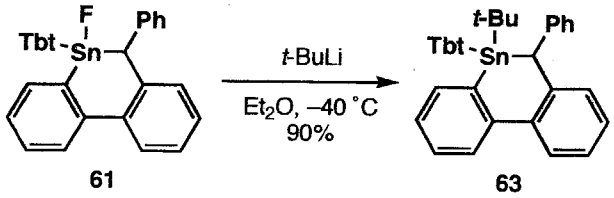

In the case of the generation of **31**, LTMP was effective for the inhibition of nuculeophilic substitution reaction. However, the reaction of **61** with LTMP resulted in the formation of a complicated mixture (Scheme 3-11).

Scheme 3-11.

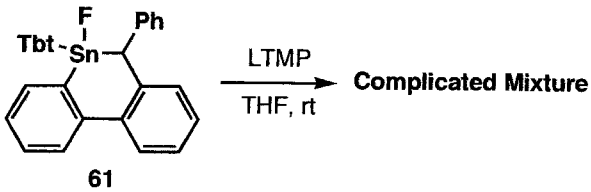

As a result, steric congestion around the proton in 10-position inhibited smooth reaction, suggesting that additional substituents should be introduced to not the 10-position but the 1-8 position.

3.3.5 Conclusion of Section 3.3

In summary, the author has succeeded in the generation of 9-stannaphenanthrene **31** for the first time and revealed its high reactivities. With the hope of isolating **31** as a stable compound, further investigation on the introduction of additional substituent(s) to the stannaphenanthrene skeleton (except the 10-position) and the cooperative stabilization method (the contribution of kinetic and thermodynamic stabilization) are currently in progress.

3.4 Synthesis of 2-Stannanaphthalene 32

3.4.1 Synthesis of the Precursor

1,2-Dihydro-2-stannanaphthalene **67** was prepared by taking advantage of *(E)-o-*(2'-lithiovinyl)benzyllithium **65**, which can be readily generated from isotellurochromene **64** according to the method reported by Sashida[23] (Scheme 3-12). The reason why the synthetic method similar to those used for the Tbt-substituted 1,2-dihydro-2-sila- and 2-germanaphthalenes **70** (Scheme 3-13) should be prevented is that the cleavage reaction of weak tin–carbon bond may proceed in the double-bond formation using excess NBS.

The following bromination of **67** with NBS afforded bromostannane **68**, a suitable precursor of 2-stannanaphthalene **32** (Scheme 3-12).

Scheme 3-12.

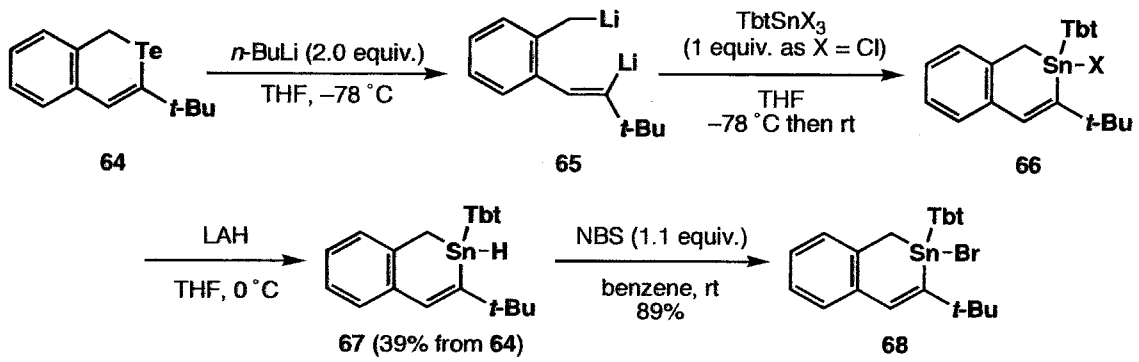

Scheme 3-13. Syntheses of the Tbt-substituted 1,2-Dihydro-2-sila- and 2-germanaphthalenes

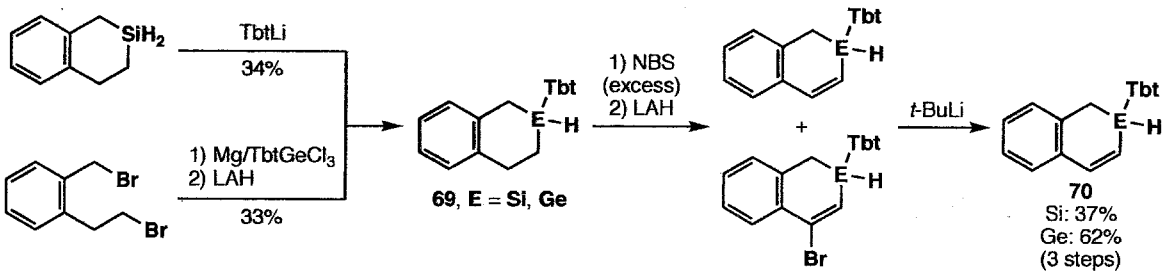

3.4.2 Synthesis of 2-Stannanaphthalene 32

2-Stannanaphthalene **32** was synthesized as pale yellow crystals by the dehydrobromination of bromostannane **68** with LDA in hexane at –40 °C (Scheme 3-14). 2-Stannanaphthalene **32** is thermally stable under an inert atmosphere either in the solid state (decomposed at 144 °C) or in solution (C_6D_6, at 80 °C for 1 h in a sealed tube).

Scheme 3-14.

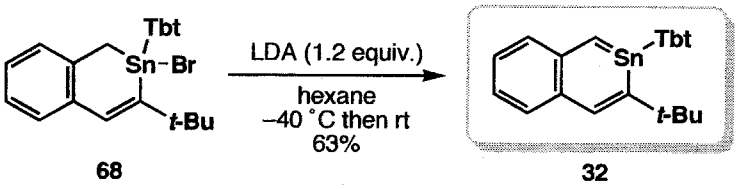

3.4.3 Crystal Structure of 2-Stannanaphthalene 32

The molecular structure of **32** was determined by X-ray crystallographic analysis (Figures 3-8, 3-9), which revealed the planarity of the 2-stannanaphthalene moiety and the completely trigonal planar geometry around the tin atom. In addition, the benzene ring of the Tbt group was found to be almost perpendicular to the 2-stannanaphthalene plane, and hence it is considered that there is very little conjugative interaction between the two aromatic units. The lengths of the two endocyclic Sn–C bonds [2.029(6) and 2.081(6) Å] are shorter than those of typical single bonds (av. 2.14 Å). In particular, the former Sn–C bond length is close to the Sn–C double bond length of the stable stannene synthesized in this work (see, Chapter 2), Tbt(Mes)Sn=CR_2 [CR_2 = fluorenylidene; 2.016(5) Å], which is stabilized by the conjugation of the Sn–C double bond with the fluorenylidene moiety. The C–C bond lengths of the 2-stannanaphthalene ring of **32** [1.356(9)-1.443(9) Å] are also roughly intermediate between those of C–C double and single bonds. These results suggest that the π–electrons are delocalized in the 2-stannanaphthalene skeleton of **32**. Furthermore, theoretical calculations for the model molecules **71-73** supported

the experimental results, indicating the effective π-conjugation in the Sn-containing aromatic ring systems (Table 3-1).

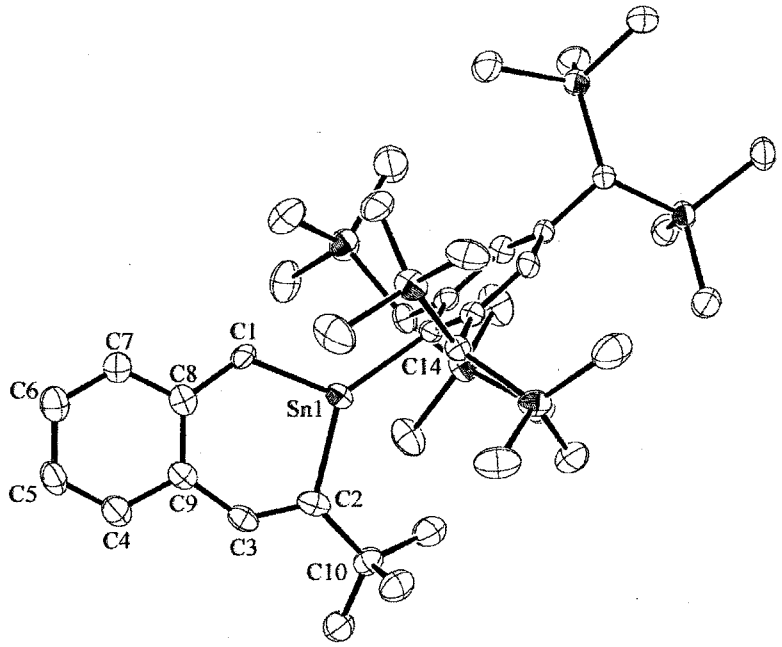

Figure 3-8. X-Ray structure of **32** (ORTEP drawing with 50% probability level). Hydrogen atoms were omitted for clarity.

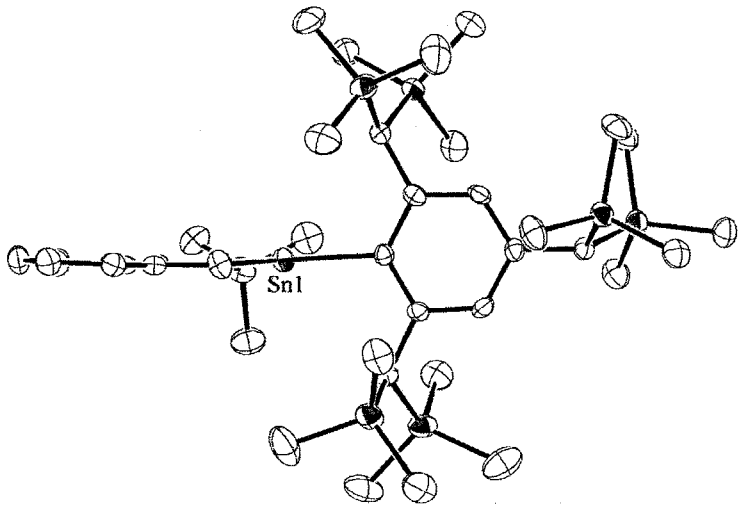

Figure 3-9. ORTEP drawing of **32** (50% probability level) along the C1→C2 atoms. Hydrogen atoms were omitted for clarity.

Chart 3-2.

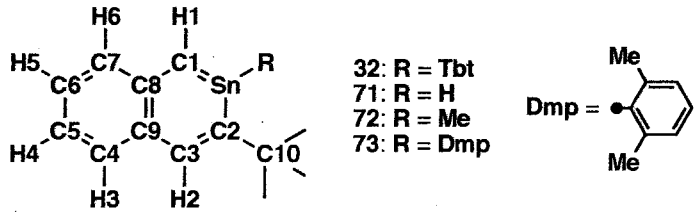

Table 3-1. Observed and calculated bond lengths (Å) for 2-stannanaphthalenes[a]

bond	**32** (obsd)	**71** (calcd)	**72** (calcd)	**73** (calcd)
C1–C8	1.394(8)	1.423	1.424	1.422
C1–Sn	2.029(6)	1.985	1.988	1.993
Sn–C2	2.081(6)	2.067	2.073	2.066
C2–C3	1.372(9)	1.374	1.374	1.380
C3–C9	1.443(9)	1.445	1.445	1.440
C4–C9	1.417(9)	1.423	1.423	1.425
C4–C5	1.356(9)	1.378	1.378	1.377
C5–C6	1.415(10)	1.411	1.411	1.413
C5–C7	1.361(9)	1.375	1.375	1.375
C7–C8	1.419(9)	1.431	1.431	1.432
C8–C9	1.436(9)	1.447	1.447	1.449
C2–C10	1.522(9)	1.535	1.535	1.541

[a] calculated at the B3LYP/6-31G(d) (LANL2DZ on Sn) level.

3.4.4 NMR Spectra of 2-Stannanaphthalene 32

The ^{119}Sn NMR spectrum of **32** in C_6D_6 showed a signal at 264 ppm, which is characteristic of the low-coordinated tin atom. All of the ^{1}H NMR signals of the protons of the 2-stannanaphthalene ring of **32** (7.05-9.28 ppm) were observed in the aromatic region, and the ^{13}C NMR signals of the stannanaphthalene ring carbons (120.0-174.0 ppm) were located in the sp^2 region. Thus, these results clearly indicate the delocalized π-electronic system of **32** even in solution. The assignments of the ^{1}H, ^{13}C, and ^{119}Sn NMR signals are listed in Table 3-2 along

with the calculated values for **71**-**73**. The observed values are in good agreement with the calculated ones.

Table 3-2. Observed and calculated ^{119}Sn, ^{1}H, and ^{13}C NMR chemical shifts (ppm) for 2-stannanaphthalenes

atom	**32** (obsd)[a]	**71** (calcd)[b]	**72** (calcd)[b]	**73** (calcd)[c]
Sn	264	123	273	150
H1	9.28	9.25	8.58	8.42
H2	8.75	8.79	8.57	8.91
H3	7.65	7.88	7.71	7.80
H4	7.05	7.38	7.01	7.17
H5	7.21	7.31	7.25	7.35
H6	7.68	7.64	7.59	7.66
C1	147.4	147.9	139.4	136.5
C2	174.0	175.4	173.8	169.9
C3	142.2	143.4	143.2	149.6
C4	135.4	137.0	136.9	136.6
C5	120.0	121.9	120.4	119.4
C6	125.3	125.3	126.0	125.4
C7	128.0	129.1	128.7	128.8
C8	147.3	149.9	148.8	151.0
C9	125.9	129.2	127.1	126.9
C10	39.7	42.5	41.2	41.8

[a] measured in benzene-d_6. [b] caluculated at the GIAO-B3LYP/6-311G+(2d,p) (TZV on Sn)//B3LYP/6-31G(d) (LANL2DZ on Sn) level. [c] caluculated at the GIAO-B3LYP/6-311G+(2d,p) (TZV on Sn)//B3LYP/6-31G(d) [TZ(2d) on Sn] level.

3.4.5 Raman Spectrum of 2-Stannanaphthalene 32

The Raman spectrum of **32** (Figure 3-10) showed planar skeletal vibration as the most intense Raman signal at 1331 cm^{-1}, which corresponds to those of 1382, 1368, and 1360 cm^{-1} for naphthalene, 2-silanaphthalene, and 2-germanaphthalene respectively. The calculated vibration

modes of **71** considerably resemble those of naphthalene, suggesting the skeletal similarity between 2-stannanaphthalene **32** and naphthalene (Figure 3-11).

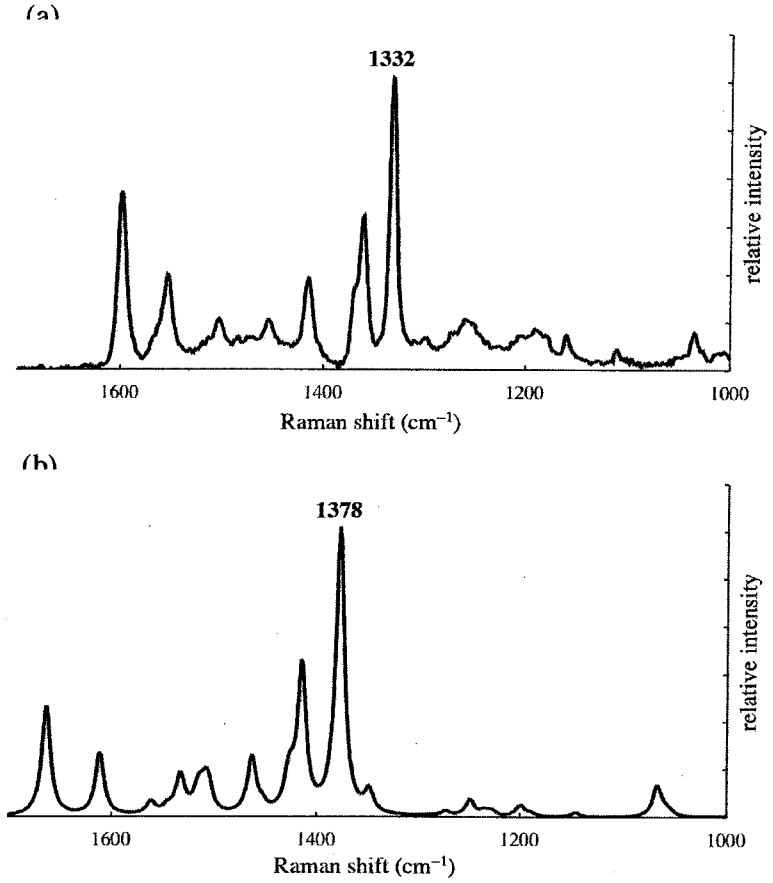

Figure 3-10. Raman spectra of 2-stannanaphthalenes. (a) FT-Raman spectrum of **32** measured with the excitation by He-Ne laser (532 nm). (b) Spectrum of **71** simulated by the theoretical calculation at the B3LYP/6-31G(d) (LANL2DZ on Sn) level.

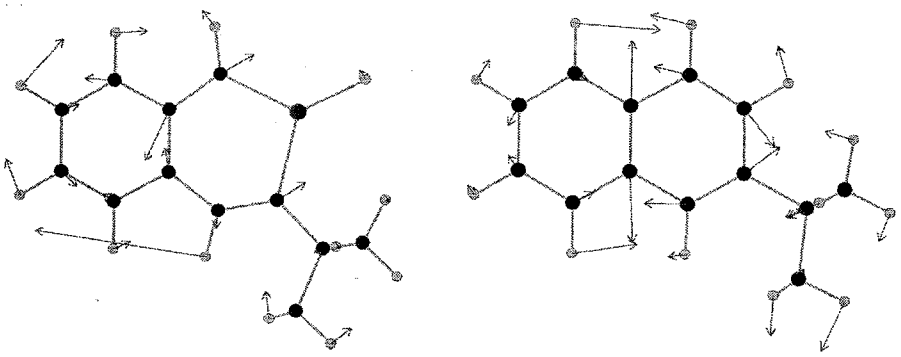

Figure 3-11. Calculated vibration modes of **71** (1378 cm^{-1}, left) and 2-*tert*-butylnaphthalene (1424 cm^{-1}, right).

3.4.6 UV/vis Spectrum of 2-Stannanaphthalene 32

In Figure 3-12 are shown the UV/vis spectrum of 2-stannanaphthalene **32** measured in hexane at room temperature. Four absorption maxima [230 (ε 5.2 × 10^4), 250 (sh, ε 3.4 × 10^4), 295 (ε 1.4 × 10^4), and 393 (ε 1.4 × 10^4) nm] were observed. The latter two maxima are most likely assignable to the β and p bands, respectively, and the weak α band may overlap to p band. These values apparently shift to longer wavelength than those for naphthalene, 2-silanaphthalene **20**, and 2-germanaphthalene **21** (Table 3-3).

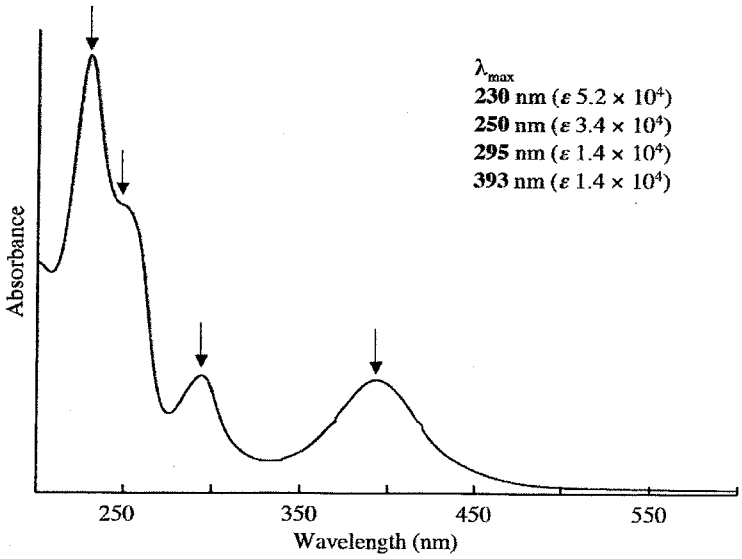

Figure 3-12. UV/vis spectrum of **32** (in hexane, rt).

Table 3-3. Absorption maxima (nm) of 2-stannanaphthalene **32**, 2-germanaphthalene **21**, 2-silanaaphthalene **20**, and naphthalene.

32	**21**	**20**	naphthalene	band
295 (ε 1.4 × 10^4)	269 (ε 2 × 10^4)	267 (ε 2 × 10^4)	221 (ε 1.3 × 10^5)	β
393 (ε 1.4 × 10^4)	335 (ε 1 × 10^4)	327 (ε 7 × 10^3)	286 (ε 9.3 × 10^3)	p
–	386 (ε 2 × 10^3)	369 (ε 1 × 10^3) 387 (ε 2 × 10^3)	312 (ε 2.9 × 10^2)	α

3.4.7 Cyclic Voltammogram of 32

A parent naphthalene is known to react with alkali metals (Li, Na, K...) to give the corresponding radical anions (metal naphthalenides) as shown in Scheme 3-15. As described above (Section 3.4.3-3.4.6), 2-stannanaphthalene **32** was found to have sufficient aromaticity comparable to parent naphthalene, judging from their structure and spectroscopic data. One can hit upon a natural question whether 2-stannanaphthalene can be reduced as in the case of a parent naphthalene or not.

Scheme 3-15.

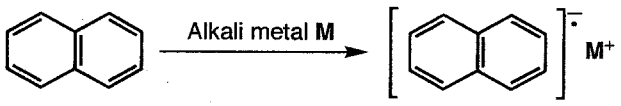

The electrochemical properties of **32** were furnished by cyclic voltammetry, measurement of which was carried out in THF with n-Bu_4NBF_4 as an electrolyte at room temperature. For comparison, the measurement of cyclic voltammetry for parent naphthalene was performed under similar conditions. The voltammograms were shown in Figure 3-13 and summarized in Table 3-4.

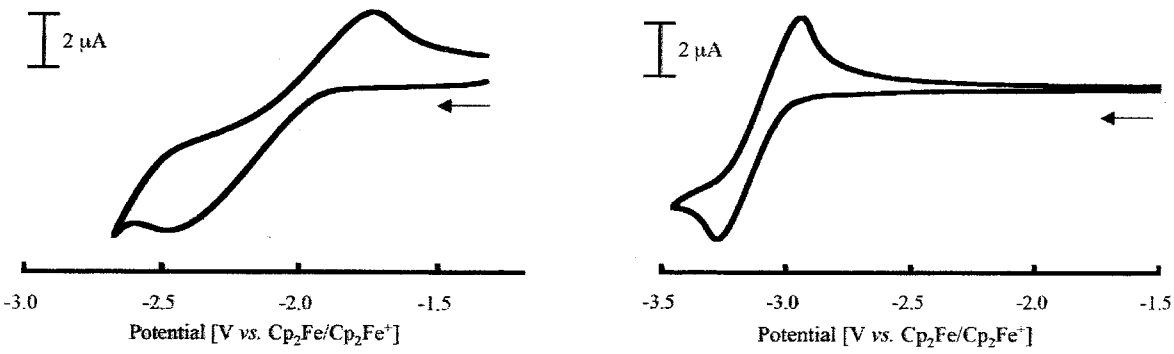

Figure 3-13. Cyclic voltammogram of **32** (left) and naphthalene (right) in THF.

Table 3-4. Redox potentials in THF [V *vs.* Cp_2Fe/Cp_2Fe^+]

	E_{pa}	E_{pc}	$E_{1/2}$
32	–2.48	–1.74	–2.11
naphthalene	–3.28	–2.94	–3.11

As in the case of parent naphthalene, pseudo-reversible one-electron reduction wave of **32** was observed at $E_{1/2}$ = –2.11 V versus Cp_2Fe/Cp_2Fe^+, the reduction potential of which was lower than that of naphthalene ($E_{1/2}$ = –3.11). These well-defined reversible redox waves indicate that the corresponding 2-stannanaphthalene radical anion can be generated with chemical stability under such conditions.

3.4.8 Complexation of 2-Stannanaphthalene 32

Tbt-substituted sila- and germabenzenes **18**, **19** are known to behave as a 6π arene system toward the complexation with transition metal carbonyl complexes leading to the formations of **74**, **75**, respectively (Scheme 3-16).[24]

Scheme 3-16.

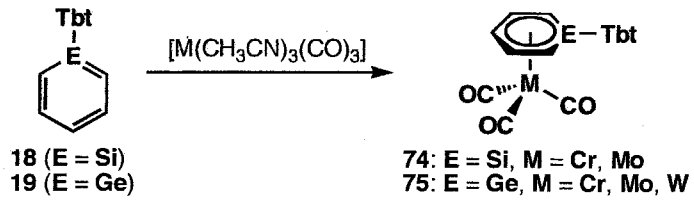

Similarly, the ligand exchange reaction of **32** with $[Cr(CH_3CN)_3(CO)_3]$ at room temperature in THF resulted in the regioselective formation of the first stable η^6-2-stannanaphthalene chromium complex **76** as brown crystals in 89% yield (Scheme 3-17).

Scheme 3-17.

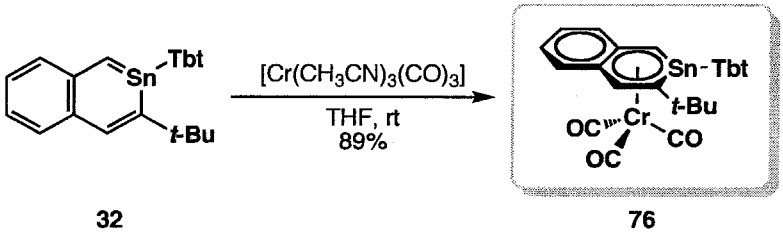

The X-ray crystallographic analysis of **76** (Figure 3-14) revealed that **76** still keeps the planarity for the 2-stannanaphthalene moiety [sum of the interior bond angles in the ring **A** (Chart 3-3): 718.7°] and the trigonal planar geometry around the tin atom (sum of the bond angles: 359.0°). The lengths of the two endocyclic Sn–C bonds of **76** [2.035(5) and 2.093(4) Å] are slightly longer than those of **32** [2.029(6) and 2.081(6) Å]. Although theoretical calculations for the Dmp-substituted model molecule **78** and the real molecule **76** supported the experimental results, the optimized structure of Me-substituted model molecule **77** showed the pyramidarized geometry at the tin atom, indicating the almost η^5-coordination of the C_5 moiety in the ring **A** (Chart 3-3, Table 3-5, Figure 3-15). This result suggests that the η^6-fashion in the coordination of the 2-stannanaphthalene ring toward the chromium observed in **76** depends on the steric requirements.

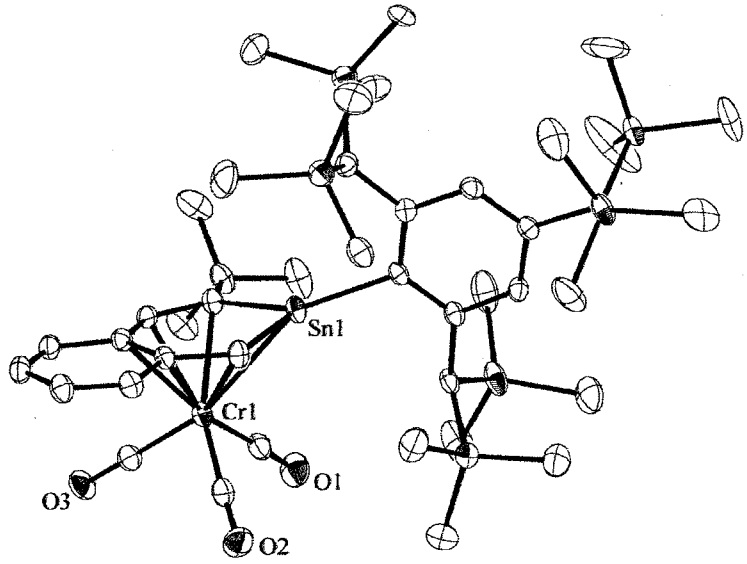

Figure 3-14. X-Ray structure of **76** (ORTEP drawing with 30% probability level). Hydrogen atoms were omitted for clarity.

Chart 3-3.

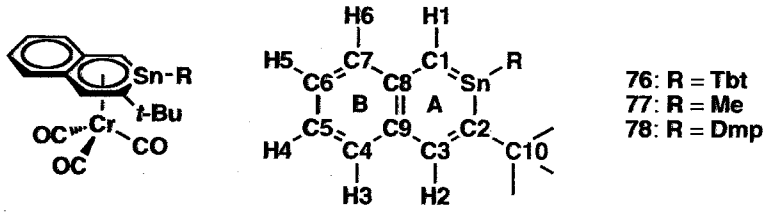

Table 3-5. Observed and calculated bond lengths (Å) for η^6-2-stannanaphthalene chromium complexes.[a]

bond	**76** (obsd)	**77** (calcd)[a]	**78** (calcd)[a]	**76** (calcd)[a]	**32** (obsd)
C1–C8	1.425(6)	1.441	1.432	1.427	1.394(8)
C1–Sn	2.036(5)	2.067	2.026	2.036	2.029(6)
Sn–C2	2.093(4)	2.119	2.090	2.103	2.081(6)
C2–C3	1.381(6)	1.395	1.392	1.391	1.372(9)
C3–C9	1.441(6)	1.457	1.455	1.453	1.443(9)
C4–C9	1.439(6)	1.428	1.431	1.432	1.417(9)
C4–C5	1.354(6)	1.374	1.372	1.371	1.356(9)
C5–C6	1.408(7)	1.415	1.417	1.419	1.415(10)
C5–C7	1.363(6)	1.373	1.371	1.370	1.361(9)
C7–C8	1.448(6)	1.431	1.435	1.438	1.419(9)
C8–C9	1.427(6)	1.445	1.445	1.445	1.436(9)
C2–C10	1.533(6)	1.546	1.546	1.547	1.522(9)
Sn–Cr	2.7536(8)	2.858	2.767	2.748	–
C1–Cr	2.306(5)	2.201	2.338	2.357	–
C2–Cr	2.417(5)	2.372	2.481	2.528	–
C3–Cr	2.244(4)	2.262	2.305	2.326	–
C8–Cr	2.317(4)	2.389	2.418	2.405	–
C9–Cr	2.284(5)	2.406	2.378	2.374	–

[a] calculated at the B3LYP/6-31G(d) [TZ(2d) on Sn] level.

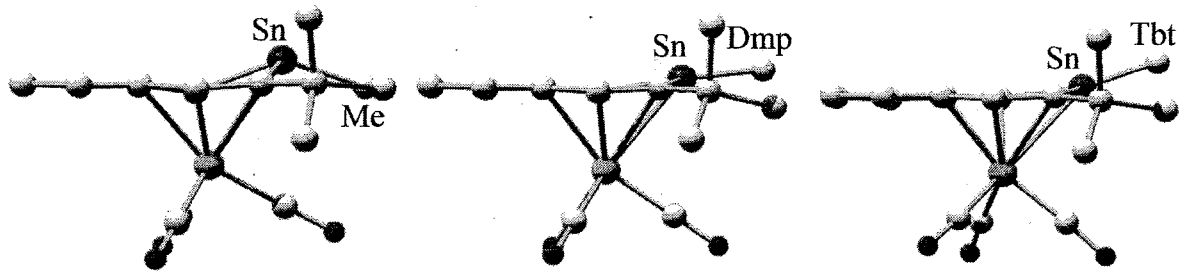

77 (calcd) **78** (calcd) **76** (obsd)

Figure 3-15. Side views of η^6-2-stannanaphthalene chromium complexes. Hydrogen atoms and the substituents on the tin atoms [except Me (**77**) and ipso carbons (**76**, **78**)] were omitted for clarity.

In ^{1}H, ^{13}C, and ^{119}Sn NMR spectra of **76**, the signals correspond to the atoms in the ring **A** (δ_{Sn}: 106, δ_{H1}: 5.10, δ_{H2}: 6.43, δ_{C}: 88.4-131.3) were shifted to upfield region relative to those for the free **32** (δ_{Sn}: 264, δ_{H1}: 9.28, δ_{H2}: 8.75, δ_{C}: 120.0-174.0). The assignments of the ^{1}H, ^{13}C, and ^{119}Sn NMR signals are listed in Table 3-6 along with the calculated values for **77**, **78**, and **76**. The observed values are in good agreement with the calculated ones for **78** and **76**.

Table 3-6. Observed and calculated ^{119}Sn, ^{1}H, and ^{13}C NMR chemical shifts (ppm) for η^{6}-2-stannanaphthalene chromium complexes.

atom	**76** (obsd)[a]	**77** (calcd)[b]	**78** (calcd)[c]	**78** (calcd)[d]	**76** (calcd)[c]	**32** (obsd)[a]
Sn	106	−150	79	70	128	264
H1	5.10	7.73	5.42	5.38	4.36	9.28
H2	6.43	6.68	6.50	6.54	6.51	8.75
H3	7.33	7.66	7.56	7.73	7.69	7.65
H4	~6.9[e]	7.43	7.26	7.41	7.29	7.05
H5	~6.9[e]	7.53	7.36	7.52	7.35	7.21
H6	~7.0[e]	7.51	7.30	7.44	7.27	7.68
C1	88.4	148.9	88.0	85.0	78.5	147.4
C2	131.3	185.8	131.7	129.5	121.1	174.0
C3	102.8	105.7	102.3	101.9	105.5	142.2
C4	134.6	136.4	129.6	131.1	129.5	135.4
C5	125.2	129.6	119.2	120.9	118.8	120.0
C6	128.7	131.0	122.9	124.8	122.6	125.3
C7	132.9	132.2	125.7	127.2	126.2	128.0
C8	116.8	121.6	114.9	114.6	116.2	147.3
C9	96.4	106.2	94.7	94.2	93.7	125.9
C10	38.4	45.2	40.2	39.4	39.1	39.7
CO	233.8	244.5	224.0	228.3	225.0	–
		246.7	224.8	228.9	225.5	
		255.1	234.0	237.6	234.8	

[a] measured in benzene-d_6. [b] caluculated at the GIAO-B3LYP/6-311G+(2d,p) (TZV on Sn)//B3LYP/6-31G(d) [TZ(2d) on Sn] level. [c] caluculated at the GIAO-B3LYP/6-31G(d) (TZV on Sn)//B3LYP/6-31G(d) [TZ(2d) on Sn] level. [d] caluculated at the GIAO-MPW1PW91/6-31G(d) (TZV on Sn)//B3LYP/6-31G(d) [TZ(2d)] on Sn level. [e] These signals are observed in the range between 6.85-7.00 but cannot be exactly assigned due to the overlap of the signals.

The IR spectrum (KBr) of **76** showed the presence of three intense ν(CO) bands at 1941, 1862, and 1851 cm^{-1}, which were observed in the region similar to those of [η^6-(naphthalene)$Cr(CO)_3$] [1941 and 1864 cm^{-1} (KBr)[25]]. The result suggests that **32** has coordination ability as an arene ligand almost the same as that of naphthalene.

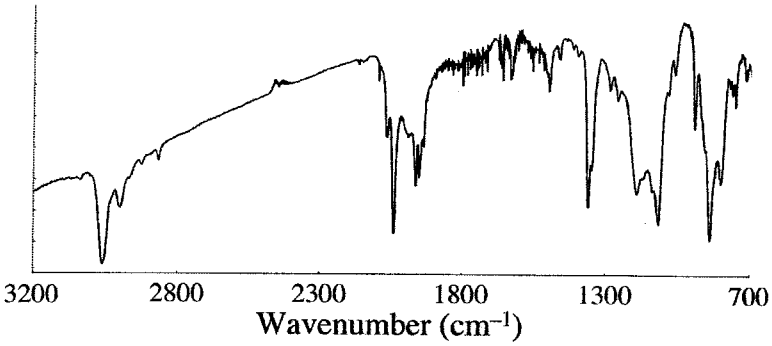

Figure 3-16. IR Spectrum of **76** (thin layer).

In Figure 3-17 are shown the UV/vis spectrum of **76**, which showed two absorption maxima observed at 228 (ε 6.1 × 10^4) and 304 (ε 1.4 × 10^4) and several absorptions (shoulder) in the range below ~600 nm. Although the assignments of these absorption were not achieved, weak absorptions in the long wavelength area (400~600 nm) might be able to be assigned metal-to-ligand charge transfer (MLCT) bands.

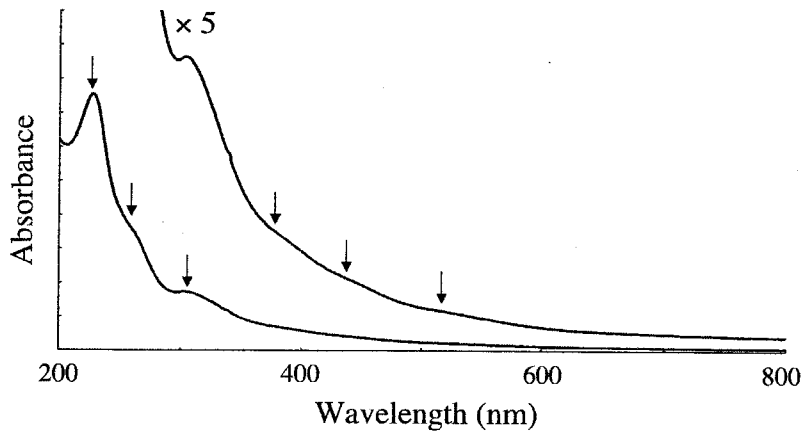

Figure 3-17. UV/vis Spectrum of **76** (in hexane, rt).

3.5 Theoretical Calculations for Stannaaromatic Compounds

As mentioned above, the thermal stability is quite different between 9-stannaphenanthrene **31** and 2-stannanaphthalene **32**. The main reason for the difference is the existence of the additional protection group, *t*-butyl on **32**. In order to elucidate the reasons for the difference, theoretical calculations for various stannaaromatic compounds were performed.

3.5.1 Optimized Structures of Stannaaromatic Compounds

The geometry optimizations for stannabenzenes **79**, 1-stannanaphthalenes **80**, 2-stannanaphthalenes **81**, and 9-stannephenanthrenes **82** bearing H, Me, and Dip substituents, respectively, were carried out at B3LYP/6-31G(d) (LANL2DZ on Sn) level. Although the optimized structures for stannabenzenes **79** and stannanaphthalenes **80** and **81** have planar geometries for the aromatic rings, those of **82** have a distorted 9-stannaphenanthrene ring and the *trans*-bent structure around the Sn=C unit in all cases of **82a-c** (Figure 3-18).

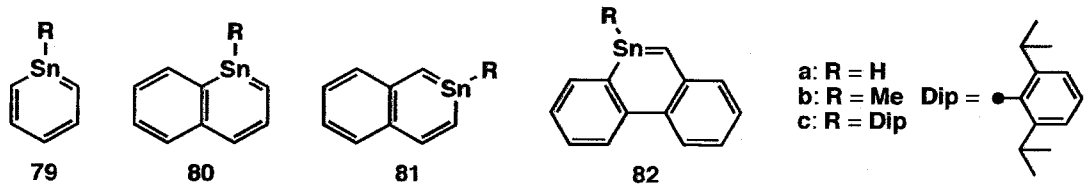

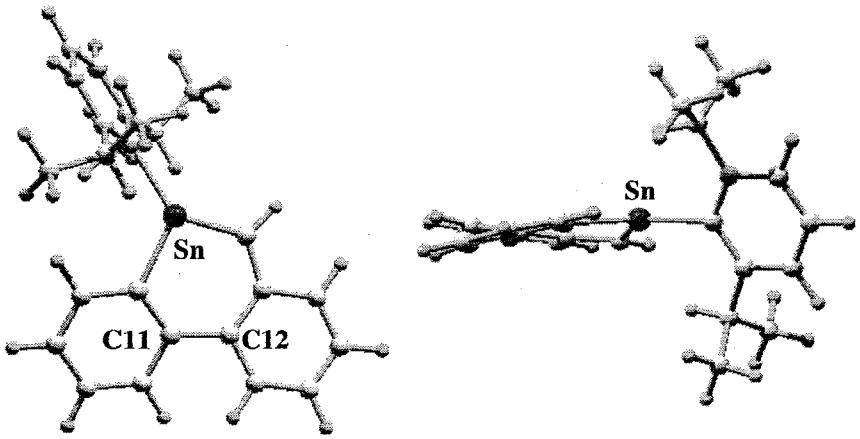

Figure 3-18. Optimized structure of **82c**. Top view (left) and side view (right) along the C11–C12 bond.

The distorted structures of 9-stannaphenanthrenes **82** are probably due to the severe repulsion between the close H4 and H5 atoms accompanied with the elongation of the Sn=C9 bonds (Figure 3-19).

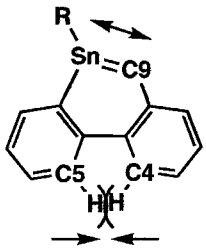

Figure 3-19.

The theoretical calculations suggest the smaller contribution of aromatic stabilization in the 9-stannaphenanthrene systems due to their non-planar structures in contrast to those of the stannabenzene and the stannanaphthalene systems. Next, the estimatation of the aromaticity for these optimized structures were performed.

3.5.2 Nucleus-Independent Chemical Shifts (NICS)

An efficient computational probe for diatropic and paratropic ring currents, associated with aromaticity and antiaromaticity, respectively, may be the calculations for nucleus-independent chemical shifts (NICS) values, which are computed as the absolute magnetic shielding at ring centers.[26] Generally, the NICS (0) and NICS(1) values are computed at the ring center and 1 Å above the ring centers, respectively, reflecting the ring current effect of the π-electrons.[27] The NICS(0) and NICS(1) values for stannaaromatic compounds **79a**-**82a** are shown in Figure 3-20 and Figure 3-21 together with those of the parent aromatic hydrocarbons and Si- and Ge-analogues.

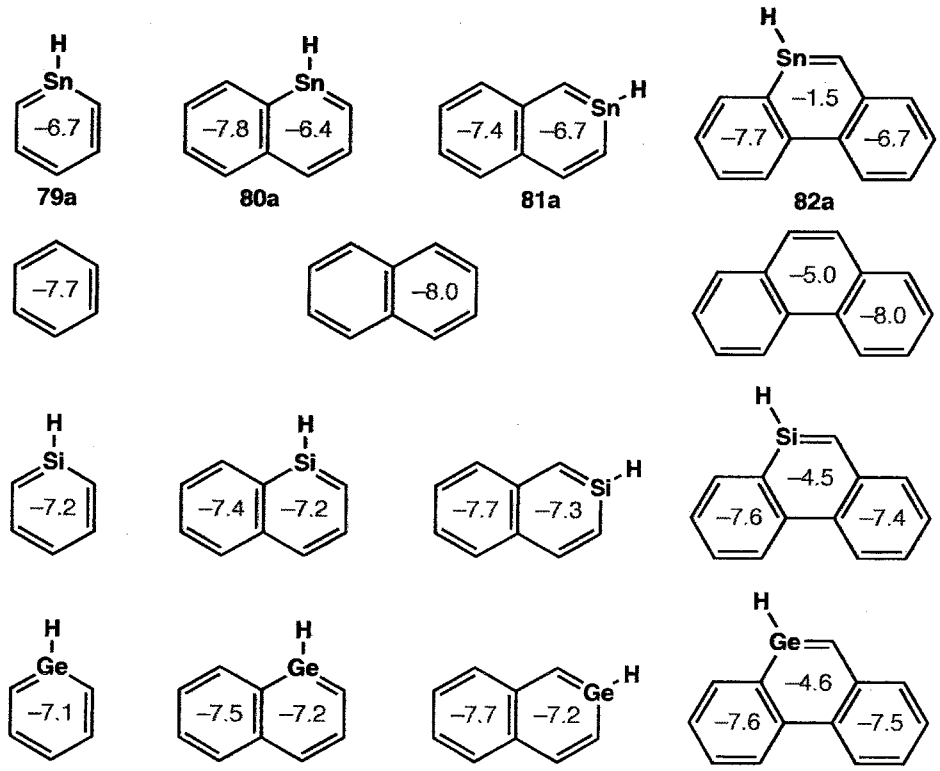

Figure 3-20. Caluculated NICS(0) (ppm) values for stannaaromatics and related aromatic rings at the GIAO-B3LYP/6-311+G(2d,p) (TZV on Sn)//B3LYP/6-31G(d) (LANL2DZ on Sn) level.

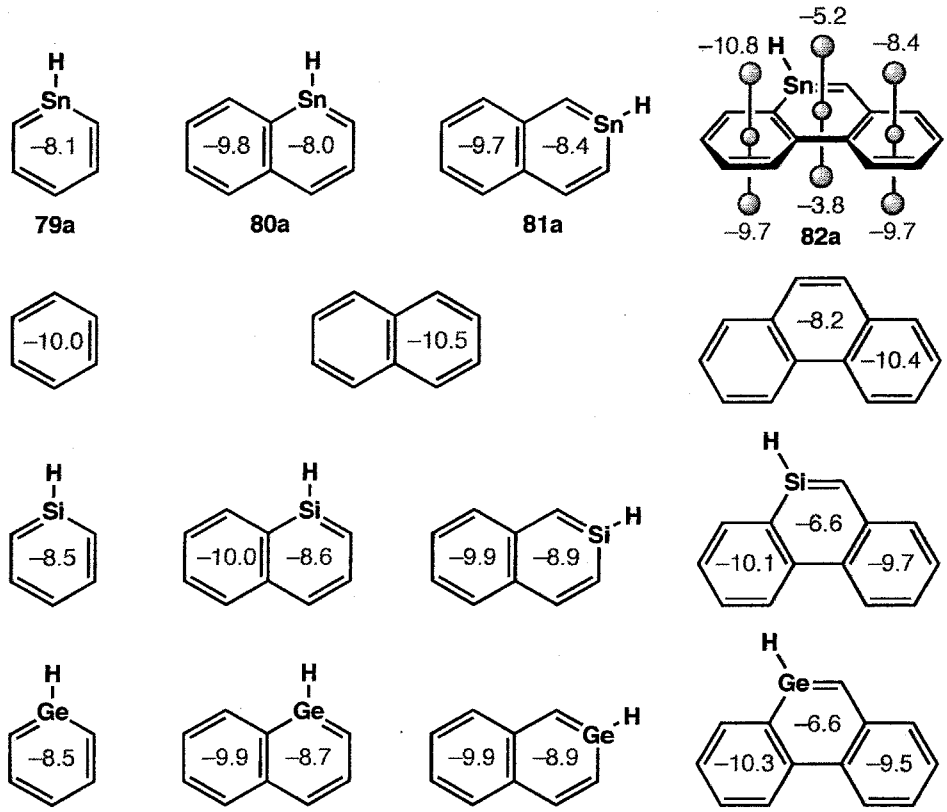

Figure 3-21. Caluculated NICS(1) (ppm) values for stannaaromatics and related aromatic rings at the GIAO-B3LYP/6-311+G(2d,p) (TZV on Sn)//B3LYP/6-31G(d) (LANL2DZ on Sn) level.

The NICS values for the C_5Sn-rings of stannabenzene **79a**, 1-stannanaphthalene **80a**, and 2-stannanaphthalene **81a** showed the large negative values, which were comparable to those for benzene and naphthalene. By contrast, those for the C_5Sn-ring of 9-stannaphenanthrene showed small negative values, indicating lower the ring current effect than that for not only phenanthrene but also other stannaaromatic systems.

3.5.3 Reaction Heats for the Addition of Hydrogen Molecule

The reaction heats in the addition reaction of hydrogen molecule should be good indicators to estimate the relative bonding energy of the π-bonds in aromatic rings. In Figure 3-22 are shown the reaction heats of stannaaromatic compounds together with those of the parent aromatic hydrocarbons.

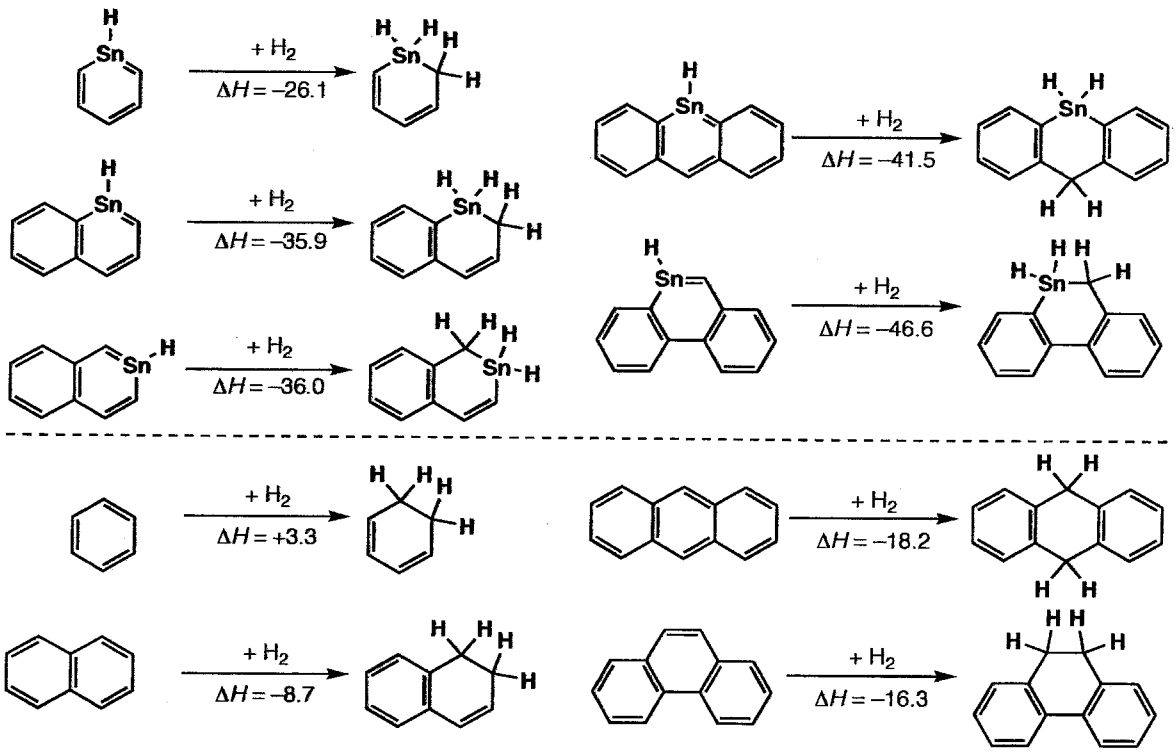

Figure 3-22. Reaction heats (kcal/mol) for the addition of hydrogen molecule to stannaaromatics and related aromatic rings [SCE, B3LYP/6-31G(d) (LANL2DZ on Sn) level].

As a result, the addition reactions of hydrogen molecule to stannaaromatic compounds are calculated to be more exothermic than those of the corresponding parent aromatic compounds by ~30 kcal/mol. The ΔH value in the hydrogenation of the parent 9-stannaphenanthrene is the

largest negative value (–46.6 kcal/mol), suggesting the lower "resonance stability" of the 9-stannaphenanthrene as compared with other stannaaromatic systems.

3.5.4 Summary of Section 3.5

Theoretical calculations suggest that 9-stannaphenanthrenes have lower aromaticity than 2-stannanaphthalenes probably due to the non-planarity of the 9-stannaphenanthrene ring. On the other hand, 2-stannanaphthalenes are considered to have sufficient aromaticity comparable to the parent naphthalene, as judged by the planarity of the 2-stannanaphthalene ring and the large negative values of its NICS.

3.6 Conclusion

In summary, the author succeeded in the generation of 9-stannaphenanthrene **31** and revealed its high reactivity. The synthesis and isolation of 2-stannanaphthalene **32** were also achieved and the structure of **32** was determined by the X-ray crystallographic analysis. Judging from the NMR and Raman spectra, the molecular structure, and reactivities, **32** has a sufficient aromatic character, which was reasonably supported by the theoretical calculations.

Table 3-7. Crystal Data for Compounds **45**, [**46**·C_6H_6], and **48**.

	45	[**46**·C_6H_6]	**48**
Empirical formula	$C_{40}H_{70}OSi_6Sn$	$C_{80}H_{136}Si_{12}Sn_2 \cdot C_6H_6$	$C_{59}H_{97}NOSi_6Sn$
Formula weight	854.19	970.39	1123.64
Temperature (K)	103(2)	103(2)	103(2)
Crystal color	colorless	colorless	colorless
Crystal dimensions	0.20 × 0.20 × 0.20	0.25 × 0.15 × 0.10	0.25 × 0.25 × 0.15
Crystal system	triclinic	triclinic	triclinic
Space group	$P\bar{1}$ (#2)	$P\bar{1}$ (#2)	$P\bar{1}$ (#2)
Lattice parameters			
a (Å)	11.147(2)	12.8898(2)	9.8361(9)
b (Å)	18.611(3)	17.9414(3)	15.5831(11)
c (Å)	24.932(5)	22.3902(5)	21.8919(17)
α (°)	77.480(6)	81.1212(8)	107.957(3)
β (°)	78.823(5)	82.9007(9)	96.281(3)
γ (°)	68.159(5)	72.8807(16)	88.936(7)
V (Å^3)	4650.1(15)	4872.49(16)	3172.5(4)
Z	4	2	2
D_{calc} (g·cm^{-3})	1.220	1.193	1.176
μ (mm^{-1})	0.732	0.699	0.552
θ range (°)	1.57 to 25.00	0.92 to 25.00	1.37 to 25.00
Independent reflections	15418	16892	10703
R_{int}	0.0177	0.0519	0.0301
Completeness to θ (%)	94.0	98.1	95.7
Restraints	0	0	24
No. of parameters	903	937	716
Goodness of fit	1.091	1.020	1.014
Final R indices [$I>2\sigma(I)$]	$R_1 = 0.0448$	$R_1 = 0.0451$	$R_1 = 0.0309$
	$wR_2 = 0.1052$	$wR_2 = 0.0907$	$wR_2 = 0.0629$
R indices (all data)	$R_1 = 0.0499$	$R_1 = 0.0849$	$R_1 = 0.0555$
	$wR_2 = 0.1082$	$wR_2 = 0.1015$	$wR_2 = 0.0907$
Largest diff. peak (e·Å^3)	1.186	1.671	0.643
Largest diff. hole (e·Å^3)	–1.211	–0.646	–0.612

Table 3-8. Crystal Data for Compounds **49**, [**59**·$CHCl_3$], and **32**.

	49	[**59**·$CHCl_3$]	**32**
Empirical formula	$C_{46}H_{78}Si_6Sn$	$C_{46}H_{73}BrSi_6Sn{\cdot}CHCl_3$	$C_{40}H_{74}Si_6Sn$
Formula weight	918.31	1112.55	842.22
Temperature (K)	103(2)	103(2)	103(2)
Crystal color	colorless	colorless	yellow
Crystal dimensions	0.20 × 0.05 × 0.05	0.20 × 0.05 × 0.05	0.20 × 0.10 × 0.10
Crystal system	hexagonal	triclinic	triclinic
Space group	$P6_3/m$ (#176)	$P\bar{1}$ (#2)	$P\bar{1}$ (#2)
Lattice parameters			
a (Å)	23.0936(5)	10.235(3)	12.4261(3)
b (Å)	23.0936(5)	12.405(4)	13.0149(3)
c (Å)	16.6637(5)	22.690(8)	17.3641(6)
α (°)	90	104.703(5)	73.4934(10)
β (°)	90	90.260(4)	74.3341(12)
γ (°)	120	94.170(5)	63.548(2)
V (Å^3)	7696.4(3)	2778.4(15)	2376.89(11)
Z	6	2	2
D_{calc} (g·cm^{-3})	1.189	1.330	1.177
μ (mm^{-1})	0.666	1.482	0.713
θ range (°)	2.04 to 25.00	2.52 to 25.00	3.15 to 25.00
Independent reflections	4691	9605	8358
R_{int}	0.1565	0.0869	0.0694
Completeness to θ (%)	99.9	98.0	99.7
Restraints	120	12	0
No. of parameters	340	578	445
Goodness of fit	1.026	1.088	1.066
Final R indices [$I>2\sigma(I)$]	$R_1 = 0.0604$	$R_1 = 0.0832$	$R_1 = 0.0655$
	$wR_2 = 0.1177$	$wR_2 = 0.1367$	$wR_2 = 0.1351$
R indices (all data)	$R_1 = 0.1406$	$R_1 = 0.1454$	$R_1 = 0.0997$
	$wR_2 = 0.1542$	$wR_2 = 0.1712$	$wR_2 = 0.1534$
Largest diff. peak (e·Å^3)	0.512	1.323	4.519
Largest diff. hole (e·Å^3)	–0.987	–0.897	–0.832

Table 3-9. Crystal Data for Compounds **72**.

	72
Empirical formula	$C_{43}H_{74}CrO_3Si_6Sn$
Formula weight	978.25
Temperature (K)	173(2)
Crystal color	brown
Crystal dimensions	0.10 × 0.10 × 0.01
Crystal system	triclinic
Space group	$P\bar{1}$ (#2)
Lattice parameters	
a (Å)	9.5178(4)
b (Å)	13.1280(7)
c (Å)	22.1764(8)
α (°)	79.6768(18)
β (°)	82.5522(15)
γ (°)	82.2722(18)
V (Å^3)	2685.5(2)
Z	2
D_{calc} (g·cm^{-3})	1.210
μ (mm^{-1})	0.833
θ range (°)	1.71 to 25.00
Independent reflections	9402
R_{int}	0.0586
Completeness to θ (%)	99.3
Restraints	0
No. of parameters	650
Goodness of fit	1.107
Final R indices [I>2σ(I)]	R_1 = 0.0493
	wR_2 = 0.0890
R indices (all data)	R_1 = 0.0880
	wR_2 = 0.1052
Largest diff. peak (e·Å^3)	0.388
Largest diff. hole (e·Å^3)	–0.388

Experimental Section

Preparation of 36 from 34. To a THF (1.0 mL) suspension of magnesium (156 mg, 6.40 mmol) was added a THF solution (11 mL) of **34** (676 mg, 2.07 mmol) and $TbtSnCl_3$[28] **35** (1.61 g, 2.07 mmol) at room temperature, and the reaction mixture was heated under reflux for 12 h. To the reaction mixture was added lithium aluminum hydride (200 mg, 5.27 mmol) at 0 °C. After stirring for 1 h at room temperature, ethyl acetate was added to the reaction mixture at 0 °C. After removal of the solvent, hexane was added to the residue. The resulting suspension was filtered through Celite®, and the solvent was removed under reduced pressure. The residue was separated by WCC (hexane) to afford **36** (291 mg, 0.347 mmol, 17%). **36**: colorless crystals; mp 103-107 °C (dec.); ^{1}H NMR (300 MHz, rt, C_6D_6) δ 0.02 (s, 9H), 0.12 (s, 9H), 0.13 (s, 36H), 1.41 (s, 1H), 1.94 (br s, 2H), 2.61 (d, ^2J = 12.3 Hz, 1H), 2.86 (d, ^2J = 12.3 Hz, 1H), 6.23 (s, 1H, Sn-H), 6.49 (br s, 1H), 6.61 (br s, 1H), 6.96-7.43 (m, 6H), 7.50-7.55 (m, 1H), 7.79-7.87 (m, 1H); ^{13}C NMR (75 MHz, rt, C_6D_6) δ 0.43 (q), 0.82 (q), 0.85 (q), 1.17 (q), 20.22 (t), 30.61 (d), 33.23 (d), 33.81 (d), 121.65 (d), 126.47 (d), 127.05 (d), 127.90 (d), 128.71 (s), 128.95 (d), 130.43 (d), 130.85 (d), 131.26 (d), 133.62 (d), 138.02 (s), 138.16 (d), 139.36 (s), 142.02 (s), 144.67 (s), 147.37 (s), 152.16 (s×2); ^{119}Sn NMR (111 MHz, rt, C_6D_6) δ –250.4. High resolution FAB-MS *m/z* calcd for $C_{40}H_{70}Si_6{}^{118}Sn$: 836.3109 [M$^+$], found: 836.3112 [M$^+$].

Preparation of 39 via 38. To a THF solution (2 mL) of 2-bromo-2'-methylbiphenyl (253 mg, 1.00 mmol) was added *n*-butyllithium (1.49 M in hexane, 0.630 mL, 0.939 mmol) at –78 °C. After stirring at the same temperature for 1 h, THF solution (8 mL) of **35** (664 mg, 0.854 mmol) was added to the mixture. After stirring for 1 h at –78 °C, the reaction mixture was warmed to room temperature and stirred for 2 h at the same temperature. After removal of the solvent,

hexane was added to the residue. The resulting suspension was filtered through Celite®, and the solvent was removed. The residue was separated by GPLC ($CHCl_3$) to afford **38** (582 mg, X_2: Cl_2/BrCl = 1/1). To a THF solution (10 mL) of **38** was added lithium aluminum hydride (53.0 mg, 1.40 mmol) at 0 °C. After stirring for 1 h at room temperature, ethyl acetate was added to the reaction mixture at 0 °C. After removal of the solvent, hexane was added to the residue. The resulting suspension was filtered through Celite®, and the solvent was removed to afford **9** (522 mg, 0.621 mmol, 73%, from **37**). **39**: colorless crystals; mp 107-111 °C (dec.); ^{1}H NMR (300 MHz, rt, C_6D_6) δ 0.14 (s, 36H), 0.17 (s, 18H), 1.47 (s, 1H), 2.03 (s, 2H), 2.20 (s, 3H), 5.70 (d, J = 19.8 Hz, 1H), 5.89 (d, J = 19.8 Hz, 1H), 6.58 (br s, 1H), 6.69 (br s, 1H), 7.13-7.19 (m, 6H), 7.29-7.32 (m, 1H), 7.80-7.83 (m, 1H); ^{13}C NMR (75 MHz, rt, C_6D_6) δ −0.41 (q), 0.92 (q), 1.26 (q), 20.67 (q), 30.59 (d), 33.21 (d), 33.60 (d), 126.03 (d), 126.54 (d), 126.90 (d), 128.18 (d), 128.80 (d), 129.29 (d), 129.31 (d), 129.81 (d), 130.34 (d), 133.79 (s), 135.75 (s), 138.21 (s), 138.86 (d), 144.45 (s), 144.68 (s), 150.43 (s), 152.50 (s×2); ^{119}Sn NMR (111 MHz, rt, C_6D_6) δ −302.0. High resolution FAB-MS *m/z* calcd for $C_{40}H_{72}Si_6{}^{120}Sn$: 840.3272 [$M^+$], found: 840.3300 [$M^+$]. Anal. Calcd for $C_{40}H_{72}Si_6Sn$: C, 57.18; H, 8.64%. Found: C, 57.27; H, 8.67%.

Preparation of 40. A CCl_4 (15 mL) solution of **39** (142 mg, 0.169 mmol) was stirred for 2 h at room temperature under the air, and the solvent was removed to afford **40** (154 mg, 0.169 mmol, quantitative). **40**: colorless crystals; mp 190-193 °C; ^{1}H NMR (300 MHz, rt, C_6D_6) δ 0.16 (s, 36H), 0.18 (s, 18H), 1.50 (s, 1H), 2.08 (s, 3H), 2.39 (br s, 1H), 2.47 (br s, 1H), 6.58 (br s, 1H), 6.71 (br s, 1H), 7.04-7.15 (m, 6H), 7.30-7.32 (m, 1H), 8.12-8.21 (m, 1H); ^{13}C NMR (75 MHz, rt, C_6D_6) δ 0.90 (q), 1.09 (q), 1.27 (q), 1.37 (q), 20.55 (q), 31.22 (d), 31.67 (d), 32.13 (d), 123.21 (d), 127.27 (d), 127.39 (d), 128.04 (d), 128.21 (d), 128.74 (d), 130.20 (d), 131.50 (d), 131.83 (d), 136.51 (d), 137.02 (s), 137.62 (s), 143.58 (s), 146.81 (s), 147.31 (s), 147.59 (s), 152.27 (s),

152.55 (s); ^{119}Sn NMR (111 MHz, rt, C_6D_6) δ –69.8. High resolution FAB-MS *m/z* calcd for $C_{40}H_{70}{}^{35}Cl_2Si_6{}^{120}Sn$: 908.2492 [M$^+$], found: 908.2505 [M$^+$]. Anal. Calcd for $C_{40}H_{70}Cl_2Si_6Sn$: C, 52.85; H, 7.76%. Found: C, 52.82; H, 7.75%.

Preparation of 41. To a CCl_4 solution (25 mL) of **40** (966 mg, 1.06 mmol) was added *N*-bromosuccinimide (190 mg, 1.07 mmol) and a catalytic amount of benzoyl peroxide at room temperature. The reaction mixture was heated under reflux for 24 h. After removal of the solvent, hexane was added to the residue. The resulting suspension was filtered through Celite®, and the solvent was removed. The residue was separated by GPLC ($CHCl_3$) to afford **41** (585 mg, 0.592 mmol, 56%). **41**: colorless crystals; mp 184-187 °C; ^{1}H NMR (300 MHz, rt, C_6D_6) δ 0.15 (s, 36H), 0.18 (s, 18H), 1.48 (s, 1H), 2.30 (br s, 1H), 2.37 (br s, 1H), 3.92 (d, ^2J = 10.5 Hz, 1H), 4.12 (d, ^2J = 10.5 Hz, 1H), 6.55 (br s, 1H), 6.68 (br s, 1H), 7.03-7.26 (m, 6H), 7.68-7.71 (m, 1H), 8.15-8.18 (m, 1H); ^{13}C NMR (75 MHz, rt, $CDCl_3$) δ 0.73 (q), 0.89 (q), 0.99 (q), 1.06 (q), 30.87 (d), 31.41 (d), 31.85 (d), 32.23 (t), 122.76 (d), 127.56 (d), 127.73 (d), 128.67 (d), 129.06 (d), 129.67 (d), 130.25 (d), 130.82 (d), 132.00 (d), 135.59 (s), 136.00 (d), 137.02 (s), 142.61 (s), 144.93 (s), 146.38 (s), 147.59 (s), 151.59 (s), 151.80 (s); ^{119}Sn NMR (111 MHz, rt, $CDCl_3$) δ –70.3. High resolution FAB-MS *m/z* calcd for $C_{40}H_{69}{}^{81}Br^{35}Cl^{37}ClSi_6{}^{118}Sn$: 988.1541 [M$^+$], found: 988.1544 [M$^+$].

Preparation of 42. To a mixture of magnesium (115 mg, 4.73 mmol) and a catalytic amount of 1,2-dibromoethane was added a THF solution (24 mL) of **41** (585 mg, 0.592 mmol) at 77 °C, and the reaction mixture was heated under reflux for 0.5 h. After removal of the solvent, hexane was added to the residue. The resulting suspension was filtered through Celite®, and the solvent was removed to afford **42** (463 mg, 0.505 mmol, 85%). **42**: colorless crystals; mp 238-241 °C (dec.);

^{1}H NMR (300 MHz, rt, C_6D_6) δ −0.04 (s, 9H), 0.06 (s, 9H), 0.10 (s, 18H), 0.17 (s, 9H), 0.22 (s, 9H), 1.42 (s, 1H), 2.16 (br s, 2H), 2.96 (d, ^2J = 12.0 Hz, 1H), 3.33 (d, ^2J = 12.0 Hz, 1H), 6.52 (br s, 1H), 6.65 (br s, 1H), 6.89-7.22 (m, 4H), 7.31-7.41 (m, 3H), 8.19-8.21 (m, 1H); ^{13}C NMR (75 MHz, rt, C_6D_6) δ 0.49 (q), 0.77 (q), 0.85 (q), 0.95 (q), 1.37 (q), 29.44 (t), 31.00 (d), 33.37 (d), 34.18 (d), 122.06 (d), 126.81 (d), 127.30 (d), 128.08 (d), 128.26 (d), 128.96 (d), 131.03 (d), 131.12 (d), 131.34 (d), 135.16 (s), 135.40 (s), 137.34 (d), 138.63 (s), 145.47 (s), 146.23 (s), 146.68 (s), 152.20 (s), 152.41 (s); ^{119}Sn NMR (111 MHz, rt, C_6D_6) δ −115.9. High resolution FAB-MS *m/z* calcd for $C_{40}H_{69}{}^{81}BrSi_6{}^{118}Sn$: 916.2220 [M$^+$], found: 916.2197 [M$^+$]. Anal. Calcd for $C_{40}H_{69}BrSi_6Sn$: C, 52.38; H, 7.58%. Found: C, 52.16; H, 7.54%.

Preparation of 36 from 42. To a THF solution (10 mL) of **42** (463 mg, 0.505 mmol) was added lithium aluminum hydride (54.1 mg, 1.42 mmol) at 0 °C. After stirring for 16 h at room temperature, ethyl acetate was added to the reaction mixture at 0 °C. After removal of the solvent, hexane was added to the residue. The resulting suspension was filtered through Celite®, and the solvent was removed to afford **36** (423 mg, 0.505 mmol, quantitative).

Preparation of 43. A CCl_4 (15 mL) solution of **36** (53.8 mg, 0.0641 mmol) was stirred for 12 h at room temperature under the air, and the solvent was removed to afford **43** (55.9 mg, 0.0641 mmol, quantitative). **43**: colorless crystals; mp 215-218 °C (dec.); ^{1}H NMR (300 MHz, rt, $CDCl_3$) δ −0.25 (s, 9H), −0.17 (s, 9H), 0.00 (s, 27H), 0.07 (s, 9H), 1.30 (s, 1H), 1.80 (br s, 1H), 1.82 (br s, 1H), 2.84 (d, ^2J = 12.6 Hz, 1H), 3.20 (d, ^2J = 12.6 Hz, 1H), 6.30 (br s, 1H), 6.43 (br s, 1H), 7.09-7.21 (m, 3H), 7.35-7.39 (m, 2H), 7.46-7.55 (m, 2H), 7.86-7.88 (m, 1H); ^{13}C NMR (75 MHz, rt, $CDCl_3$) δ −0.41 (q), 0.00 (q), 0.18 (q), 0.25 (q), 0.56 (q), 28.63 (t), 30.29 (d), 32.80 (d), 33.54 (d), 121.11 (d), 125.89 (d), 126.58 (d), 127.39 (d), 127.42 (d), 128.27 (d), 130.29 (d),

130.42 (d), 130.46 (d), 134.29 (s), 135.50 (d), 137.78 (s), 141.44 (s), 144.91 (s), 145.66 (s), 146.11 (s), 150.57 (s), 151.35 (s); ^{119}Sn NMR (111 MHz, rt, C_6D_6) δ –89.6. High resolution FAB-MS *m/z* calcd for $C_{40}H_{69}{}^{35}ClSi_6{}^{120}Sn$: 872.2725 [$M^+$], found: 872.2722 [$M^+$]. Anal. Calcd for $C_{40}H_{69}ClSi_6Sn{\cdot}H_2O$: C, 53.94; H, 8.03%. Found: C, 53.96; H, 8.03%.

Reaction of 43 with lithium hexadisilazide at room temperature. In a glovebox filled with argon, lithium hexadisilazide (17.0 mg, 0.102 mmol) was added to a benzene solution (2 mL) of **43** (80.3 mg, 0.0920 mmol) at room temperature. The reaction mixture was stirred at the same temperature for 12 h. After removal of the solvent, hexane was added to the residue. The resulting suspension was filtered through Celite®, and the solvent was removed. A C_6D_6 solution of the residue was placed in a 5 mm ϕ NMR tube. The tube was evacuated and sealed. The observed ^{1}H NMR signals were assignable to the starting material **43** and lithium hexadisilazide.

Reaction of 43 with DBU at room temperature. In a glovebox filled with argon, DBU (1,8-diazabicyclo[5.4.0]undec-7-ene, 0.0095 mL, 0.064 mmol) was added to a benzene solution (2 mL) of **43** (55.2 mg, 0.0633 mmol) at room temperature. The reaction mixture was stirred at the same temperature for 4 days. After removal of the solvent, hexane was added to the residue. The resulting suspension was filtered through Celite®, and the solvent was removed. A C_6D_6 solution of the residue was placed in a 5 mm ϕ NMR tube. The tube was evacuated and sealed. The observed ^{1}H NMR signals were assignable to the starting material **43** and DBU.

Reaction of 43 with *t*-butyl lithium at room temperature. In a glovebox filled with argon, *t*-butyllithium (2.2 M in pentane, 0.045 mL, 0.099 mmol) was added to a benzene solution (2 mL) of **43** (78.1 mg, 0.0895 mmol) at room temperature. The reaction mixture was stirred at the same

temperature for 1 h. After removal of the solvent, hexane was added to the residue. The resulting suspension was filtered through Celite®, and the solvent was removed. A C_6D_6 solution of the residue was placed in a 5 mm ϕ NMR tube. The tube was evacuated and sealed. The observed ^{1}H NMR signals were assignable to the starting material **43**.

Reaction of 43 with LDA at room temperature. In a glovebox filled with argon, LDA (2 M in heptane/THF/ethylbenzene, 0.029 mL, 0.058 mmol) was added to a benzene solution (2 mL) of **43** (50.1 mg, 0.0574 mmol) at room temperature. The reaction mixture was stirred at the same temperature for 15 min. After removal of the solvent, hexane was added to the residue. The resulting suspension was filtered through Celite®, and the solvent was removed. A C_6D_6 solution of the residue was placed in a 5 mm ϕ NMR tube. The tube was evacuated and sealed. After measurement of ^{1}H NMR spectrum [suggesting the generation of **44**, judged by the signals assignable to $(C\underline{H}_3)_2C\underline{H}$-], the sealed tube was opened. The NMR signals were assignable only to **45**. However, compound **45** gradually decomposed in solution. **45**: colorless crystals; ^{1}H NMR (300 MHz, rt, C_6D_6) δ –0.03 (s, 9H), 0.07 (s, 9H), 0.10 (s, 18H), 0.12 (s, 18H), 1.46 (s, 1H), 1.99 (s, 1H), 2.06 (s, 1H), 2.68 (d, ^2J = 12.2 Hz, 1H), 2.84 (d, ^2J = 12.2 Hz, 1H), 6.53 (br s, 1H), 6.65 (br s, 1H), 6.94-7.56 (m, 7H), 7.81-7.87 (m, 1H); ^{13}C NMR (75 MHz, rt, C_6D_6) δ 0.35 (q), 0.81 (q), 0.85 (q), 1.15 (q), 26.94 (t), 30.83 (d), 33.40 (d), 33.94 (d), 121.82 (d), 126.47 (d), 126.72 (d), 127.52 (d), 128.54 (d), 128.99 (d), 130.78 (d), 131.20 (d), 131.30 (d), 135.62 (d), 136.58 (s), 138.72 (s), 143.14 (s), 145.82 (s), 146.26 (s), 147.42 (s), 152.15 (s×2); ^{119}Sn NMR (111 MHz, rt, C_6D_6) δ –112.0.

X-Ray crystallographic analysis of 45. Crystal data for **45** are shown in Table 3-7. Colorless and prismatic single crystals of **45** were grown by the slow evaporation of its hexane solution.

The intensity data were collected on a Rigaku/MSC Mercury CCD diffractometer with graphite monochromated MoKα radiation (λ = 0.71069 Å) to $2\theta_{max}$ = 50° at 103 K. The structure was solved by Patterson methods (DIRDIF-99.2[29]) and refined by full-matrix least-squares procedures on F^2 for all reflections (SHELXL-97[30]). All hydrogen atoms were placed using AFIX instructions, while all the other atoms were refined anisotropically.

Reaction of 43 with LTMP at room temperature. To a THF solution (2 mL) of **43** (60.4 mg, 0.0692 mmol) was added a THF solution (0.5 mL) of LTMP (0.0719 mmol) at room temperature. The reaction mixture was stirred at the same temperature for 1 h. After removal of the solvent, hexane was added to the residue. The resulting suspension was filtered through Celite®, and the solvent was removed. The residue was separated by PTLC ($CHCl_3$/hexane = 1:9) to afford **46** (26.5 mg, 0.0158 mmol, 46%). **46**: colorless crystals; mp 178 °C (dec.); ^{1}H NMR (300 MHz, rt, C_6D_6) δ 0.01 (s, 18H), 0.07 (s, 18H), 0.14 (s, 18H), 0.15 (s, 36H), 0.19 (s, 18H), 1.47 (s, 2H), 1.92 (s, 2H), 2.10 (s, 2H), 4.64 (s, 2H), 6.56-6.61 (m, 2H), 6.63 (br s, 2H), 6.69 (br s, 2H), 6.86-6.92 (m, 4H), 7.02-7.05 (m, 2H), 7.15-7.18 (m, 4H), 7.57-7.60 (m, 4H); ^{13}C NMR (75 MHz, rt, C_6D_6) δ 0.97 (q), 1.12 (q), 1.19 (q), 1.26 (q), 1.35 (q), 30.70 (d), 31.89 (d), 32.38 (d), 44.27 (d), 122.94 (d), 125.04 (d), 125.46 (d), 126.90 (d), 128.29 (d), 129.29 (d), 129.97 (d), 131.57 (d), 132.02 (d), 137.12 (s), 137.17 (d), 138.27 (s), 138.33 (s), 140.66 (s), 144.29 (s), 146.72 (s), 151.52 (s), 152.01 (s); ^{119}Sn NMR (111 MHz, rt, C_6D_6) δ −160.2. High resolution FAB-MS *m/z* calcd for $C_{80}H_{136}Si_{12}{}^{120}Sn_2$: 1672.5917 [$M^+$], found: 1672.5924 [$M^+$]. Anal. Calcd for $C_{80}H_{136}Si_{12}Sn_2$: C, 57.45; H, 8.20%. Found: C, 57.16; H, 8.35%.

X-Ray crystallographic analysis of [46·C_6H_6]. Crystal data for [**46**·C_6H_6] are shown in Table 3-7. Colorless and prismatic single crystals of [**46**·C_6H_6] were grown by the slow evaporation of its

benzene solution. The intensity data were collected on a Rigaku/MSC Mercury CCD diffractometer with graphite monochromated MoKα radiation (λ = 0.71070 Å) to $2\theta_{max}$ = 50° at 103 K. The structure was solved by Patterson methods (DIRDIF-99.2[29]) and refined by full-matrix least-squares procedures on F^2 for all reflections (SHELXL-97[30]). All hydrogen atoms were placed using AFIX instructions, while all the other atoms were refined anisotropically.

Reaction of 31 with MeOD at –78 °C. To a THF solution (2 mL) of **43** (62.1 mg, 0.0712 mmol) was added LTMP (0.30 M in THF, 0.29 mL, 0.087 mmol) at –78 °C. After stirring at the same temperature for 1 h, MeOD (0.5 mL) was added. After removal of the solvent, hexane was added to the residue. The resulting suspension was filtered through Celite®, and the solvent was removed. ^{1}H NMR spectrum of this residue showed the signals of only **47-*d*** (*cis*-adduct/*trans*-adduct = 1/1; D content: 100%) and 2,2,6,6-tetramethylpiperidine.

Synthesis of 47. To a THF solution (1 mL) of **43** (28.3 mg, 0.0324 mmol) was added lithium methoxide (8.2 mg, 0.22 mmol) at room temperature. The reaction mixture was stirred at the same temperature for 1 h. After removal of the solvent, hexane was added to the residue. The resulting suspension was filtered through Celite®, and the solvent was removed to afford **47** (28.1 mg, 0.0324 mmol, quantitative). **47**: colorless crystals, ^{1}H NMR (300 MHz, rt, C_6D_6) δ –0.03 (s, 9H), 0.08 (s, 9H), 0.115 (s, 9H), 0.120 (s, 9H), 0.14 (s, 9H), 0.20 (s, 9H), 1.43 (s, 1H), 1.99 (br s, 1H), 2.07 (br s, 1H), 2.52 (d, ^2J = 12.6 Hz, 1H), 3.19 (d, ^2J = 12.6 Hz, 1H), 3.66 (s, 3H, -O<u>Me</u>), 6.53 (br s, 1H), 6.66 (br s, 1H), 6.94-7.00 (m, 1H), 7.02-7.07 (m, 1H), 7.13-7.18 (m, 1H), 7.14-7.19 (m, 1H), 7.22-7.27 (m, 1H), 7.37 (dd, ^3J = 8 Hz, ^4J = 2 Hz, 1H), 7.51 (dd, ^3J = 8 Hz, ^4J = 1 Hz, 1H), 7.89 (dd, ^3J = 8 Hz, ^4J = 2 Hz, 1H); ^{13}C NMR (75 MHz, rt, C_6D_6) δ 0.23 (q), 0.62 (q), 0.80 (q), 0.83 (q), 1.14 (q), 22.79 (t), 30.81 (d), 33.34 (d), 33.95 (d), 55.88 (q, -O<u>Me</u>), 121.79 (d),

126.50 (d), 126.75 (d), 127.20 (d), 128.09 (d), 129.39 (d), 130.87 (d), 131.35 (d), 131.56 (d), 132.21 (s), 135.84 (d), 136.42 (s), 138.59 (s), 143.02 (s), 145.90 (s), 148.03 (s), 152.13 (s), 152.32 (s); ^{119}Sn NMR (111 MHz, rt, C_6D_6) δ –95.85. High resolution FAB-MS *m/z* calcd for $C_{40}H_{69}OSi_6{}^{120}Sn$: 853.2991 ([M–Me]$^+$), found: 853.2996 ([M–Me]$^+$). Elemental analysis of **47** was unsuccessful in spite of several trials, because of its high hygroscopicity and the ready hydrolysis in the open air.

Reaction of 31 with Mes*CNO at –78 °C. To a THF solution (2 mL) of **43** (68.8 mg, 0.0788 mmol) was added LTMP (0.35 M in THF, 0.27 mL, 0.095 mmol) at –78 °C. After stirring at the same temperature for 1 h, Mes*CNO (30.3mg, 0.105 mmol) was added. The reaction mixture was stirred for 12 h at the same temperature and warmed to room temperature. After removal of the solvent, hexane was added to the residue. The resulting suspension was filtered through Celite®, and the solvent was removed. The residue was separated by GPLC (toluene) to afford **48** (38.3 mg, 0.0341 mmol, 43%). **48**: colorless crystals; mp 208-211 °C (dec.); ^{1}H NMR (300 MHz, rt, $CDCl_3$) δ –0.14 (s, 18H), –0.02 (s, 18H), 0.040 (s, 9H), 0.044 (s, 9H), 0.64 (s, 9H), 1.28 (s, 9H), 1.36 (s, 1H), 1.43 (s, 9H), 1.62 (br s, 2H), 3.69 (s, 1H), 6.12-6.15 (m, 1H), 6.39 (br s, 1H), 6.50 (br s, 1H), 6.75-6.79 (m, 1H), 7.06-7.07 (m, 1H), 7.13-7.18 (m, 1H), 7.40-7.46 (m, 1H), 7.418 (s, 1H), 7.424 (s, 1H), 7.51-7.53 (m, 1H), 7.60-7.63 (m, 1H), 7.72-7.74 (m, 1H); ^{13}C NMR (75 MHz, rt, $CDCl_3$) δ 0.20 (q), 0.48 (q), 0.62 (q), 0.82 (q), 30.67 (d), 31.30 (q+d), 33.80 (q), 33.81(d), 34.41 (q), 34.56 (s), 38.33 (s), 38.37 (s), 45.4 (d), 122.05 (d), 123.00 (d), 123.70 (d), 126.70 (d×2), 126.96 (d), 127.08 (d), 127.28 (d), 128.26 (s), 130.68 (d), 131.27 (d), 132.73 (s), 133.25 (s), 135.58 (d), 136.31 (d), 139.40 (s), 140.94 (s), 146.31 (s), 146.91 (s), 147.10 (s), 147.83 (s), 148.92 (s), 151.18 (s), 151.36 (s), 157.72 (s); ^{119}Sn NMR (111 MHz, rt, C_6D_6) δ –17.1. High resolution FAB-MS *m/z* calcd for $C_{59}H_{98}NOSi_6{}^{120}Sn$: 1124.5281 ([M+H]$^+$), found:

1124.5309 ([M+H]$^+$). Anal. Calcd for $C_{59}H_{97}NOSi_6Sn{\cdot}H_2O$: C, 62.07; H, 8.74; N, 1.23%. Found: C, 62.35; H, 8.73; N, 1.41%.

X-Ray crystallographic analysis of 48. Crystal data for **48** are shown in Table 3-7. Colorless and prismatic single crystals of **48** were grown by the slow evaporation of its hexane solution. The intensity data were collected on a Rigaku/MSC Mercury CCD diffractometer with graphite monochromated MoKα radiation (λ = 0.71070 Å) to $2\theta_{max}$ = 50° at 103 K. The structure was solved by Patterson methods (DIRDIF-99.2[29]) and refined by full-matrix least-squares procedures on F^2 for all reflections (SHELXL-97[30]). Two trimethylsilyl groups of the $CH(SiMe_3)_2$ groups at *para*-position of the Tbt group were disordered. The occupancies of the disordered parts were refined (0.88:0.12). The U_{ij} values of the disordered trimethylsilyl groups were restrained using SIMU instructions. All hydrogen atoms were placed using AFIX instructions, while all the other atoms were refined anisotropically.

Reaction of 31 with 2,3-dimethyl-1,3-butadiene at –78 °C. To a THF solution (2 mL) of **43** (59.0 mg, 0.0676 mmol) was added LTMP (0.30 M in THF, 0.37 mL, 0.111 mmol) at –78 °C. After stirring at the same temperature for 1 h, 2,3-dimethyl-1,3-butadiene (0.5 mL, excess) was added. After removal of the solvent, hexane was added to the residue. The resulting suspension was filtered through Celite®, and the solvent was removed. The residue was separated by WCC (eluent: hexane) to afford [2+4] adduct **49** (41.5 mg, 0.0452 mmol, 67%). In addition, the residue does not contain dimer **46**, indicating that **31** readily reacted with 2,3-dimethyl-1,3-butadiene. **49**: colorless crystals; mp 170-173 °C (dec.); ^{1}H NMR (300 MHz, rt, C_6D_6) δ 0.02 (s, 18H), 0.125 (s, 9H), 0.132 (s, 9H), 0.17 (s, 9H), 0.20 (s, 9H), 1.43 (s, 1H), 1.68 (s, 3H), 1.72 (s, 3H), 1.93 (br s, 1H), 2.03 (br s, 1H), 2.10 (d, ^2J = 13.6 Hz, 1H), 2.14 (d, ^2J = 13.6 Hz, 1H), 2.39 (dd, ^2J = 13.6

Hz, ^3J = 4.4 Hz, 1H), 2.59 (dd, ^2J = 13.6 Hz, ^3J = 11.2, 1H), 2.78 (dd, ^3J = 4.4 Hz, ^3J = 11.2 Hz, 1H), 6.53 (br s, 1H), 6.65 (br s, 1H), 7.05-7.32 (m, 5H), 7.46-7.48 (m, 1H), 7.56-7.59 (m, 1H), 7.80-7.83 (m, 1H); ^{13}C NMR (75 MHz, rt, C_6D_6) δ 0.43 (q), 0.62 (q), 0.85 (q), 0.92 (q), 1.20 (q), 21.83 (q), 22.28 (t), 23.48 (q), 30.61 (d), 33.33 (d), 33.90 (d), 34.34 (d), 40.58 (t), 121.92 (d), 126.68 (d), 127.01 (d), 127.28 (d), 127.79 (d), 128.00 (d), 129.00 (s), 129.51 (d), 131.62 (d), 132.31 (d), 135.81 (s), 138.76 (d), 140.38 (s), 142.88 (s), 144.06 (s), 144.38 (s), 147.78 (s), 151.75 (s), 151.98 (s). The signal of an olefin carbon might be overlapped on the signals of C_6D_6.; ^{119}Sn NMR (111 MHz, rt, C_6D_6) δ –179.63. High resolution FAB-MS *m/z* calcd for $C_{46}H_{79}Si_6{}^{120}Sn$: 919.3814 ([M+H]$^+$), found: 919.3837 ([M+H]$^+$).

X-Ray crystallographic analysis of 49. Crystal data for **49** are shown in Table 3-8. Colorless and prismatic single crystals of **49** were grown by the slow evaporation of its hexane solution. The intensity data were collected on a Rigaku/MSC Mercury CCD diffractometer with graphite monochromated MoKα radiation (λ = 0.71070 Å) to $2\theta_{max}$ = 50° at 103 K. The structure was solved by Patterson methods (DIRDIF-99.2[29]) and refined by full-matrix least-squares procedures on F^2 for all reflections (SHELXL-97[30]). There was a pseudo mirror plane on the molecule due to the 1:1 disorder of the molecule. The U_{ij} values of the carbon atoms of the disordered central moiety were restrained using SIMU instructions. All hydrogen atoms were placed using AFIX instructions, while all the other atoms were refined anisotropically.

Preperations of 52 and 53. The syntheses of **52** and **53** have been already reported.[31] In the reported method, bromination of **52** was performed by using HBr gas. The author used PBr_3 instead of HBr gas in the step as shown below. To alcohol **52** (1.91 g, 5.64 mmol) was added PBr_3 (ca. 0.6 mL, 6.4 mmol) at 0 °C. After stirring for 2 days at room temperature, the reaction

was quenched by water at 0 °C. To the mixture added diethylether and the organic layer was washed with water. The organic layer was dried over $MgSO_4$, and solvent was evaporated to afford almost pure **53** (2.27 g, .5.64 mmol, quantitative).

Preperation of 54. To a diethylether solution (30 mL) of **53** (4.78 g, 11.9 mmol) was added lithium aluminum hydride (1.4 g, 37 mmol) at 0 °C. The reaction mixture was heated under reflux for 10 h. The reaction was quenched by ethyl acetate at 0 °C. After removal of the solvent, hexane was added to the residue. The resulting suspension was filtered through Celite®, and the solvent was removed. The residue was separated by WCC (eluent: hexane) to afford **54** (2.81 g, 8.69 mmol, 73%). **54**: colorless crystals; mp 57-59 °C; ^{1}H NMR (300 MHz, rt, $CDCl_3$): δ 3.81 (d, ^2J = 15.6 Hz, 1H), 3.95 (d, ^2J = 15.6 Hz, 1H), 7.03-7.08 (m, 2H), 7.17-7.44 (m, 10H), 7.71-7.74 (m, 1H); ^{13}C NMR (75 MHz, rt, $CDCl_3$): δ 39.30 (t), 123.93 (s), 125.81 (d), 125.99 (d), 127.00 (d), 128.07 (d), 128.15 (d), 128.78 (d), 129.05 (d), 129.69 (d), 129.75 (d), 131.31(d), 132.47 (d), 139.03 (s), 140.64 (s), 141.03 (s), 142.11 (s); LRMS (EI): *m/z* 322 (M^+), 243 [$(M–Br)^+$].

Preparation of 56 via 55. To a THF solution (6 mL) of **54** (849 mg, 2.63 mmol) was added *n*-butyllithium (1.53 M in hexane, 1.72 mL, 2.63 mmol) at –78 °C. After stirring at the same temperature for 1 h, THF solution (14 mL) of **35** (2.05 g, 2.63 mmol) was added to the mixture. After stirring for 6 h at –78 °C, the reaction mixture was warmed to room temperature and stirred for 12 h at the same temperature. After removal of the solvent, hexane and chloroform were added to the residue. The resulting suspension was filtered through Celite®, and the solvents were removed. The residue was separated by GPLC ($CHCl_3$) to afford **55** (726 mg). To a THF solution (20 mL) of **55** was added lithium aluminum hydride (252 mg, 6.64 mmol) at 0 °C. After stirring for 12 h at room temperature, ethyl acetate was added to the reaction mixture at 0 °C.

After removal of the solvent, hexane was added to the residue. The resulting suspension was filtered through Celite®, and the solvent was removed to afford **56** (636 mg, 0.694 mmol, 26%, from **54**). **56**: colorless crystals; ^{1}H NMR (300 MHz, rt, C_6D_6) δ 0.14 (s, 18H), 0.17 (s, 36H), 1.47 (s, 1H), 2.04 (s, 2H), 3.95 (s, 2H), 5.81 (s, 2H, Sn–H), 6.58 (br s, 1H), 6.67 (br s, 1H), 6.95-7.20 (m, 11H), 7.33-7.36 (m, 1H), 7.77-7.80 (m, 1H); ^{13}C NMR (75 MHz, rt, C_6D_6) δ 1.03 (q), 1.29 (q), 30.63 (d), 33.28 (d), 33.64 (d), 39.99 (t), 122.00 (d), 126.21 (d), 126.45 (d), 126.60 (d), 127.00 (d), 128.54 (d), 128.56 (d), 129.11 (d), 129.47 (d), 129.81 (d), 130.25 (d), 130.43 (d), 133.84 (s), 138.61 (s), 138.77 (d), 139.11 (s), 141.27 (s), 144.47 (s), 144.67 (s), 149.86 (s), 152.47 (s×2).

Preparation of 57. A CCl_4 (15 mL) solution of **56** (636 mg, 0.694 mmol) was stirred for 3 h at room temperature under the air, and the solvent was removed to afford **57** (685 mg, 0.694 mmol, quantitative). **57**: colorless crystals; ^{1}H NMR (300 MHz, rt, $CDCl_3$) δ 0.02 (s, 9H), 0.06 (s, 27H), 0.11 (s, 18H), 1.40 (s, 1H), 2.06 (br s, 1H), 2.13 (br s, 1H), 3.90 (s, 2H), 6.38 (br s, 1H), 6.51 (br s, 1H), 6.95-7.35 (m, 10H), 7.40-7.46 (m, 1H), 7.50-7.60 (m, 1H), 7.90-8.20 (m, 1H); ^{13}C NMR (75 MHz, rt, $CDCl_3$) δ 0.75 (q), 0.81 (q), 0.93 (q), 1.04 (q), 1.14 (q), 30.88 (d), 31.31 (d), 31.76 (d), 39.33 (t), 122.78 (d), 125.93 (d), 127.13 (d), 127.42 (d), 127.61 (d), 128.21 (d), 128.35 (d), 128.47 (d), 129.41 (d), 129.89 (d), 131.06 (d), 131.35 (d), 136.01 (s), 136.04 (d), 140.02 (s), 140.89 (s), 143.00 (s), 146.21 (s), 146.58 (s), 147.41 (s), 151.67 (s), 151.89 (s); ^{119}Sn NMR (111 MHz, rt, C_6D_6) δ –72.7.

Preparation of 59 via 58. A benzene solution (25 mL) of **57** (483 mg, 0.490 mmol), *N*-bromosuccinimide (95.8 mg, 0.537 mmol) and AIBN [2,2'-azobis(isobutyronitrile), 30.5 mg, 0.186 mmol] was heated under reflux for 2 h. After removal of the solvent, hexane was added to

the residue. The resulting suspension was filtered through Celite®, and the solvent was removed. The residue was separated by GPLC ($CHCl_3$) to afford **58** (459 mg, $X_2 = Br_2$. BrCl, Cl_2 and their *dl/meso* isomers). To a mixture of magnesium (83.9 mg, 3.45 mmol) and a catalytic amount of 1,2-dibromoethane was added a THF solution (30 mL) of **58** (459 mg) at 77 °C, and the reaction mixture was heated under reflux for 1 h. After removal of the solvent, hexane and benzene were added to the residue. The resulting suspension was filtered through Celite®, and the solvents were removed to afford **59** almost diastereoselectively (395 mg, 0.397 mmol, 81% from **57**). **59**: colorless crystals; mp 252-256 °C; ^{1}H NMR (300 MHz, rt, $CDCl_3$) δ –0.19 (s, 9H), –0.15 (s, 9H), 0.03 (s, 18H), 0.07 (s, 9H), 0.12 (s, 9H), 1.33 (s, 1H), 1.98 (br s, 1H), 2.01 (br s, 1H), 4.56 (s, 1H), 6.34 (br s, 1H), 6.46 (br s, 1H), 6.90-7.23 (m, 7H), 7.32-7.74 (m, 6H); ^{13}C NMR (75 MHz, rt, $CDCl_3$) δ 0.33 (q), 0.62 (q), 0.76 (q), 0.81 (q), 1.24 (q), 30.67 (d), 33.15 (d), 33.94 (d), 45.40 (d), 121.65 (d), 124.88 (d), 126.42 (d), 127.33 (d), 127.75 (d), 128.15 (d), 128.24 (d), 128.42 (d), 128.54 (d), 130.99 (d), 131.38 (d), 133.36 (d), 135.48 (s), 135.98 (s), 137.72 (d), 139.73 (s), 140.56 (s), 140.81 (s), 146.30 (s), 146.35 (s), 151.63 (s), 151.74 (s); ^{119}Sn NMR (111 MHz, rt, $CDCl_3$) δ –90.8. Low resolution FAB-MS: *m/z* 993 [$(M+H)^+$].

X-Ray crystallographic analysis of [59·CHCl$_3$]. Crystal data for [**59**·$CHCl_3$] are shown in Table 3-8. Colorless and prismatic single crystals of [**59**·$CHCl_3$] were grown by the slow evaporation of its chloroform and acetonitrile solution. The intensity data were collected on a Rigaku/MSC Mercury CCD diffractometer with graphite monochromated MoKα radiation (λ = 0.71070 Å) to $2\theta_{max}$ = 50° at 103 K. The structure was solved by Patterson methods (DIRDIF-99.2[29]) and refined by full-matrix least-squares procedures on F^2 for all reflections (SHELXL-97[30]). Chloroform molecule was disordered. The occupancies of the disordered parts were refined (0.58:0.42). The U_{ij} values of two carbon atoms (in the majority and minority of

disordered chloroform molecules) were restrained not to be non-positive values using ISOR instructions. All hydrogen atoms were placed using AFIX instructions, while all the other atoms were refined anisotropically.

Preparation of 60. A CH_2Cl_2 (15 mL) solution of **59** (216 mg, 0.217 mmol) and AgOTf (87.3 mg, 0.320 mmol) was stirred for 12 h at room temperature. After removal of the solvent, the reaction mixture was taken into a glovebox filled with argon. Hexane was added to the residue and the resulting suspension was filtered through Celite®. The solvent was removed to afford **60** (228 mg, 0.211 mmol, 97%). **60**: colorless crystals; ^{1}H NMR (300 MHz, rt, C_6D_6) δ –0.15 (s, 9H), 0.31 (s, 9H), 0.09 (s, 18H), 0.23 (s, 9H), 0.28 (s, 9H), 1.44 (s, 1H), 2.25 (br s, 1H), 2.26 (br s, 1H), 4.83 (s, 1H), 6.58 (br s, 1H), 6.70 (br s, 1H), 6.87-7.43 (m, 12H), 8.38 (d, ^3J = 7.2 Hz, 1H); ^{13}C NMR (75 MHz, rt, C_6D_6) δ 0.52 (q), 0.81 (q), 0.86 (q), 1.11 (q), 1.51 (q), 31.52 (d), 33.69 (d), 34.36 (d), 49.23 (d), 119.33 (q, $^1J_{CF}$ = 320 Hz, –$\underline{C}F_3$), 122.37 (d), 126.38 (d), 127.16 (d), 127.70 (d), 128.30 (d), 128.90 (d), 129.06 (d), 129.26 (d), 129.28 (d), 132.30 (d), 132.61 (d), 133.85 (d), 134.27 (s), 136.08 (s), 138.18 (d), 138.40 (s), 139.07 (s), 140.43 (s), 147.51 (s), 148.63 (s), 153.28 (s), 153.39 (s); ^{19}F NMR (283 MHz, rt, $CDCl_3$): δ –75.5; ^{119}Sn NMR (111 MHz, rt, C_6D_6) δ –44.6.

Preparation of 61. In a glovebox filled with argon, a THF (3 mL) solution of **60** (228 mg, 0.211 mmol) and LiF (102 mg, 3.92 mmol) was stirred for 18 h at room temperature. After removal of the solvent, hexane was added to the residue. The resulting suspension was filtered through Celite®, and the solvent was removed to afford **61** (202 mg, 0.217 mmol, quantitative). **61**: colorless crystals; mp 198-201 °C (dec.); ^{1}H NMR (300 MHz, rt, C_6D_6) δ –0.21 (s, 9H), –0.13 (s, 9H), –0.01 (s, 9H), 0.02 (s, 9H), 0.03 (s, 9H), 0.04 (s, 9H), 1.34 (s, 1H), 1.65 (br s, 1H), 1.73 (br s,

1H), 4.47 (s, 1H), 6.35 (br s, 1H), 6.48 (br s, 1H), 6.92-7.63 (m, 13H); ^{119}Sn NMR (111 MHz, rt, C_6D_6) δ −113.8 ($^1J_{SnF}$ = 2530 Hz). Anal. Calcd for $C_{46}H_{73}FSi_6Sn$: C, 59.26; H, 7.89%. Found: C, 59.33; H, 8.00%.

Reaction of 59 with LDA. In a glovebox filled with argon, LDA (2 M in heptane/THF/ethylbenzene, 0.020 mL, 0.040 mmol) was added to a THF solution (2 mL) of **59** (40.6 mg, 0.0409 mmol) at −40 °C. The reaction mixture was stirred at room temperature for 1 h. After removal of the solvent, hexane was added to the residue. The resulting suspension was filtered through Celite®, and the solvent was removed. A C_6D_6 solution of the residue was placed in a 5 mm ϕ NMR tube, and the tube was sealed. The ^{1}H NMR signals were assignable to the starting material **59**. The tube was opened, and the solvent was evaporated. The residue was purified by WCC (hexane) to afford **59** (37.2 mg, 0.0375 mmol, 92%).

Reaction of 61 with LDA. In a glovebox filled with argon, LDA (2 M in heptane/THF/ethylbenzene, 0.021 mL, 0.042 mmol) was added to a THF solution (2 mL) of **61** (38.3 mg, 0.0411 mmol) at room temperature. The reaction mixture was stirred at the same temperature for 1 h. After removal of the solvent, hexane was added to the residue. The resulting suspension was filtered through Celite®, and the solvent was removed. A C_6D_6 solution of the residue was placed in a 5 mm ϕ NMR tube, and the tube was evacuated and sealed. The observed ^{1}H NMR signals were assignable to one diasteroisomer of aminostannane **62**. **62**: ^{1}H NMR (300 MHz, rt, C_6D_6) δ 0.13 (s, 9H), 0.14 (s, 36H), 0.18 (s, 9H), 0.90 (d, ^3J = 6.6 Hz, 3H), 1.28 (d, ^3J = 6.6 Hz, 3H), 1.44 (s, 1H), 2.43 (br s, 1H), 2.51 (br s, 1H), 3.35 (sept, ^3J = 6.6 Hz, 1H), 4.50 (s, 1H), 6.48 (br s, 1H), 6.63 (br s, 1H), 6.76-7.66 (m, 12H), 8.24-8.26 (m, 1H).

Reaction of 61 with *t*-butyllithium. In a glovebox filled with argon, *t*-butyllithium (0.95 M in hexane, 0.051 mL, 0.048 mmol) was added to a diethylether solution (2 mL) of **61** (44.2 mg, 0.0474 mmol) at –40 °C. After stirring for 0.5 h at the same temperature, the reaction mixture was stirred at room temperature for 1 h. After removal of the solvent, hexane was added to the residue. The resulting suspension was filtered through Celite®, and the solvent was removed. A C_6D_6 solution of the residue was placed in a 5 mm ϕ NMR tube, and the tube was evacuated and sealed. The observed ^{1}H NMR signals were assignable to two isomers of **63**. The tube was opened, and the solvent was evaporated. The residue was purified by WCC (hexane→chloroform) to afford **63** (*dl*/*meso* = 1/1, 41.3 mg, 0.0426 mmol, 90%). **63**: a mixture of isomers; colorless crystals; mp 221-224 °C (dec.); ^{1}H NMR (300 MHz, rt, $CDCl_3$, *: one isomer) δ –0.62 (s, 4.5H*), –0.63 (s, 4.5H*), –0.03 (s, 4.5H*), 0.00 (s, 4.5H*), 0.01 (s, 4.5H*), 0.03 (s, 4.5H*), 0.05 (s, 4.5H*), 0.07 (s, 4.5H*), 0.12 (4.5H*), 0.15 (s, 4.5H*), 0.25 (s, 4.5H*), 0.26 (s, 4.5H*), 0.88 (s, 9H, *t*-Bu), 1.53 (s, 1H), 1.85 (br s, 1H), 2.46 (br s, 1H), 4.38 (s, 0.5H*), 4.40 (s, 0.5H*), 6.22 (br s, 0.5H*), 6.34 (br s, 0.5H*+0.5H*), 6.46 (br s, 0.5H*), 6.89-7.34 (m, 9H), 7.47-7.53 (m, 2H), 7.74-7.86 (m, 2H); ^{119}Sn NMR (111 MHz, rt, $CDCl_3$): δ –182.6, –183.0.

Reaction of 61 with LTMP. In a glovebox filled with argon, LTMP [0.054 mmol, prepared from 2,2,6,6-tetramethylpiperidine (10.1 mg, 0.0715 mmol) and *n*-butyllithium (1.5 M in hexane, 0.036 mL, 0.054 mmol) in THF (0.5 mL)] was added to a THF solution (2 mL) of **61** (45.8 mg, 0.0491 mmol) at room temperature. The reaction mixture was stirred at the same temperature for 1 h. After removal of the solvent, hexane was added to the residue. The resulting suspension was filtered through Celite®, and the solvent was removed. A C_6D_6 solution of the residue was placed in a 5 mm ϕ NMR tube, and the tube was sealed. After the measurement of ^{1}H NMR

spectrum (complicated mixture), the tube was opened, and the solvent was evaporated. The residue was purified by HPLC (toluene), but any isolable products were not obtained.

Synthesis of 67 via 65. To a THF solution (16 mL) of **64** (493 mg, 1.64 mmol) was added *n*-butyllithium (1.5 M in hexane, 2.2 mL, 3.3 mmol) at –78 °C. After stirring at the same temperature for 10 min, THF solution (33 mL) of $TbtSnX_3$ (X = Cl or Br, ca. 75% purity; 1.63 g, ca 1.6 mmol as X = Cl) was added to the mixture. After stirring for 3 h at –78 °C, the reaction mixture was warmed to room temperature. After removal of the solvent, hexane was added to the residue. The resulting suspension was filtered through Celite®, and the solvent was removed. The residue was separated by GPLC ($CHCl_3$) to afford 3-*t*-Bu-2-Tbt-2-X-1,2-dihydro-2-stannanaphthalene **66** (567 mg, X: Cl/Br = 7/3). To a THF solution (10 mL) of **66** was added lithium aluminum hydride (88.5 mg, 2.33 mmol) at 0 °C. After stirring for 1 h at the same temperature, ethyl acetate was added to the reaction mixture at 0 °C. After removal of the solvent, hexane was added to the residue. The resulting suspension was filtered through Celite®, and the solvent was removed. This crude product was separated by WCC (hexane) to afford **67** (509 mg, 0.603 mmol, 37%, from **64**). **67**: colorless crystals; mp 179-181 °C (dec.); ^{1}H NMR (300 MHz, rt, C_6D_6): δ 0.05 (s, 9H), 0.10 (s, 9H), 0.137 (s, 9H), 0.144 (s, 9H), 0.16 (s, 9H), 0.21 (s, 9H), 1.39 (s, 9H), 1.44 (s, 1H), 1.65 (br s, 1H), 2.34 (br s, 1H), 2.58 (d, ^2J = 15.0 Hz, 1H), 2.78 (dd, ^2J = 15.0 Hz, ^3J = 0.9 Hz, 1H), 5.95 (d, ^3J = 0.9 Hz, 1H), 6.52 (br s, 1H), 6.67 (br s, 1H), 6.91-7.10 (m, 5H); ^{13}C NMR (75 MHz, rt, C_6D_6): δ 0.96 (q), 1.00 (q), 1.18 (q), 17.21 (t), 30.63 (d), 32.12 (d), 32.24 (q), 32.88 (d), 37.81 (s), 122.29 (d), 125.98 (d), 127.12 (d), 127.35 (d), 132.95 (d), 133.50 (d), 135.91 (s), 135.95 (s), 139.61 (d), 143.92 (s), 151.79 (s×2), 158.66 (s); ^{119}Sn NMR (111 MHz, rt, C_6D_6): δ –293.3; High resolution FAB-MS *m/z* calcd for $C_{40}H_{76}Si_6{}^{120}Sn$: 844.3585 ([M]$^+$), found: 844.3589 ([M]$^+$). Anal. Calcd for $C_{40}H_{76}Si_6Sn$: C, 56.91; H, 9.07. Found: C, 56.93; H, 9.23.

Synthesis of 68. A benzene (50 mL) solution of **67** (509 mg, 0.603 mmol) and *N*-bromosuccinimide (118 mg, 0.663 mmol) was stirred for 1 h at room temperature. After removal of the solvent, hexane was added to the residue. The resulting suspension was filtered through Celite®, and the solvent was removed to afford **68** (509 mg, 0.552 mmol, 91%). **68**: colorless crystals; mp 162-165 °C (dec.); ^{1}H NMR (300 MHz, rt, C_6D_6): δ –0.13 (s, 9H), –0.03 (s, 9H), –0.01 (s, 9H), 0.04 (s, 18H), 0.11 (s, 9H), 1.25 (s, 1H), 1.39 (s, 9H), 1.59 (br s, 1H), 2.42 (s, 1H), 3.02 (d, J = 15.0 Hz, 1H), 3.24 (d, J = 15.0 Hz, 1H), 6.29 (br s, 1H), 6.44 (br s, 1H), 7.01-7.11 (m, 5H); ^{13}C NMR (75 MHz, rt, C_6D_6): δ 0.96 (q), 0.98 (q), 1.21 (q), 30.44 (t), 30.83 (d), 31.24 (d), 31.75 (d), 33.09 (q), 38.51 (s), 123.46 (d), 126.41 (d), 127.48 (d), 128.00 (d), 132.55 (d), 133.65 (d), 134.02 (s), 135.81 (s), 136.10 (s), 142.01 (d), 145.42 (s), 151.13 (s), 152.35 (s), 160.65 (s); ^{119}Sn NMR (111 MHz, rt, C_6D_6): δ –93.0; High resolution FAB-MS *m/z* calcd for $C_{40}H_{75}{}^{79}BrSi_6{}^{120}Sn$: 922.2690 ([M]$^+$), found: 922.2695 ([M]$^+$). Anal. Calcd for $C_{40}H_{75}BrSi_6Sn$: C, 52.04; H, 8.19. Found: C, 52.31; H, 8.44.

Synthesis of 32. In a glovebox filled with argon, **68** (46.2 mg, 0.0500 mmol) was dissolved in hexane (2 mL, dried over K mirror and distilled by trap-to-trap method), and LDA (2.0 M in heptane/THF/ethylbenzene, 0.0300 mL, 0.0600 mmol) was added to the solution at –40 °C. After stirring for 1 h at room temperature, the solvents were removed under reduced pressure and hexane was added to the residue. The resulting suspension was filtered through Celite®, and the solvent was removed. The residue was recrystallized from hexane to give **32** (26.7 mg, 0.0317 mmol, 63%). **32**: yellow crystals; mp 144-147 °C (dec.); ^{1}H NMR (300 MHz, rt, C_6D_6): δ 0.18 (br s, 54H), 1.06 (s, 1H), 1.53 (s, 9H), 2.04 (br s, 1H), 2.08 (s, 1H), 6.68 (br s, 1H), 6.81 (br s, 1H), 7.05 (dd, ^3J = 9 Hz, ^3J = 7 Hz, 1H), 7.21 (dd, ^3J = 9 Hz, ^3J = 7 Hz, 1H), 7.65 (d, ^3J = 9 Hz, 1H), 7.68 (d, ^3J = 9 Hz, 1H), 8.75 (s, 1H), 9.28 (s, 1H); ^{13}C NMR (75 MHz, rt, C_6D_6): δ 0.91 (q),

1.55 (q), 30.84 (d), 34.93 (q), 39.36 (d), 39.72 (s), 39.90 (q), 119.97 (d), 122.12 (d), 125.30 (d), 125.92 (s), 126.76 (d), 127.93 (d), 135.39 (d), 141.58 (s), 142.22 (d), 146.02 (s), 147.26 (s), 147.38 (d), 150.92 (s×2), 174.03 (s); ^{119}Sn NMR (111 MHz, rt, C_6D_6): δ 264; High resolution FAB-MS *m/z* calcd for $C_{40}H_{75}Si_6{}^{120}Sn$: 843.3506 ($[M+H]^+$), found: 843.3531 ($[M+H]^+$).

X-Ray crystallographic analysis of 32. Crystal data for **32** are shown in Table 3-8. Yellow and prismatic single crystals of **32** were grown by the slow evaporation of its hexane solution in a glovebox filled with argon. The intensity data were collected on a Rigaku/MSC Saturn CCD diffractometer with graphite monochromated MoKα radiation (λ = 0.71069 Å) to $2\theta_{max}$ = 50° at 103 K. The structure was solved by Patterson methods (DIRDIF-99.2[29]) and refined by full-matrix least-squares procedures on F^2 for all reflections (SHELXL-97[30]). All hydrogen atoms were placed using AFIX instructions, while all the other atoms were refined anisotropically. A residual peak may be derived from the ghost peak near the tin atom and the inevitable disorder of 2-stannanaphthalene skeleton, similarly to the cases of Tbt-substituted 2-silanaphthalene[32] and 2-germanaphthalene.[21g] Although the ratio of the minor disorder in **1a** was too low to find all atoms of the disordered minor part, only the strong peak corresponding to the tin atom of the minor part was found as the residual peak.

Measurement of UV/vis spectrum of 32. In a glovebox filled with argon, **32** (1.0 mg, 1.2 × 10^6 mol) was dissolved in hexane (3 mL, dried over K mirror and distilled by trap-to-trap distillation). This solution (4.0 × 10^4 M) was put into UV cell (pathlength 1 mm), and UV/vis spectrum was measured with JASCO Ubest-50 UV/vis spectrometer at room temperature.

Measurement of Raman spectrum of 32. In a glovebox filled with argon, **32** was powdered and put into a glass capillary. The capillary was evacuated and sealed. FT-Raman spectrum was measured with the excitation by He-Ne laser (532 nm) at room temperature in the solid state with Spex 1877 Triplemate and EG&G PARC 1421 intensified photodiode array detector by Prof. Furukawa at Waseda University.

Synthesis of 74. In a glovebox filled with argon, **32** (34.2 mg, 0.0406 mmol) and $[Cr(CH_3CN)_3(CO)_3]$[33] (14.6 mg, 0.0563 mmol) were dissolved in THF (1 mL, dried over K mirror and distilled by trap-to-trap method) at room temperature. After stirring for 4 h, the solvents were removed under reduced pressure and hexane was added to the residue. The resulting suspension was filtered through Celite®, and the solvent was removed to give almost pure **74** (35.5 mg, 0.0363 mmol, 89%). **74**: brown crystals; mp 154 °C (dec.); ^{1}H NMR (300 MHz, C_6D_6, 70 °C) δ 0.15 (s, 18H), 0.18 (s, 18H), 0.27 (s, 18H), 1.36 (s, 9H), 1.52 (s, 1H), 2.24 (s, 2H), 5.10 (s, 1H), 6.43 (s, 1H), 6.81 (br s, 2H), 6.85-6.95 (m, 3H), 7.33 (d, ^3J = 8 Hz, 1H); ^{13}C NMR (75 MHz, C_6D_6, 50 °C) δ 0.86 (q), 0.95 (q), 1.34 (q), 31.42 (d), 34.31 (q), 38.40 (s), 39.79 (d), 40.27 (d), 88.37 (d), 96.41 (s), 102.75 (d), 116.84 (s), 122.70 (d), 125.19 (d), 125.70 (d), 128.68 (d), 131.31 (s), 132.89 (d), 134.59 (d), 134.91 (s), 147.69 (s), 151.87 (s×2), 233.77 (s, <u>C</u>O); ^{119}Sn NMR (111 MHz, 50 °C, C_6D_6) δ 106. High resolution FAB-MS *m/z* calcd for $C_{43}H_{74}O_3CrSi_6{}^{120}Sn$ ($[M]^+$): 978.2681, found: 978.2675.

X-Ray crystallographic analysis of 72. Crystal data for **72** are shown in Table 3-9. Brown and prismatic single crystals of **72** were grown by the slow evaporation of its benzene solution in a glovebox filled with argon. The intensity data were collected on a RIGAKU Saturn70 CCD system with VariMax Mo Optic MoKα radiation (λ = 0.71069 Å) to $2\theta_{max}$ = 50° at 173 K. The

structure was solved by Patterson methods (DIRDIF-99.2[29]) and refined by full-matrix least-squares procedures on F^2 for all reflections (SHELXL-97[30]). Four trimethylsilyl groups of the $CH(SiMe_3)_2$ groups at *para*-position and one of the *ortho*-positions of the Tbt group were disordered. The occupancies of the disordered parts were refined (*p*-: 0.60:0.40, *o*-: 0.66:0.34). The U_{ij} values of the disordered trimethylsilyl groups were restrained using SIMU instructions. All hydrogen atoms were placed using AFIX instructions, while all the other atoms were refined anisotropically.

Measurement of UV/vis spectrum of 74. In a glovebox filled with argon, **74** (1.5 mg, 1.5×10^6 mol) was dissolved in hexane (2 mL, dried over K mirror and distilled by trap-to-trap distillation). This solution (7.7×10^4 M) was put into UV cell (pathlength 1 mm), and UV/vis spectrum was measured with JASCO Ubest-50 UV/vis spectrometer at room temperature.

Refferences

1. Minkin, V. J.; Glukhovtsev, M. N.; Simkin, Y. B. *Aromaticity and Antiaromaticity; Electronic and Structural Aspects*; Wiley: New York, 1994.
2. Faraday, M. *Phil. Trans. Roy. London.* **1825**, 440.
3. Schleyer, P. v. R.; Jiao, H. *Pure. Appl. Chem.* **1996**, *68*, 209.
4. For a review on phosphabenzenes, see: Märkl, G. In *Multiple Bonds and Low Coordination in Phosphorus Chemistry*; Regitz, M., Scherer, O. J., Eds.; Thieme Stuttgart, 1990; chapter D.5.
5. Ashe, A. J., III. *Acc. Chem. Res.* **1981**, *11*, 153.
6. For reviews on boratabenzenes, see: (a) Herberich, G. E.; Ohst, H. *Adv. Organomet. Chem.* **1986**, *25*, 119. (b) Ashe, A. J., III; Al-Ahmad, S.; Fang, X. *J. Organomet. Chem.* **1999**, *581*, 92.
7. For recent work on boratabenzene π-complexes, see: (a) Rogers, J. S.; Bu, X.; Bazan, G. C. *Organometallics* **2000**, *19*, 3948. (b) Ashe, A. J., III.; Al-Ahmad, S.; Fang, X.; Kampf, J. W. *Organometallics* **2001**, *20*, 468. (c) Zheng, X.; Herberich, G. E. *Organometallics* **2001**, *20*, 3097.
8. Ashe III, A. J.; Al-Ahmad, S.; Kampf, J. W. *Angew. Chem. Int. Ed. Ennl.* **1995**, *34*, 1357.
9. For reviews on silaaromatic compounds, see: (a) Raabe, G.; Michl, J. *Chem. Rev.* **1985**, *85*, 419. (b) Raabe, G.; Michl, J. In *The Chemistry of Organic Silicon Compounds*; Patai, S., Rappoport, Z., Eds.; Wiley: New York, 1989; pp 1102–1108. (c) Apeloig Y. *ibid.*, pp 151–166. (d) Brook, A. G.; Brook, M. A. *Adv. Organomet. Chem.* **1996**, *39*, 71. (e) Apeloig, Y.; Karni, M. In *The Chemistry of Organic Silicon Compounds, Volume 2*; Rappoport, Z., Apeloig, Y., Eds.; Wiley: New York, 1998; chapter 1.

10. For a review on germaaromatic compounds, see: Lee, V. Y.; Sekiguchi, A.; Ichinohe, M.; Fukaya, N. *J. Organomet. Chem.* **2000**, *611*, 228.

11. For related works on silole anion and dianion species, see: (a) Hong, J.-H.; Boudjouk, P. *J. Am. Chem. Soc.* **1993**, *115*, 5883. (b) Hong, J.-H.; Boudjouk, P.; Castellino, S. *Organometallics* **1994**, *13*, 3387. (c) West, R.; Sohn, H.; Bankwitz, U.; Calabrese, J.; Apeloig, Y.; Mueller, T. *J. Am. Chem. Soc.* **1995**, *117*, 11608. (d) Freeman, W. P.; Tilley, T. D.; L-Sands, L. M.; Rheingold, A. L. *J. Am. Chem. Soc.* **1996**, *118*, 10457. (e) Choi, S.-B.; Boudjouk, P.; Wei, P. *J. Am. Chem. Soc.* **1998**, *120*, 5814. (f) Liu, Y.; Stringfellow, T. C.; Ballweg, D.; Guzei, I. A.; West, R. *J. Am. Chem. Soc.* **2002**, *124*, 49.

12. For related works on germole dianion species, see: (a) Hong, J.-H.; Boudjouk, P. *Bull. Chem. Soc. Fr.* **1995**, *132*, 495. (b) West, R.; Sohn, H.; Powell, D. R.; Müller, T.; Apeloig, Y. *Angew. Chem., Int. Ed. Engl.* **1996**, *35*, 1002. (c) Choi, S.-B.; Boudjouk, P.; Hong, J.-H. *Organometallics* **1999**, *18*, 2919. (d) Choi, S.-B.; Boudjouk, P.; Qin, K. *Organometallics* **2000**, *19*, 1806.

13. Goldfuss, B.; Schleyer, P. v. R. *Organometallics* **1995**, *14*, 1553.

14. Lee, V. Ya.; Kato, R.; Ichinohe, M.; Sekiguchi, A. *J. Am. Chem. Soc.* **2005**, *127*, 13142.

15. (a) Freeman, W. P.; Tilley, T. D.; Rheingold, A. L.; Ostrander, R. L. Angew. Chem., Int. Ed. Engl. 1993, 32, 1744. (b) Freeman, W. P.; Tilley, T. D.; Rheingold, A. L. *J. Am. Chem. Soc.* **1994**, *116*, 8248. (c) Dysard, J. M.; Tilley, T. D. *J. Am. Chem. Soc.* **1998**, *120*, 8245. (d) Dysard, J. M.; Tilley, T. D. *J. Am. Chem. Soc.* **2000**, *122*, 3097. (d) Dysard, J. M.; Tilley, T. D.; Woo, T. K. *Organometallics* **2001**, *20*, 1195.

16. (a) Freeman, W. P.; Tilley, T. D.; Rheingold, A. L.; Ostrander, R. L. *Angew. Chem., Int. Ed. Engl.* **1993**, *32*, 1774. (b) Dysard. J. M.; Tilley, T. D. *J. Am. Chem. Soc.* **1998**, *120*, 8245.

(c) Freeman, W. P.; Dysard. J. M.; Tilley, T. D. Rheingold, A. L. *Organometallics* **2002**, *21*, 1734.

17. Sekiguchi, A.; Tsukamoto, M.; Ichinohe, M. *Science*. **1997**, *275*, 60.

18. Ichinohe, M.; Igarashi, M.; Sanuki, K.; Sekiguchi, A. *J. Am. Chem. Soc.* **2005**, *127*, 9978.

19. Denk, M.; Lennon, R.; Hayashi, R.; West, R.; Belyakov, A. V.; Verne, H. P.; Haaland, A.; Wagner, M.; Metzler, N. *J. Am. Chem. Soc.* **1994**, *116*, 2691.

20. Denk, M.; Green, J. C.; Metzler, N.; Wagner, M. *J. Chem. Soc., Dalton Trans.* **1994**, 2405.

21. (a) Tokitoh, N.; Wakita, K.; Okazaki, R.; Nagase, S.; Schleyer, P. v. R.; Jiao, H. *J. Am. Chem. Soc.* **1997**, *119*, 6951. (b) Wakita, K.; Tokitoh, N.; Okazaki, R.; Nagase, S. *Angew. Chem. Int. Ed.* **2000**, *39*, 636. (c) Wakita, K.; Tokitoh, N.; Okazaki, R.; Takagi, N.; Nagase, S. *J. Am. Chem. Soc.* **2000**, *122*, 5648. (d) Takeda, N.; Shinohara, A.; Tokitoh, N. *Organometallics* **2002**, *21*, 256. (e) Takeda, N.; Shinohara, A.; Tokitoh, N. *Organometallics* **2002**, *21*, 4024. (f) Shinohara, A.; Takeda, N.; Tokitoh, N. *J. Am. Chem. Soc.* **2003**, *125*, 10805. (g) Nakata, N.; Takeda, N.; Tokitoh, N. *Organometallics* **2001**, *20*, 5507. (h) Nakata, N.; Takeda, N.; Tokitoh, N. *J. Am. Chem. Soc.* **2002**, *124*, 6914.

22. (a) Saito, M.; Haga, R.; Yoshioka, M. *Chem. Commun.* **2002**, 1002. (b) Saito, M.; Haga, R.; Yoshioka, M. *Chem. Lett.* **2003**, *32*, 912. (c) Saito, M.; Haga, R.; Yoshioka, M.; Ishimura, K.; Nagase, S. *Angew. Chem. Int. Ed.* **2005**, *44*, 6553

23. Sashida, H. *Synthesis* **1999**, *11*, 1866.

24. (a) Nakata, N.; Takeda, N.; Tokitoh, N. *Angew. Chem. Int. Ed.* **2003**, *42*, 115. (b) Shinohara, A.; Takeda, N.; Tokitoh, N. *Organometallics*, **2005**, *24*, 6141.

25. (a) Morley, J. A.; Woolsey, N. F. *J. Org. Chem.* **1992**, *57*, 6487. (b) There is another report for the IR spectral data [1958 and 1862 (broad) cm^{-1} (KBr)] for the same compound. See, Fischer, R. D. *Chem. Ber.* **1960**, *93*, 165.

26. Schleyer, P. v. R.; Maerker, C.; Dransfeld, A.; Jiao, H.; Hommes, N. J. R. v. E. *J. Am. Chem. Soc.* **1996**, *118*, 6317.

27. Schleyer, P. v. R.; Jiao, H.; van Eikema Hommes, N.J.R.; Malkin, V. G.; Malkina, O. J. *J. Am. Chem. Soc.* **1997**, *119*, 12669.

28. Matsuhashi, Y.; Tokitoh, N.; Okazaki, R.; Goto, M.; Nagase, S. *Organometallics* **1993**, *12*, 1351.

29. Beurskens, P. T.; Beurskens, G.; de Gelder, R.; Garcia-Granda, S.; Gould, R. O.; Israel, R.; Smits, J. M. M. *The DIRDIF–99.2 program system, Crystallography Laboratory*; University of Nijmegen: The Netherlands, 1999.

30. Sheldrick, G. M. *SHELX-97, Program for the Refinement of Crystal Structures*; University of Göttingen: Göttingen, Germany, 1997

31. Cookson, E. A.; Crofts, P. C. *J. Chem. Soc. Section C: Organic* **1966**, *21*, 2003.

32. Wakita, K.; Tokitoh, N.; Okazaki, R. *Bull. Chem. Soc., Jpn.* **2000**, *73*. 2157.

33. Tate, D. P.; Knipple, W. R.; Augl, J. M. *Inorg. Chem.* **1962**, *1*, 433.

Chapter 4

Conclusion and Outlook

The chemistry of multiple-bond compounds containing (a) tin atom(s) has the longest history among those of the multiple bonds to the heavier main group elements. However, it has developed rapidly in the last decade and is still insufficient to make systematic elucidation of the multiply bonded systems containing (a) tin atom(s). In order to study the chemical behaviour of tin–carbon double bond in detail, the author described in Chapter 2 the synthesis and properties of the kinetically stabilized stannenes bearing only carbon substituents. In Chapter 3, the synthesis and properties of 9-stannaphenanthrene and 2-stannanaphthalene, stannaaromatic compounds having a formal Sn=C fragment in their aromatic rings, have been reported.

In Chapter 2, the author succeeded in the synthesis of the first donor-free tetraarylstannene **1** stable at ambient temperature by taking advantages of an efficient steric protection group, 2,4,6-tris[bis(trimethylsilyl)methyl]phenyl (Tbt).

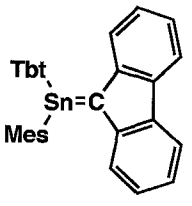

1

The X-ray crystallographic analysis showed the shortest the tin–carbon bond length (2.016 Å) among those previously reported and the completely trigonal planar geometries around the central tin (359.9°) and carbon (359.9°) atoms, indicating the formation of a π-bond between tin and carbon atoms. Their NMR, UV/vis, and Raman spectra and reactivity supported the double-bond characters of **1**.

The fact that the synthesis and isolation of tin–carbon double-bond compound was achieved by suitable protecting groups, prompted the author to expand this chemistry to stannaaromatic compounds.

In Chapter 3, the author succeeded in the generation of 9-stannaphenanthrene **2** and the synthesis and isolation of 2-stannanaphthalene **3** by taking advantages of a Tbt group.

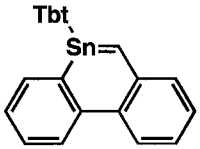

2

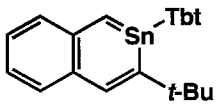

3

9-Stannaphenanthrene **2** was thermally unstable and underwent ready dimerization at room temperature in sharp contrast to the high stability of the Tbt-substituted 9-sila- and germaphenanthrenes, which are known to be stable at 100 °C in C_6D_6. By contrast, 2-stannanaphthalene **3** was thermally stable. The X-ray crystallographic analysis of **3** showed the planar geometry of 2-stannanaphthalene ring and the bond-alternation, which are eventually the same features as those of a parent naphthalene. Judging from their structure, NMR, UV/vis, and Raman spectra, and reactivity, 2-stannanaphthalene **3** has sufficient aromatic characters.

The main reason for the difference of the stability between **2** and **3** may be the introduction of an additional substituent (*t*-Bu) on **3**. However, theoretical calculations for stannaaromatic compounds implied the general conclusion that 9-stannaphenaathrene had lower aromaticity than 2-stannanaphthalene and that 2-stannanaphthalene had sufficient aromaticity comparable to the parent naphthalene.

In summary, the author disclosed in this Doctor Thesis that a tin atom, one of the fifth row elements, can forms a sufficient π-bond with a carbon atom as not only silicon and germanium atoms but also a carbon atom can do. In the light of these results, he hopes the synthesis of the unprecedented species containing (a) tin–carbon multiple bond(s), 1,3-distannaallene, polystannaaromatic compounds, stannaacetylene, and so on in the near future.

Acknowledgment

This thesis summarizes the author's study that has been carried out under the direction of Prof. Norihiro Tokitoh at Institute for Chemical Research of Kyoto University during the period of April 2003 to March 2006.

The author was assisted by many persons throughout this study. The author wishes to express his sincerest gratitude to all of them, especially to:

Prof. Norihiro Tokitoh for his kind guidance, helpful suggestions, and hearty encouragement.

Dr. Nobuhiro Takeda for his useful advice, suggestions and kind encouragement.

Dr. Takahiro Sasamori for his kind suggestions and helping in many aspects.

Dr. Yasushi Kawai for his kind suggestions and helping in the measurement and instruction of X-ray crystallographic analysis.

Assoc. Prof. Kaoru Nakamura, Dr. Takashi Sugiyama and Dr. Norimasa Yamazaki for helpful discussions from various points of view.

Ms. Toshiko Hirano for taking the elemental analysis.

Ms. Tomoko Terada for the measurement of mass spectra.

Ms. Kyoko Ohmine for the measurement of NMR spectra.

Prof. Yukio Furukawa, Waseda University for the measurement of Raman spectra.

Dr. Noriyoshi Nagahora for the measurement of cyclic voltammetry.

Dr. Norio Nakata for his useful advice, suggestions, technical assistance and kind encouragement.

Dr. Takashi Kajiwara, Dr. Akihiro Shinohara, and Dr. Tomoyuki Tajima for their valuable discussions and suggestions on various points.

Mr. Daisuke Shimizu and Mr. Yusuke Sugiyama for their technical suggestions and friendship.

The author thanks Research Fellowships of the Japan Society for the Promotion of Science for Young Scientists.

The author would like to express his deep appreciation to his parents, Mr. Yoshiro Mizuhata and Ms. Yukiko Mizuhata for their financial support, constant help and encouragement.

Finally, the author thanks to all members of Tokitoh Laboratory for their supports and communications:

Prof. Norihiro Tokitoh, Assoc. Prof. Kaoru Nakamura,

Dr. Nobuhiro Takeda, Dr. Takahiro Sasamori,

Dr. Takashi Sugiyama, Dr. Yasushi Kawai, Dr. Norimasa Yamazaki, Ms. Toshiko Hirano, Ms. Fuyuko Totani,

Dr. Motoko Hayashi, Dr. Kenji Ito, Dr. Hitomi Takao, formerly Yamaguchi,

Dr. Noriyoshi Nagahora, Dr. Kazuto Nagata, Dr. Norio Nakata, Dr. Rio Yamanaka,

Dr. Takashi Kajiwara, Ms. Mariko Hori, Dr. Akihiro Shinohara, Dr. Tomoyuki Tajima,

Mr. Satoshi Kimura, Mr. Daisuke Shimizu, Mr, Yusuke Sugiyama,

Mr. Masaki Fujiwara, Mr. Hirofumi Hamaki, Ms. Megumi Kobayashi, Ms. Misato Tomuro, formerly Shiraishi, Mr. Takayuki Yamasaki,

Mr. Wataru Hoshino, Mr. Toru Isobe, Mr. Takeshi Matsumoto, Ms. Eiko Mieda,

Mr. Masahiro Kawai, Mr. Shuhei Ozaki, Mr. Taro Tanabe,

Mr. Koji Inamura, Mr. Teruyuki Matsumoto, and Mr. Akihiro Tsurusaki.

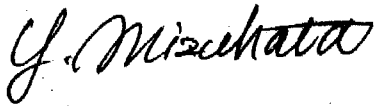

Yoshiyuki Mizuhata
Kyoto University
March 2006

List of Publications

Publications for This Thesis

1. "Generation of 9-Stannaphenanthrene and Its Reactivities"
   Mizuhata, Y.; Takeda, N.; Sasamori, T.; Tokitoh, N. *Chem. Lett.*, **2005**, *34*, 1088-1089.

2. "Synthesis and properties of a stable 6-stannapentafulvene"
   Mizuhata, Y.; Takeda, N.; Sasamori, T.; Tokitoh, N. *Chem. Commun.*, **2005**, 5876-5878.

3. "A Stable Neutral Stannaaromatic Compound: Synthesis, Structure and Complexation of a Kinetically Stabilized 2-Stannanaphthalene"
   Mizuhata, Y.; Sasamori, T.; Takeda, N.; Tokitoh, N. *J. Am. Chem. Soc.*, **2006**, *128*, 1050-1051.

Related Publications

4. "Generation of 1,6-Disilahexapentaene in the Reduction of an Overcrowded Bis(bromodiaryl)butadiyne Leading to the Unexpected Formation of 2-Allenyl-1-benzosilole"
   Mizuhata, Y.; Takeda, N.; Sasamori, T.; Tokitoh, N. *Chem. Lett.*, **2004**, *33*, 420-421.

5. "REDUCTION OF BIS(BROMO(MESITYL){2,4,6-TRIS[BIS(TRIMETHYLSILYL)-METHYL]PHENYL}SILYL)BUTADIYNE WITH POTASSIUM GRAPHITE: UN-EXPECTED FORMATION OF 2-ALLENYL-1-BENZOSILOLE"
   Mizuhata, Y.; Takeda, N.; Tokitoh, N. *Phosphorus, Sulfur and Silicon and the Related Elements*, **2004**, *179*, 947-948.

Other Publication

6. "Palladium-Catalyzed Asymmetric Synthesis of Axially Chiral (Allenylmethyl)silanes and Chirality Transfer to Stereogenic Carbon Centers in S_E' Reactions"
   Ogasawara, M.; Ueyama, K.; Nagano, T.; Mizuhata, Y.; Hayashi, T. *Org. Lett.*, **2003**, *5*, 217-219.